ENGINEERING VASCULARIZED BONE GRAFTS WITH ADIPOSE-DERIVED STEM CELLS

By

Daphne Hutton

A dissertation submitted to The Johns Hopkins University in conformity with the requirements for the degree of Doctor of Philosophy.

Baltimore, MD

December 2014

Abstract

Tissue engineered bone grafts could potentially revolutionize treatments for massive bone defects, offering greater tissue quantities and graft customization over the gold standard autograft. However, scale-up of cell-seeded grafts requires rapid vascularization in order to maintain high cell viability and function after implantation. Engineering vasculature inside the graft may greatly accelerate blood perfusion of the whole tissue, rather than relying solely on slow angiogenic ingrowth. Development of a complex tissue graft poses several challenges, including the concurrent stimulation of two lineages, as well as the selection of clinically relevant cell source(s). Therefore, the **objective** of this thesis was to develop a protocol to engineer vascularized bone grafts with a single, clinically relevant cell source: adipose-derived stem cells (ASCs). ASCs can be harvested autologously via liposuction with very high yield and are unique in that they have both osteogenic and vascular potential, making them a promising cell source to supply key components of a vascularized bone graft.

This body of work describes a multistep approach towards the aforementioned objective. First, the potential of ASCs to form functional vasculature networks was explored. By increasing the direct physical interactions amongst cells, it was demonstrated that small lingering sub-populations of vascular cells are capable of spontaneously proliferating and self-assembling into three-dimensional pericyte-stabilized vascular networks. The next two chapters describe the development of a step-wise *in vitro* protocol to induce vascularized bone by recapitulating the biochemical environment of native bone repair. This study highlighted factors derived from platelets and inflammatory cells that promote vascular growth and stability, as well as osteogenic mineralization. Lastly, the effects of hypoxia on vascular assembly and stability were studied to understand how ASC-seeded grafts may

behave in an ischemic bone injury environment. This investigation revealed that hypoxia severely inhibits *de novo* vascular assembly, but promotes growth and stability of pre-formed vessels. Taken together, these findings have significant implications for how ASCs could be applied clinically for bone regeneration.

Advisor: Warren L. Grayson, Ph.D.

Acknowledgements

First, I would like to thank my advisor, Warren Grayson, for his advice and support. It has been such an honor to be his first PhD student and to have the opportunity to work closely with him as he developed his lab. He was persistently helpful as a mentor – coming to the lab to teach me a few techniques or to look at my cells, making himself available whenever I needed to discuss something, and always encouraging me to challenge myself. I am grateful for his mentorship and support, which have undoubtedly contributed to my successes throughout the challenging PhD process.

I would also like to thank my thesis committee members: HaiQuan Mao, Douglas DiGirolamo, and Kevin Yarema. I am grateful for their time, input, criticisms, insightful questions, and thoughtful discussion of my work. Their feedback and kind words of encouragement were incredibly helpful in the refinement and completion of my thesis.

Throughout my tenure in the Grayson Lab, I have had the great pleasure of getting to know and work with so many wonderful people. I am so thankful for everyone's friendship, support, and collaboration. Our group started small, but has grown into such a diverse group of sweet, friendly, funny, and smart people. I had a lot of fun at all of the group activities, potlucks, and of course daily lunches at the Outpatient Cafeteria. I have enjoyed working side-by-side (literally, as we only had one cell culture hood), learning together, and giving and receiving so much helpful advice. Years of chatting, venting, and laughing together made it so enjoyable to get to know everyone on a personal level.

Several collaborators have helped me in many ways with my research. Jeffrey Gimble not only supplied our lab with adipose-derived stem cells in the early years, but also reviewed my first two manuscripts and provided very insightful and critical feedback regarding stem cell

biology. Feilim Mac Gabhann and Elizabeth Logsdon collaborated on the monolayer vascular morphogenesis studies, providing helpful suggestions and commentary about vascular biology. Xiaofeng Jia conducted the *in vivo* studies that were included in this thesis and also collaborated in the development of future surgical procedures for the lab. Amir Dorafshar and Angelo Leto Barone helped at various stages of the process to obtain adipose tissue samples. The Wilmer Core Module for Microscopy and Imaging allowed me to use the Zeiss LSM 510 Meta confocal microscope.

I must also thank my sources of funding, which were critical to supporting my research. The American Heart Association granted me a Pre-Doctoral Fellowship (2012-2014), which was very meaningful to me as a young researcher and essential to the financial support of my research project. My project was also supported over the years by grants awarded to Warren Grayson by the Maryland Stem Cell Research Fund, Johns Hopkins Center for Musculoskeletal Research, American Society for Bone and Mineral Research, and the National Science Foundation CAREER award.

These acknowledgements would never be complete without mentioning the most important people in my life: my family. My parents and sister are such hardworking, intelligent, motivated, kind, and giving people, and I have missed them a lot since moving to Baltimore. They have been indescribably loving and supportive throughout my entire life, and never stop telling me how proud they are of my accomplishments and who I have become. Of course my family also now includes my husband Suneil, who I met soon after starting at Hopkins. I am so grateful for his loving friendship, emotional support, and guidance throughout the entire PhD process. He has truly made a huge positive impact in my life, and I cannot wait to see what the future holds!

Table of Contents

List of Tables

List of Figures

List of Abbreviations

ANOVA	Analysis of variance
ASC	Adipose-derived stem cell
αSMA	Alpha smooth muscle actin
BM	Bone marrow
BMP-2	Bone morphogenetic protein-2
BrdU	Bromodeoxyuridine
Col I/IV	Collagen I/IV
DAPI	4',6-diamidino-2-phenylindole
DMEM	Dulbecco's Modified Eagle's Medium
EBM-2	Endothelial Basal Medium-2
EC	Endothelial cell
EIM	Endothelial induction medium
ELISA	Enzyme-linked immunosorbent assay
FBS	Fetal bovine serum
FGF-2	Basic fibroblast growth factor
H&E	Hematoxylin and Eosin
Lam	Laminin
MSC	Mesenchymal stem cell
OCN	Osteocalcin
OM	Osteogenic medium
PBS	Phosphate buffered saline
PCL	Polycaprolactone
PDGF	Platelet-derived growth factor
PDGFR-β	Platelet-derived growth factor receptor beta
PTw	PBS + 0.1% (v/v) Tween
RT-PCR	Reverse transcription polymerase chain reaction
RUNX-2	Runt-related transcription factor-2
SVF	Stromal vascular fraction
TNF	Tumor necrosis factor
VE-Cad	Vascular endothelial-cadherin
VEGF	Vascular endothelial growth factor
VEGFR-2	Vascular endothelial growth factor receptor-2
VM	Vascular Medium
vWF	von Willebrand Factor

Chapter 1

Introduction

1.1 Critical-Size Bone Defects

Bone is a highly regenerative tissue that has considerable potential to fully heal itself following traumatic injury. However, when the size of the defect is beyond a critical healing threshold (approximately a few centimeters in humans), normal healing cascades are disrupted (**Fig. 1.1**), and the defect may never completely heal. These defects are termed 'critical-size' and may be due to trauma, congenital defects, or disease. Complicating factors that can impede healing include missing critical sources of regenerative cues (i.e. periosteum, hematoma) and may be prone to mechanical / structural instability and infection [1]. Bone grafting is often required to facilitate healing of these defects.

More than one million Americans each year require bone grafts for the regeneration of critical-size bone defects, with an economic burden in excess of $1B annually [2]. The gold standard for treatment is autologous bone grafts, which are often harvested from the iliac crest, fibula, or ribs. Autografts contain viable bone cells and osteoinductive factors, which facilitate rapid osteogenesis and remodeling at the site of transplant. However, the limited availability of autografts and donor site complications pose challenges for their use [3]. Allogeneic bone grafts and synthetic grafting materials (e.g. tricalcium phosphate) are more abundant alternatives that have osteoinductive and osteoconductive properties, but require massive cellular infiltration from surrounding tissues to populate large volume defects.

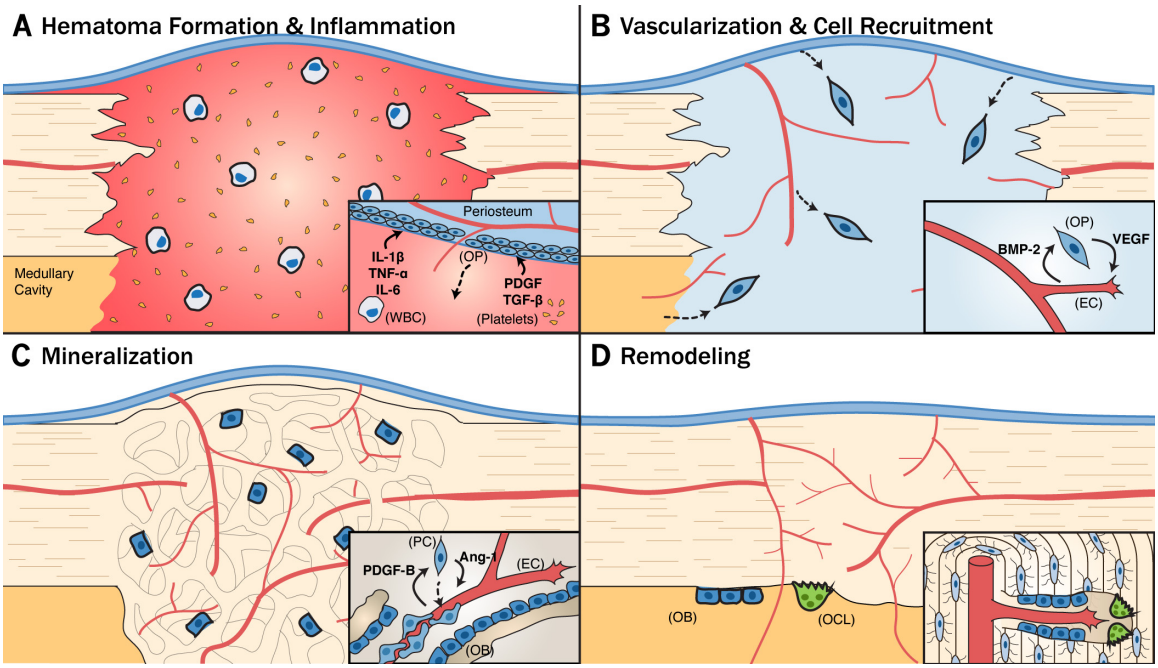

Figure 1.1. Normal bone healing and its coupling with vascularization. (A) Vascular damage occurs concomitantly with bone fracture, resulting in local bleeding that clots to form a hematoma. An acute inflammatory phase begins immediately, wherein white blood cells (WBCs) secrete pro-inflammatory cytokines and degranulating platelets release growth factors. These inflammatory factors signal the recruitment and proliferation of osteoprogenitor cells (OPs) from the periosteum, bone marrow, muscle, and/or perivascular position. The periosteum not only serves as a major source of OPs and vasculature, but also structural support (if still in tact). **(B)** Over the course of a few weeks, the hematoma is resorbed and replaced by granulation tissue, followed by fibrocartilagenous tissue ('soft callus'). Lack of blood flow within the defect results in hypoxia, which causes an increase in expression of VEGF by OPs. Invading endothelial cells (ECs) respond to VEGF gradients via increased angiogenesis into the defect site. These ECs express BMP-2, which induces differentiation of OPs into osteoblasts (OB). **(C)** After a few weeks, the callus becomes mineralized into woven bone ('hard callus') that completely bridges the defect (i.e. union). During this regeneration phase, growing vessels secrete PDGF-B to recruit pericytes (PCs) who secrete factors that help stabilize and mature the vessels (e.g. Ang-1). These vessels pattern the newly forming bone trabeculae, as OBs orient around the vessel and begin secreting osteoid outward. **(D)** Long-term remodeling via osteoclasts (OCL) and OBs transforms the hard callus into ordered lamellar bone. Osteocytes orient in circumferential lamellae around blood vessels.

1.2 Cell Transplantation & Vascularization

Bone tissue engineering is a promising alternative that allows the combination of supportive scaffolds, regenerative cells, and inductive cues to recapitulate the normal fracture healing environment within large void volumes. Stem cell transplantation has been shown to

significantly improve bone healing over acellular grafts [4-6] and has been employed clinically in a small number of cases [7-9]. However, its adoption into clinical practice has been limited by issues regarding reproducibility, efficacy, cost-effectiveness, and safety [10].

Vascularization of tissue-engineered grafts is critical to the survival and efficacy of transplanted cells to ensure adequate delivery of oxygen and nutrients. The vascular damage that occurs with bone injury renders sites of large bone defects highly ischemic. Delivering cells to the defect site further increases the local metabolic demand and exacerbates the detrimental effects arising form the lack of adequate oxygen supply. Vascularization of an implant that is several centimeters in size may take weeks. Therefore, encouraging vascular growth within cell-seeded grafts has become an important topic of research.

1.3 Approaches to Engineer Vascularized Bone

Several approaches have been developed to vascularize an engineered bone graft, including engineering vasculature before implantation, as well as encouraging vascular growth *in vivo* (**Fig. 1.2**). Engineering vascular networks within grafts prior to implantation (termed "pre-vascularization") may accelerate the rate of blood perfusion if they can quickly fuse ("anastomose") with established vasculature in surrounding tissues (**Fig. 1.2 top**). Several studies have shown this is possible [11-13], with a more recent study shedding light on the novel 'wrapping and tapping' mechanism by which engineered vessels anastomose with host vessels [14]. With this in mind, numerous approaches to engineer vascularized bone have implemented an *in vitro* pre-vascularization strategy [15] in order to maintain high cell viability during the vascularization process as well as greater control over the microenvironment. Despite the close relationship between bone and vascular growth *in vivo*

[16], establishing *in vitro* cultivation protocols that enable robust, synergistic development of both bone and vasculature has remained a persistent challenge since the biochemical cues that are present in the culture medium to stimulate bone development impede vascular growth and vice-versa [17-20]. Therefore, to develop tissue grafts that have both vascular and mineral components, groups have primarily either (i) utilized staged-induction approaches where angiogenic factors are provided for a period to stimulate vessel formation prior to introducing osteogenic supplements [17, 21-23] or (ii) cultured cells separately in medium optimized for vessel formation or osteogenic differentiation prior to recombining the various cell populations in a single tissue graft [24-27]. Additional studies have utilized perfusion or rotating-wall bioreactors to increase transport of oxygen and nutrients, as well as provide mechanical cues via shear stress, which increases tissue formation [28-30]. Further studies are required to understand how bioreactor culture affects vascularized bone development, as the direct effects on vasculature remain unclear. In addition, extensive and/or complex *in vitro* cultivation methods may not be readily adopted in the clinic in the near future due to logistical, regulatory, and financial hurdles.

Rather than pre-culture vasculature *in vitro*, it is possible to utilize the body itself as an *in vivo* 'bioreactor' to pre-vascularize the scaffold in an ectopic site (**Fig. 1.2 middle**). This two-step procedure involves implanting a scaffold within a highly vascularized bed, such as muscle or within an arteriovenous (AV) loop, for several weeks until extensive vascular networks have penetrated the graft. This scaffold can then be transplanted as a free flap to the orthotopic site with surgical anastomosis of major vessels to immediately perfuse the graft with blood [31, 32]. Clinically, there have been a few successful cases of ectopic pre-vascularization within muscle for craniofacial reconstruction. Autologous bone marrow

aspirate or ASCs have been combined with osteoinductive cues within titanium mesh cages, then implanted within muscle tissues to vascularize [7, 9]. Grafts were subsequently transplanted to defect sites. While partially successful, complications related to infections and necrosis ultimately occurred [33].

To enhance clinical applicability, it may be advantageous to seed a scaffold with cells and immediately implant into the defect site for *in situ* tissue formation (**Fig. 1.2 bottom**). However once *in vivo*, it is much more difficult to control the graft microenvironment. Successful regeneration may require tight control over the delivery of inductive cues to guide robust formation of perfusable vascular networks surrounded by mature, organized bone.

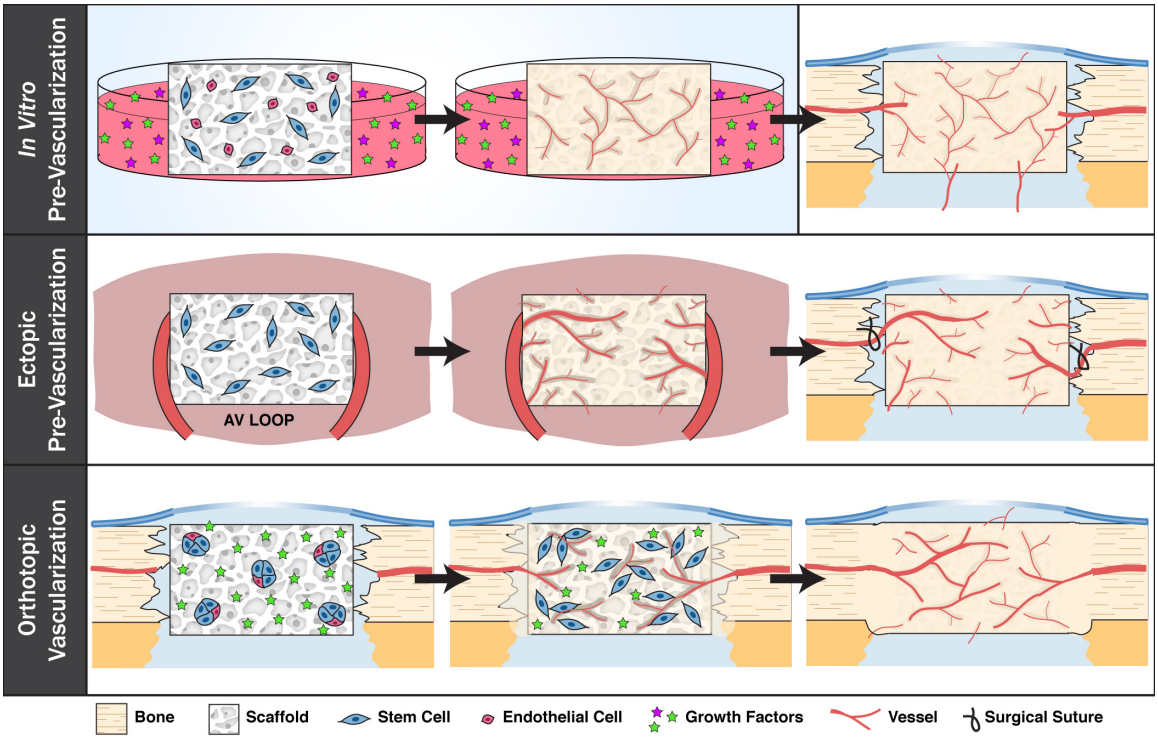

Figure 1.2. Vascularization approaches for bone tissue engineering. (TOP) *In vitro* pre-vascularization techniques induce cell-seeded scaffolds to form vasculature with exogenous growth factors. **(MIDDLE)** *In vivo* ectopic pre-vascularization involves implantation of a cell-seeded scaffold into a highly vascularized bed to allow angiogenic ingrowth before free flap transplantation with surgical anastomosis. **(BOTTOM)** *In vivo* orthotopic vascularization involves direct implantation of scaffolds into the bone defect for *in situ* tissue development. Scaffolds can be functionalized for the controlled release of growth factors (stars) that guide tissue regeneration.

1.4 Clinically Relevant Cell Sources

Numerous autologous stem / progenitor cell sources have been utilized in bone tissue engineering research (**Table 1.1**), often involving mesenchymal stem cells (MSCs) from bone marrow or adipose tissue because of their osteogenic potential. Adipose-derived stem cells (ASCs) are particularly attractive for clinical application because their multipotency, abundance, and ease of harvest via liposuction.

Table 1.1. Autologous stem / progenitor cell sources for engineering vascularized bone.

Cell Population	Advantages	Disadvantages
Minimally Processed Tissue Sources		
Bone Marrow (BM)	• Osteoinductive properties (e.g. bone chips in reamed / 'enhanced' BM) • Endothelial sub-population • Intraoperative use	• Limited tissue availability • Composition will vary amongst donors and isolation procedures
Adipose Stromal Vascular Fraction (SVF)	• Abundant tissue • Easily harvested via liposuction • High proportion of stem cells and endothelial cells • Intraoperative use	• Cell population varies amongst donors and isolation procedures • 2 – 3 hour multi-step isolation procedure
Isolated Adult Stem / Progenitor Cells		
Mesenchymal Stem Cells from BM (BM-MSC)	• Osteogenic potential • Studied extensively	• Very low yield from BM, requiring extensive *in vitro* expansion • Requires addition of endothelial cells to form vessels
Adipose-Derived Stem Cells (ASC)	• Osteogenic potential • High yield from adipose tissue • Vascular potential	• Loses vascular sub-populations after several passages
Endothelial Progenitor Cells (EPC)	• Autologous endothelial source • Non-invasively harvested from blood • Capable of maturation into functional vascular networks	• Very low yield, requiring extensive *in vitro* expansion • Not capable of forming bone
Pluripotent Stem Cells		
Induced Pluripotent Stem Cells (iPSC)	• Autologous pluripotent cells • Capable of differentiating into all cell types in bone	• Reprogramming efficiency very low, requiring extensive expansion • Safety concerns, limited clinical application

Adipose tissue is primarily composed of adipocytes and pre-adipocytes. The remaining population of cells is termed the stromal vascular fraction (SVF), which yields approximately

40 million cells per 100 milliliters of adipose tissue. SVF contains mesenchymal stem cells (ASCs, ~25-50%), endothelial cells (ECs, ~15-30%), pericytes (2-5%), and immune / hematopoietic lineage cells (~20-30%) [34-36]. After culturing and serial passaging SVF, the majority of the endothelial and hematopoietic lineage cells are lost, either because of non-adherence, slow proliferation, or death. This results in a seemingly pure population of ASCs by passage 2 or 3 [35].

Co-culture of stem cells with an EC source, such as endothelial progenitor cells or mature ECs, has demonstrated promise in promoting bone vascularization *in vitro* and *in vivo* [15, 37-39]. However, the separate harvest, purification, and expansion of additional cell types complicate these approaches. Yet, ASCs may not require co-culture, as they have been reported to give rise to both endothelial [40-42] and perivascular cells [43-47], each of which is essential to form mature, stabilized vessels [48, 49]. However, prior to these studies the ability of ASCs to form vascular networks was debated and poorly understood. Therefore, this thesis first explores the vascular properties of these cells, and then demonstrates that they can be utilized as a single, clinically relevant cell source to give rise to both osteogenic and vascular components of a complex tissue graft.

1.5 Specific Aims

The overall goal of this thesis was to elucidate the biochemical and biophysical cues that can induce ASCs to form robust vascularized bone. To accomplish this goal, initial studies determined if and how ASCs could form 3D vascular networks. After setting this groundwork, a protocol was developed to induce the co-development of both vasculature and bone within the same culture by mimicking aspects of the native bone healing

environment. Lastly, the effects of hypoxia on ASC vascularization were investigated to simulate the challenging hypoxic environment of a bone defect. These studies are summarized by three Specific Aims:

Aim 1. Induce functional assembly of vascular networks by ASCs (**Chapter 2**)

1.1. Understanding the vascular potential of ASCs

1.2. Spatial organization of cells

Aim 2. Develop an induction protocol to engineer robust vascularized bone by recapitulating factors in native bone repair (**Chapter 3-4**)

2.1. PDGF-BB

2.2. Inflammatory cytokines

Aim 3. Evaluate the effects of hypoxia on ASC viability and vascularization (**Chapter 5**)

3.1. *De novo* vascular assembly

3.2. Stability and growth of pre-formed vessels

Chapter 2

Vascular Morphogenesis: Major Role of a Minority Endothelial Sub-Population

2.1 Introduction and Background

Heterogeneity in adipose-derived stromal/stem cell (ASC) cultures can give rise to novel cellular interactions that may be useful for regeneration of complex tissues comprised of multiple cellular phenotypes. Yet, the importance of cell population heterogeneity is an under-explored concept in tissue engineering. ASCs hold great promise as an autologous cell source for regenerative medicine due to their abundance, ease of harvest via liposuction, and multipotency [50]. In addition to their well-studied potential towards the classic mesenchymal lineages (bone, cartilage, fat) [51], ASCs possess vascular properties and can give rise to both endothelial [40-42] and perivascular cells [43-47]. Each of these populations is essential to form stable vascular networks [48, 49]. Therefore, the potential to supply all tissue components from a single autologous cell source would be a powerful tool in engineering complex vascularized grafts.

Several studies have investigated the perivascular and endothelial potentials of ASCs. Intriguingly, it has been demonstrated that ASCs may be resident in perivascular sites in native adipose tissues [46, 47]. They also possess the ability to secrete pro-angiogenic factors and stabilize vascular networks [47, 52-54]. However, the potential of ASCs alone to yield

vascular networks is less clear. Approaches towards *in vitro* endothelial differentiation are typically growth factor-mediated [40, 41, 55], and involve Matrigel [40, 56], hypoxia [57], shear stress [58, 59], or spontaneous transformation [42, 60]. All of these studies have reported successfully increasing the overall endothelial phenotype in cultures, though the functional characteristics of these cells and the phenotypes of the non-endothelial cells remain unclear. There is also evidence that ASCs differentiate into endothelial cells *in vivo* and engraft into host vasculature [41, 42]. These studies have been counter-balanced by the assertion that ASCs inherently have limited endothelial potential due to epigenetic restrictions of endothelial gene promoters [61]. Each of these studies raises important questions regarding the robustness of the endothelial potential of ASCs and whether it is possible to simultaneously obtain endothelial and perivascular subpopulations within the same culture.

These questions may be answered by studying their phenotypic profiles. ASCs are isolated from adipose tissue by selecting for the plastic-adherent population of the stromal vascular fraction (SVF) [62, 63]. These cells have been extensively characterized by multiple laboratories who have reported on their phenotypes across multiple donors [35, 41, 59], passages [35, 64], extraction methods [41, 65], and clonal differentiation potentials [66]. While they do exhibit increasingly homogenous profiles with sustained *in vitro* cultivation, demonstrating greater than 90% positive expression of mesenchymal surface markers CD13, CD29, CD73, and CD90 by passage 3 [35, 64], ASCs are still widely considered a heterogeneous population. There also often exists a minority subpopulation that expresses endothelial cell-associated markers, such as CD31. This CD31+ population can range between 1 to 25% in early passage ASC cultures [35, 41, 42, 61], but diminishes substantially

with sustained *in vitro* cultivation. More interestingly, this inherent heterogeneity might even be intentionally utilized to induce formation of complex tissue structures in engineered grafts.

The current study aims to investigate the ability of ASCs to form stable vascular structures *in vitro*. By modulating the spatial organization of the cells in 2D culture (seeding density) and in 3D culture (multicellular aggregation), we demonstrated that multiple ASC subpopulations are able to closely interact and spontaneously self-assemble into three-dimensional vascular structures. This report explores this phenomenon and elucidates the cellular behaviors that are necessary to generate stable vascular networks with ASCs.

2.2 Materials and Methods

ASC Isolation and Culture

ASCs were isolated at the Stem Cell Biology Laboratory, Pennington Biomedical Research Center, under an Institutional Review Board approved protocol according to published methods [67]. Briefly, fresh human subcutaneous adipose lipoaspirates were obtained under informed consent from five healthy Caucasian female donors undergoing elective liposuction surgery with a mean age of 47.6 ± 1.9 years and mean body mass index of 27.1 ± 0.6. Fat depots included (number of donors denoted): thighs (3), abdomen (2), hips and flanks (2). The lipoaspirate tissue was extensively washed with warm phosphate buffer solution to remove erythrocytes and then digested in PBS supplemented with 0.1% Collagenase Type I (Worthington Biochemical Corp.), 1% BSA, and 2 mM $CaCl_2$ for one hour at 37 ºC. Following room temperature centrifugation at 300 g and resuspension in Stromal Medium (DMEM/Hams F-12 Medium supplemented with 10% FBS (Hyclone) and 1% antibiotic/antimycotic), the stromal vascular pellet obtained from 35 ml of lipoaspirate

digest was plated in a T175 flask (0.2 ml per cm^2). After 24 hrs of incubation at 37 ºC, 5% CO_2, the adherent cells were washed with warm PBS and maintained in Stromal Medium until 80-90% confluent. The adherent population ("passage 0") was harvested by digestion with trypsin (0.05%)/EDTA (1 mM) at 37 ºC for five minutes, washed with Stromal Medium and cryopreserved [68] for shipment to Johns Hopkins University. Prior studies have demonstrated no deleterious effects on ASCs due to cryopreservation, such as loss of viability or multipotency [68-70]. For expansion, ASCs were thawed and cultured in expansion medium: high glucose DMEM (GIBCO Invitrogen) with 10% fetal bovine serum (FBS; Atlanta Biologicals), 1% penicillin/streptomycin (GIBCO Invitrogen), and 1 ng/ml bFGF (PeproTech). Cells were used at passage three for monolayer experiments and passage two for 3D fibrin gel experiments. Observations were confirmed with four additional donors.

Flow Cytometry

ASCs were assessed for surface expression of mesenchymal (CD73, CD105) and vascular markers (CD34, VEGFR2, CD31, αSMA). Detached cells were suspended in PBS containing 2% FBS and incubated with monoclonal antibodies conjugated to fluorescein isothiocyanate or phycoerythrin for 30 min at 4ºC. Cells were analyzed with a flow cytometer (BD Accuri C6). All antibodies were purchased from BD Biosciences.

Monolayer Seeding Density

ASCs were seeded at 3000, 10000, or 20000 cells per cm^2 and cultured for 14 days in endothelial induction medium (EIM). The composition of EIM was optimized in preliminary experiments for monolayer experiments and consisted of: Endothelial Basal

Medium-2 (EBM2; Lonza) supplemented with 2% FBS, 1% penicillin/streptomycin, 2 ng/ml $VEGF_{165}$ (PeproTech), 10 ng/ml bFGF, and 1 μg/ml L-ascorbic acid-2-phosphate (Sigma). Endothelial phenotype was assessed via quantitative RT-PCR and immunocytochemistry. The DNA content was assessed at various time points to evaluate growth patterns and final cell densities within the cultures.

Vascular Morphogenesis in Monolayer

ASCs were seeded at 20000 cells per cm^2 and cultured for up to 14 days in EIM. Cells were assayed extensively over several timepoints (0, 3, 7, 10, 14 days) and passages (2 through 4) via immunocytochemistry for endothelial and perivascular markers. Day 0 samples were taken 4 hours after seeding. Quantitative RT-PCR was also conducted on passage 3 cells after 1, 7, and 14 days.

BrdU Incorporation

To identify proliferating cells in the culture, 10 μM bromodeoxyuridine (BrdU; Sigma) was added to culture medium for 24 hours. This was followed by washing and fixation with 3.7% formaldehyde for 20 min. Samples were first immunostained for CD31 and αSMA in order to identify the subpopulations, followed by 10 min post-fixation to preserve the signal. DNA was denatured by incubating cells with 4N HCl plus 0.5% triton X-100 in PBS for 15 min at room temperature. Following extensive washes, samples were incubated with mouse anti-BrdU conjugated to Alexa Fluor 647 (1:50; Invitrogen) overnight at 4ºC. Nuclei were then counterstained with DAPI (4',6-diamino-2-phenylindole) and samples were mounted for analysis.

PDGFR Inhibition

The effects of platelet-derived growth factor-B (PDGF-B) signaling on the vascular morphogenesis in our system were assessed by blocking its receptor. ASCs were seeded at 20000 cells per cm^2 and cultured for 14 days in EIM supplemented either with vehicle only (dimethyl sulfoxide) or 50 μM tyrphostin AG1295 (Santa Cruz Biotechnology), a selective inhibitor of PDGF receptor (PDGFR) tyrosine kinase activity. Morphological effects were evaluated via immunocytochemistry.

DNA Content

In order to evaluate proliferation, cells were grown in 24-well plates for 0, 3, 7, 10, or 14 days and lysed with 250 μl of digestion buffer (10 mM Tris, 1 mM EDTA, 0.1% Triton X-100, and 0.1 mg/mL proteinase K). Samples were incubated at 50 ºC overnight and DNA content was assessed using a PicoGreen dsDNA quantitation kit (Molecular Probes). Briefly, PicoGreen dye was added to samples in duplicate in black 96-well plates (50 μl sample, 50 μl 1X Tris-EDTA buffer, 100 μl PicoGreen diluted 1:200) and read with a fluorescent plate reader (excitation 485 nm, emission 530 nm). DNA content was determined using a λDNA standard curve and compared against known cell numbers from day 0 samples to determine cell number.

Quantitative RT-PCR

Cells were grown in 12-well plates (n = 4 per group) for up to 14 days. Total RNA was isolated using a TRIzol (Invitrogen) extraction method and quantified using a NanoDrop

spectrophotometer (Thermo Scientific). Reverse transcription was performed with 1 μg of total RNA using iScript cDNA Synthesis Kit (BioRAD). Complementary DNA was amplified using SYBR Green PCR Master Mix (Applied Biosystems) and a StepOnePlus Real-Time PCR System (Applied Biosystems). The primer sequences used for PCR analysis are listed in **Table 2.1**. Expression levels were calculated by the comparative C_T method using GAPDH (seeding density study) as an endogenous reference gene.

Table 2.1. Quantitative RT-PCR Primer Sequences

Gene	Primer Sequence (5' – 3')	
αSMA	Forward	CGGACCTTTGGCTTGGCTT
	Reverse	TGGGGTGCGGACAGGAATT
β-Actin	Forward	AGTTGCGTTACACCCTTTCTTG
	Reverse	TCACCTTCACCGTTCCAGTTT
CD31 (PECAM-1)	Forward	TCAGCAGCATCGTGGTCAAC
	Reverse	TGGAGCAGGACAGGTTCAGT
GAPDH	Forward	CACCCACTCCTCCACCTTTGA
	Reverse	TCCACCACCCTGTTGCTGTAG
VE-Cadherin	Forward	ATGGACCCTGATGCGGCTA
	Reverse	TGTGACTCGGAAGAACTGGC
VEGF-A	Forward	GCCTTGCCTTGCTGCTCTA
	Reverse	GATTCTGCCCTCCTCCTTCTG
VEGFR-2 (KDR)	Forward	AGTCTGTGGCATCTGAAGGC
	Reverse	ACGGTGGTGTCTGTGTCATC
vWF	Forward	GGGCTGTGTGGCAACTTTAAC
	Reverse	ATAAGGGTCCGAGGTCAAGGT

Immunocytochemistry

Cells were fixed with 3.7% formaldehyde for 20 min, permeabilized with 0.2% triton X-100 for 10 min, and then blocked with 10% normal donkey serum (Sigma) for 30 min. Briefly, samples were then incubated with antigen-specific primary antibodies overnight at 4ºC, followed by secondary antibodies for 1 hour at room temperature. When using multiple primary antibodies from the same species (i.e. mouse), antigens were stained sequentially with slight modification of the first bound primary antibody: mouse IgG were masked with

goat anti-mouse IgG monovalent Fab fragments (20 μg/ml) for 2 hours at room temperature, and then detected with Cy3-conjugated donkey anti-goat IgG. Antibody complexes were lightly fixed with 1.85% formaldehyde for 10 min, and cells were blocked with 10% normal goat serum (Sigma) for 30 min. Samples were then co-stained for the remaining antigens following standard protocol using species-specific secondary antibodies (DyLight 488- or 649-conjugated goat anti-mouse or anti-rabbit IgG, respectively). Coverslips were mounted in ProLong Gold Antifade Reagent (Invitrogen) containing DAPI, and imaged using a Zeiss Axio Observer inverted fluorescence microscope and a Zeiss LSM 510 confocal microscope with 63x/1.4 oil objective. Primary antibodies were purchased from Santa Cruz Biotechnology [mouse anti-CD31 (1:50), mouse anti-vascular endothelial-cadherin (VE-Cad; 1:50), rabbit anti-desmin (1:50), mouse anti-collagen IV (1:100)], Sigma [rabbit anti-von Willebrand factor (vWF; 1:200), rabbit anti-laminin (1:100)], and Invitrogen [mouse anti-alpha smooth muscle actin (αSMA; 1:50)]. All secondary antibodies were purchased from Jackson Immunoresearch and used at a 1:200 dilution.

Image Analysis (Immunocytochemistry)

Morphological measurements of immunostaining were performed using Image J software (NIH). At least eight vessels per group were used for quantification of vessel length and width. Length was measured along the entire structure from tip to tip. For branched vessels, segment lengths were summed. The width of each vessel was averaged among discrete measurements (spaced ~25 μm apart) along the entire length of the vessel. The area covered by αSMA+ cells was averaged from 5 random view fields per sample, and across

three samples per group. Images were thresholded to measure percent positive area. All groups were normalized to "day 0" values.

Spheroid Formation via Hanging Drop

Cells were trypsinized and resuspended in culture medium containing 0.24% (w/v) methylcellulose (Sigma). Cell concentrations were varied (0.1, 0.4, or 1 x 10^6 cells/mL) to control the total cell number per spheroid. Cell suspensions were pipetted as 10 μl drops onto inverted Petri dish caps, which were then reverted and placed on dish bottoms containing sterile water to reduce evaporation. Dishes were incubated at 37 ºC overnight to allow cellular aggregation at the air-liquid interface. The dish caps were then flooded with PBS to allow bulk collection and transfer of the spheroids to conical tubes.

Vascular Morphogenesis in 3D Fibrin Gels

To study the effects of cellular aggregation on three-dimensional vascular assembly, cells were encapsulated either monodispersed (single-cell suspension) or aggregated into multicellular spheroids (1000, 4000, or 10000 cells each). Cells were resuspended at 4571 cells/μl in fibrinogen (8 mg/ml final; Sigma), followed by the addition of thrombin (2 U/ml final; Sigma) to initiate gelation. Fibrin gels (35 μl) were pipetted into 6-mm diameter wells and incubated at 37 ºC for 30 minutes to allow complete gelation prior to the addition of culture medium. Samples were cultured for two weeks in vascular medium: Endothelial Basal Medium-2 (Lonza), 6% FBS, 1% penicillin/streptomycin, 10 ng/ml $VEGF_{165}$, 1 ng/ml FGF-2, and 1 μg/ml L-ascorbic acid-2-phosphate (Sigma).

Whole-Mount Immunostaining

All incubation and washing steps were carried out at 4 ºC with gentle agitation. Samples were fixed with 3.7% formaldehyde for 3 hrs, and then washed with PBS three times for 30

min each. Fixed gels were carefully removed from their wells and transferred to microcentrifuge tubes for subsequent staining procedures. Gels were permeabilized and blocked for 4 hrs with 0.2% triton X-100 and 5% normal goat serum (Sigma) in PBS with 0.1% Tween (PTw). Samples were then incubated overnight with primary antibodies diluted in blocking solution: mouse anti-CD31 (4 μg/ml; Santa Cruz Biotechnology) and rabbit anti-laminin (7 μg/ml; Sigma). After three 1-hr washes in PTw, samples were incubated overnight with DyLight 488-conjugated goat anti-mouse and DyLight 649-conjugated goat anti-rabbit (both 1:400; Jackson ImmunoResearch) diluted in blocking solution, followed by three 1-hr washes in PTw. Lastly, samples were blocked in 5% normal mouse serum for 4 hrs, incubated overnight with Cy3-conjugated mouse anti-αSMA (7 μg/ml; Sigma), and then washed three times for 1 hr each. Gels were mounted in 70% glycerol in chamber slides and imaged using a Zeiss LSM 510 confocal microscope with a 5x objective.

Image Analysis (Whole-Mount Immunostaining)

Confocal z-stacks of immunostained gels were z-projected and thresholded for subsequent quantification of vessel network parameters (n = 6 images per group). Thresholded images were analyzed with AngioQuant software[71] to quantify total vessel length, area, and interconnectivity. ImageJ software (NIH) was used to quantify pericyte coverage of vessels, which was defined as αSMA+ area within at least 5 μm of the abluminal face of vessel networks. Briefly, vessel networks were selected in the CD31 channel of thresholded image composites, and selections were enlarged by 5 μm at all edges. These enlarged selections were applied to the αSMA channel, and percent αSMA+ area within the selection was quantified (denoted as "% vessel pericyte coverage"). To quantify the amount

of basement membrane protein deposited along the vessels, the enlarged vessel selection was applied to the non-thresholded laminin channel, and the mean pixel intensity within the selection area was quantified (denoted as "laminin mean intensity").

Statistical Analysis

Quantitative data are expressed as mean ± standard error. Unpaired t-test was used for two-group comparisons. One-way ANOVA was used for multi-group comparisons, with Tukey's post-hoc analysis. Significance levels denoted as *P < 0.05, **P < 0.01, ***P < 0.001.

2.3 Results

Cell Characterization

The majority of ASCs were positive for mesenchymal markers, with a small minority (<1%) expressing vascular markers at passage 2 and 3 (**Table 2.2**).

Table 2.2. Flow cytometric analysis of human ASCs.

Surface Marker	Passage 2	Passage 3
Vascular Markers		
CD31	0.8%	0.1%
CD34	5.2%	1.2%
VEGFR2	0.3%	0.1%
αSMA	1.1%	0.6%
Mesenchymal Markers		
CD73	98.4%	99.4%
CD105	80.1%	88.3%

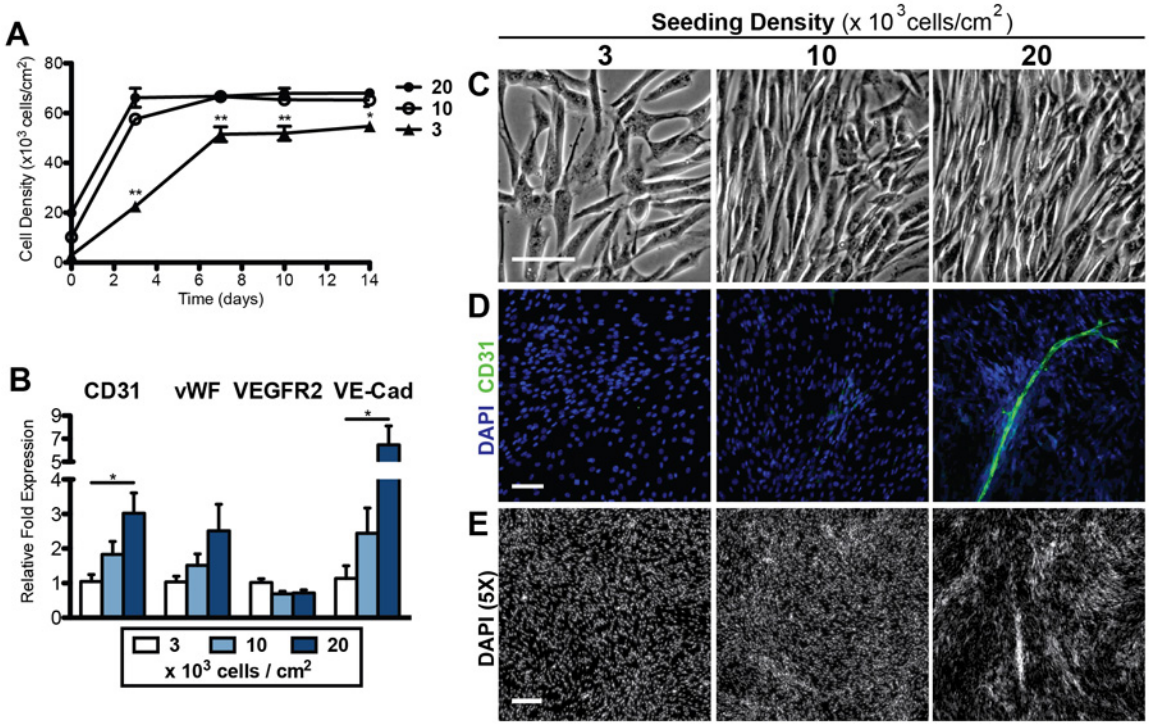

Figure 2.1. Effects of cell seeding density on the endothelial phenotype of ASCs. (**A**) DNA content revealed that ASCs seeded at the two higher densities reached a final density of 65,000 cells/cm² within three days, while those seeded at 3,000 cells/cm² took longer to reach a final density that was still significantly less. (**B**) mRNA expression of endothelial markers increased with increasing seeding density by day 14. (**C**) Morphologically, ASCs seeded at higher densities were more densely packed and aligned. (**D**) Only ASCs seeded at 20,000 cells/cm² gave rise to CD31+ vessels. (**E**) Cells remained uniformly distributed when seeded at 3,000 and 10,000 cells/cm², while those seeded at 20,000 cells/cm² aggregated into dense clusters by day 14. Significance indicated as $*P < 0.05$. Scale bars = 100 μm (C-D) and 250 μm (E).

Cell Seeding Density in Monolayer

Passage 3 ASCs were cultured at 3000, 10000, and 20000 cells/cm^2 for 14 days in EIM. ASCs seeded at the two higher densities attained a final density of approximately 65,000 cells/cm^2 as determined by DNA content by day 3 (20000 per cm^2) or day 7 (10000 per cm^2), at which they stayed for the remainder of the differentiation period. Cells seeded at 3000 cells/cm^2 grew to 50000 cells/cm^2 by day 7 and remained constant thereafter, never attaining the density of the other two groups (**Fig. 2.1A**). At higher seeding densities there was increased mRNA expression of CD31, vWF, and VE-cadherin by day 14. VEGF receptor-2

(VEGFR-2) expression was not significantly affected by seeding density (**Fig. 2.1B**). After 14 days, cells seeded at 10000 to 20000 cells/cm^2 became densely packed with cells aligning locally with neighboring cells, while those seeded at 3000 cells/cm^2 remained sub-confluent with random cell orientation (**Fig. 2.1C**). Positive staining for CD31 was only observed when cells were seeded at 20000 cells/cm^2, with specific staining of vessel-like structures enveloped within dense cell clusters (**Fig. 2.1D**). Low magnification images of DAPI stains confirmed that the non-uniform aggregation occurred only in the 20000 cells/cm^2 group, while those seeded at 3000 or 10000 cells/cm^2 were uniformly distributed (**Fig. 2.1E**). In all subsequent experiments, cells were seeded at 20000 cells/cm^2.

Vascular Phenotypes and Morphology

Vascular structures stained positively for three endothelial markers: CD31 located at cell junctions and filopodia, VE-cadherin located at cell junctions, and vWF with a granular pattern in the cytoplasm (**Fig. 2.2A**). Many of the cells surrounding the vessels were positive for pericyte markers (αSMA and desmin) (**Fig. 2.2B**). Vascular basement membrane proteins, collagen IV and laminin, were also present along vessel tracks (**Fig. 2.2C**). The pan-laminin antibody, which is reactive against all laminin isoforms, also faintly stained other cellular regions beyond the vessels.

Optical slices from 63x confocal z-stacks revealed the relative locations of the cells comprising the vascular structures (**Fig. 2.2D-F**). Many of the αSMA+ cells were stretched out against the glass (**Fig. 2.2D**), blanketing the area beneath the endothelial vessels. Some of the αSMA+ cells were also visible along the sides or on top of vessels, assuming classic pericyte morphology (**Fig. 2.2E**). Additional CD31-/αSMA-cells were located on top of the

vessels (**Fig. 2.2F**), indicating that the vessels were fully encased within a three-dimensional cellular microenvironment. Many vessels contained large voids that appeared to be patent lumens (**Fig. 2.2G**) as shown in a cross-sectional view of one representative vessel, which measured an internal width of 9.7 μm and height of 5.4 μm, similar in size to a capillary (**Fig. 2.2H**). Vessel tips were dense with filopodia (**Fig. 2.2I**).

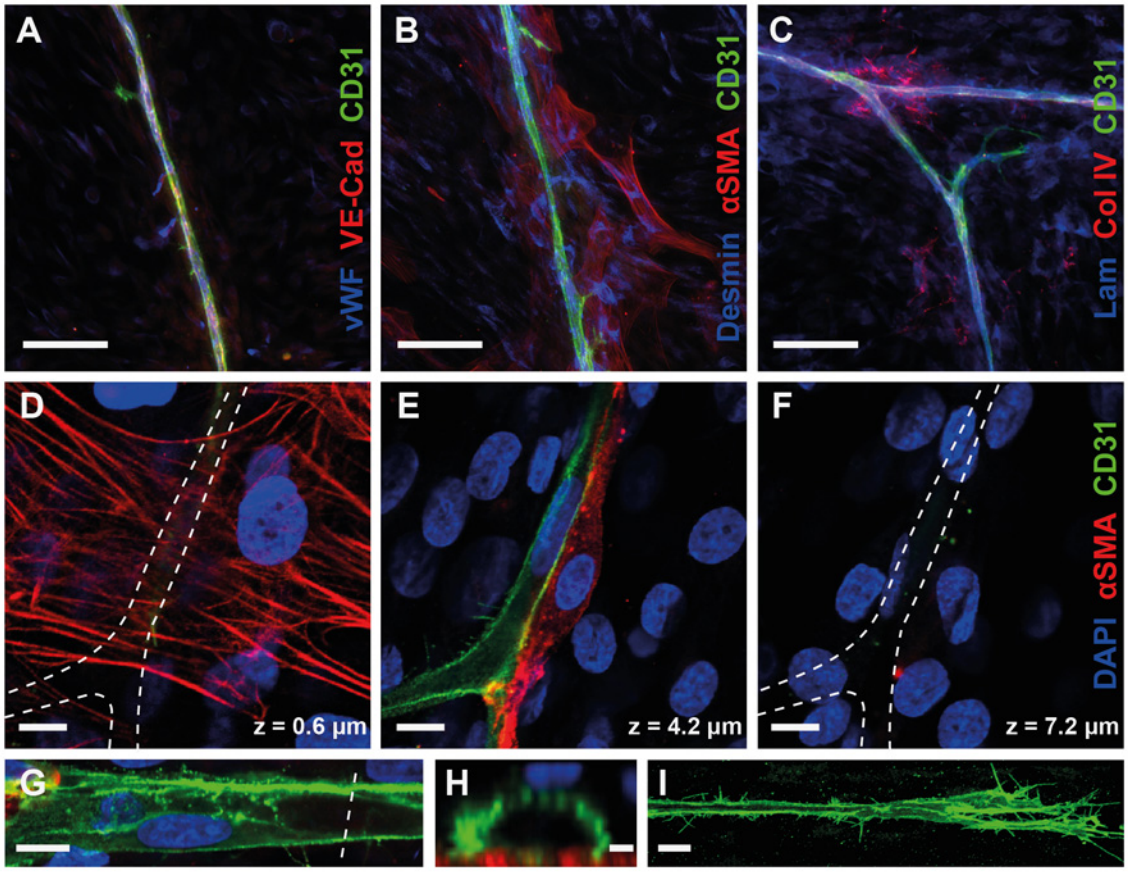

Figure 2.2. Vascular phenotypes and morphology. (**A**) Vessels stained positively for CD31, VE-cadherin, and vWF (endothelial markers). (**B**) Cells clustered around the vessels were positive for αSMA and desmin (pericyte markers). (**C**) Vascular basement membrane proteins, collagen IV and laminin, were found along vessel tracks. (**D-F**) Optical slices from a confocal z-stack: (**D**) αSMA+ cells (red) stretched out against the glass beneath the vessels. (**E**) CD31+ vessels (green) propagated on top of this layer of cells, with some αSMA+ cells invested alongside. (**F**) Additional αSMA-/CD31- cells were located on top of the vessels (indicated by DAPI, blue), fully enveloping the vessel in a three-dimensional cellular environment. (**G**) Some vessels contained voids resembling patent lumens, demonstrated by the cross-section (dotted line) shown in (**E**). (**F**) Vessel tips were dense with filopodia. Scale bars = 100 μm (A-C), 10 μm (D-G,I), and 2 μm (H).

Time Course of Morphogenesis

Four hours after seeding ("day 0"), the culture contained small numbers of αSMA+ cells (0.5%) and CD31+ cells (0.02%) (**Fig. 2.4A**), which similarly reflected the flow cytometry analysis. All CD31+ cells were in direct contact with another cell after attachment (**Fig. 2.3**). During the first week, individual CD31+ cells began to elongate into multicellular vessels, while the spatially independent αSMA+ cells increased in number and appeared to migrate towards the vessels (**Fig. 2.4A**). In the second week, αSMA+ cells co-localized with the vessels and continued to increase in number. DAPI stains revealed that cells began forming dense clusters around the vessels very early on, even before contact with αSMA+ cells (**Fig. 2.4B**). From an orthogonal view, the initially flat vessel (Day 3) increased in height over time, while additional cells in the surrounding monolayer migrated on top of one another to form a multilayered cluster of cells (**Fig. 2.4C**). Quantification of vessel morphology revealed a steady temporal increase in vessel length (up to 1.2 mm at day 14) and pericyte coverage, while vessel width remained fairly constant (~12 μm) (**Fig 2.4D**). Expression of endothelial genes (CD31, VE-cadherin, VEGFR-2) and pericyte genes (αSMA) increased significantly over time (**Fig 2.4E**).

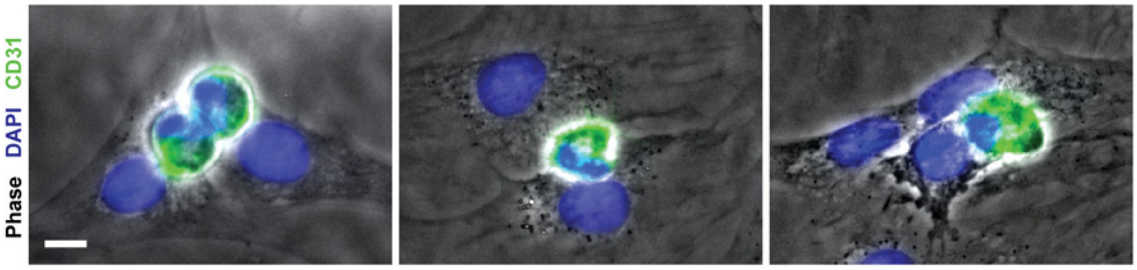

Figure 2.3. Attachment of CD31+ cells. Four hours post-seeding, all CD31+ cells were directly contacting other cells, facilitated by the high seeding density. Scale bar = 10 μm.

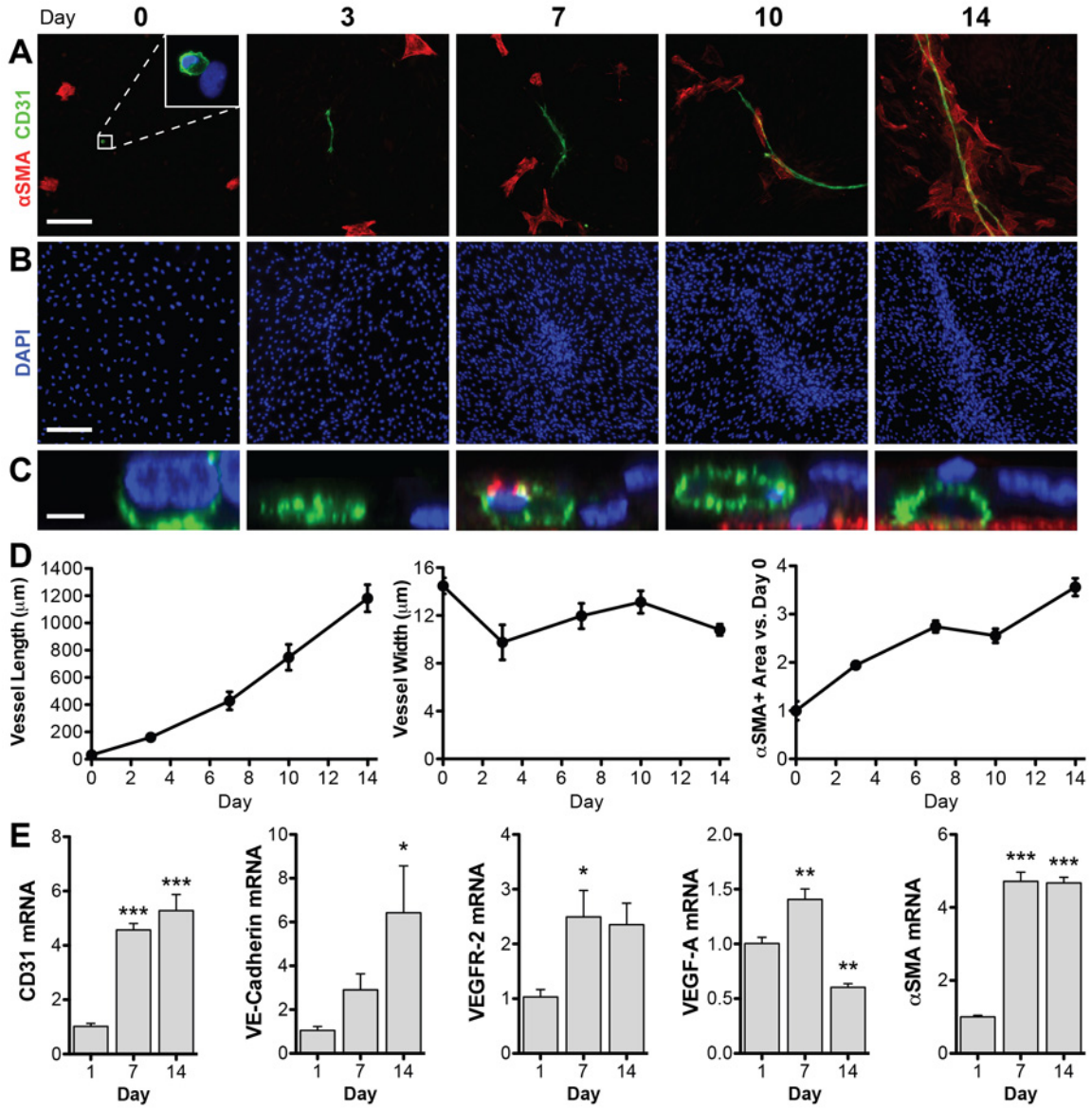

Figure 2.4. Time course of vascular morphogenesis. (**A**) Four hours post-seeding ("day 0"), the culture contained small numbers of αSMA+ cells (0.5%; red) and CD31+ cells (0.02%; green; inset magnified). CD31+ cells elongated into vessels over time. αSMA+ cell density increased over time as they migrated towards the vessels. (**B**) DAPI staining (blue) of the same view fields illustrate dense cell clustering around the vessel. (**C**) Cross-sectional views of the vessels depict lumen formation, accompanied by cell migration on top of the vessel. Scale bars = 200 μm (**A-B**) and 5 μm (**C**). (**D**) Quantification of vessel morphology and pericyte area throughout the culture. (**E**) Gene expression of vascular markers. Significance indicated as $*P < 0.05$, $**P < 0.01$, or $***P < 0.001$ vs. day 1.

Proliferation & Pericyte Recruitment

BrdU incorporation revealed that the primary mode of vessel growth was proliferation (**Fig. 2.5A**), with most CD31+ cell nuclei staining positively for BrdU at days 3, 7, 10, and 14 (single timepoint shown). αSMA+ cells distant from the vessel were most often BrdU+, whereas those in direct contact were not (**Fig. 2.5B**).

Inhibition of PDGFR with significantly reduced αSMA+ cell vessel coverage (**Fig. 2.5C**) and their overall presence in the culture (**Fig. 2.5D**). Vessel length was not significantly affected by AG1295 (**Fig. 2.5E**); however, the vessels were significantly thinner (**Fig. 2.5F**).

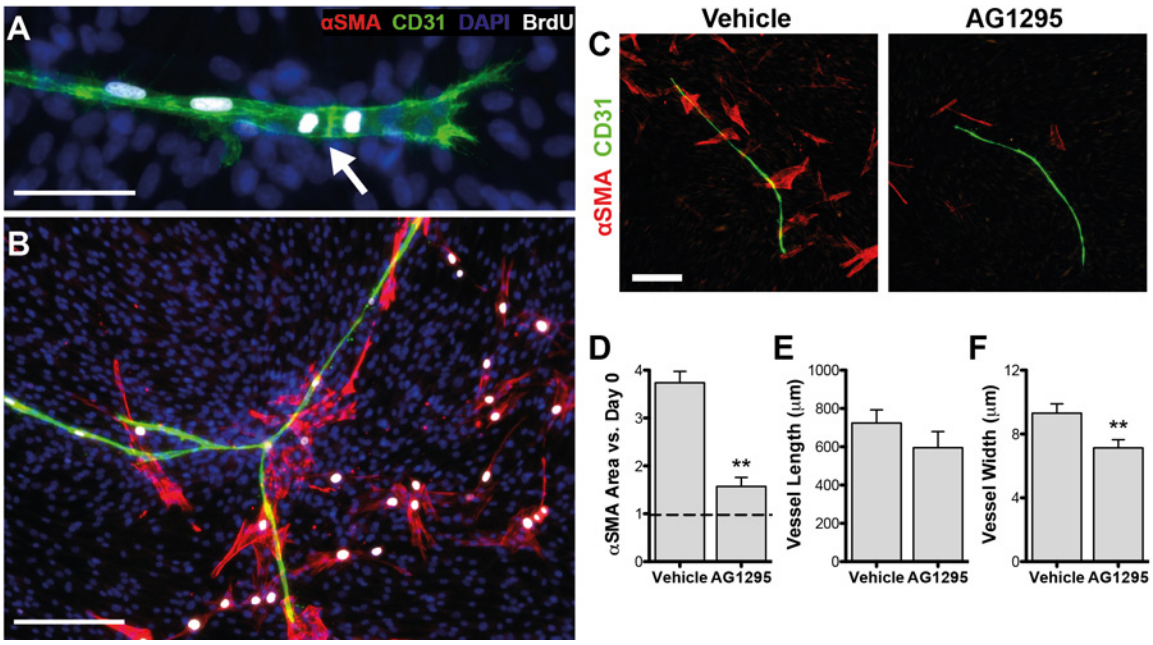

Figure 2.5. Proliferation and pericyte recruitment. ASCs were incubated with BrdU at multiple stages of vascular formation. (**A**) BrdU+ vessels (shown at day 7). Arrow indicates a dividing tip cell. (**B**) BrdU+ pericytes (shown at day 14). (**C**,**D**) Inhibition of PDGFR with AG1295 significantly reduced pericyte coverage. (**E**) Vessel length was not affected by AG1295, but (**F**) vessels were thinner. Scale bars = 50 μm (**A**) and 200 μm (**B**,**C**). Significance indicated as $^{**}P < 0.01$ vs. vehicle.

Serial Passaging

ASCs from passage 2 through 4 were grown to assess the effects of serial passaging on vascular assembly. On the day of seeding, the initial density of CD31+ cells decreased with

increasing passage number (**Fig. 2.6A**), which corroborates the flow cytometry data (**Table 2.2**). This trend correlated with the degree of vascular growth by day 14, which was substantially greater at passage 2 and non-existent at passage 4 (**Fig. 2.6B**). Cells were used at passage 2 for all subsequent studies.

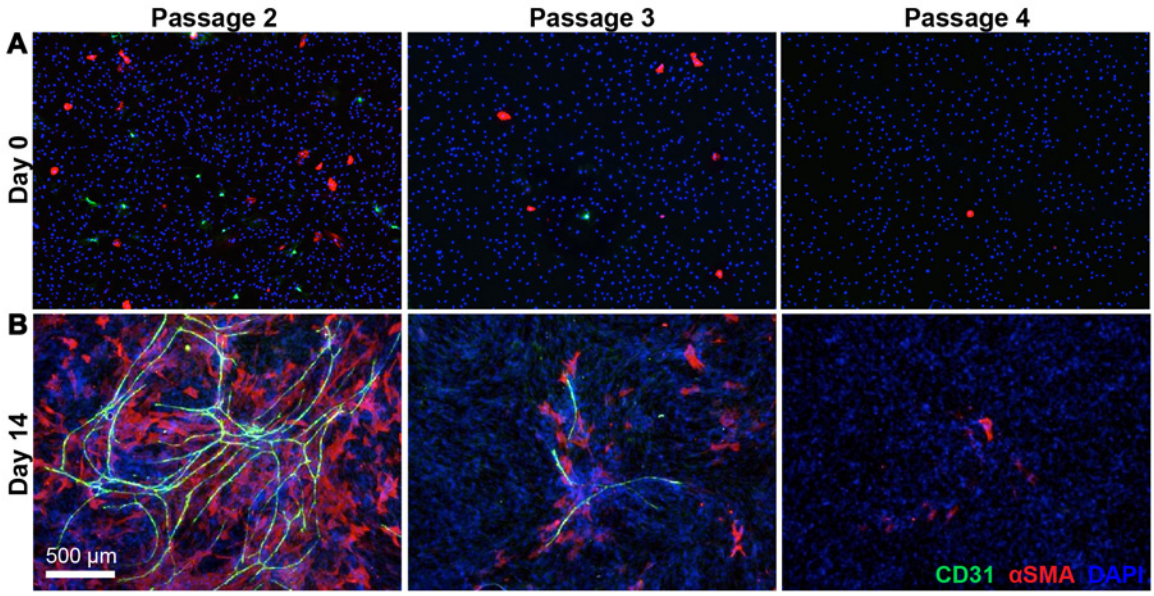

Figure 2.6. Effects of serial passaging on the endothelial sub-population. (**A**) Vascular subpopulations four hours post-seeding. (**B**) Vessels after 14 days of culture.

Cellular Aggregation in 3D Fibrin Gel

To study the effects of cellular aggregation on vascular morphogenesis of ASCs in 3D fibrin gel, passage 2 cells were encapsulated either as a monodispersed cell suspension or spheroids containing various cell numbers (1000, 4000, or 10,000 cells per spheroid), with total cell number held constant (**Fig. 2.7A**). After 14 days of culture in VM, spheroid aggregates yielded significantly larger (up to 2.1-fold) and more interconnected (up to 5.5-fold) vessel networks than monodispersed cells (**Fig. 2.7B-D**). Vessel coverage with pericytes and laminin also increased with increased initial aggregation, up to 4000 cells per

spheroid (**Fig. 2.7E-F**). With the largest spheroid size (10000 cells per spheroid), the spatial distribution of the networks was less uniform.

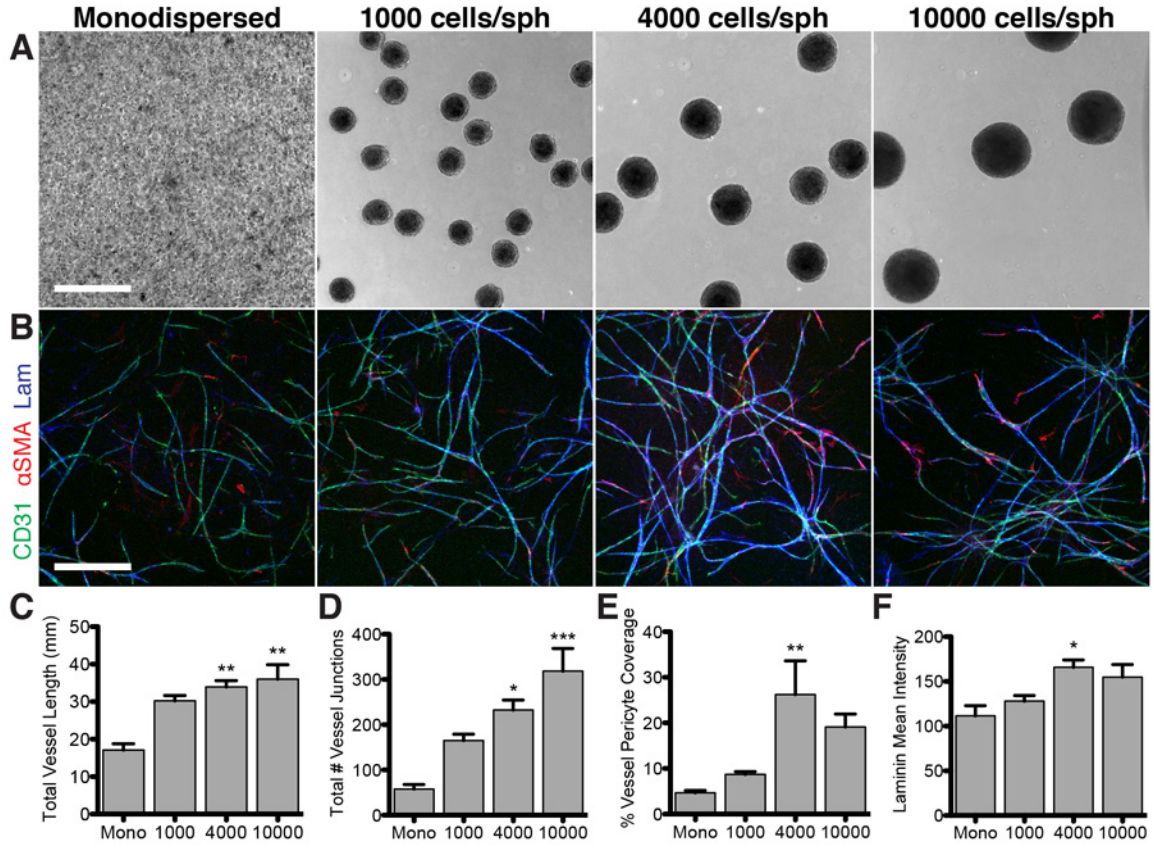

Figure 2.7. Effects of cellular aggregation on 3D vascular morphogenesis. (**A**) ASCs were encapsulated in fibrin gel as monodispersed cells or as spheroid aggregates ("sph") of different sizes. (**B**) Vascular networks developed after 14 days of culture in vascular medium, staining positively for CD31 (green), αSMA (red), and laminin (blue). Compared to monodispersed cultures vascular networks derived from spheroids were longer (**C**), more interconnected (**D**), and displayed greater coverage by pericytes (**E**) and laminin (**F**). Scale bars = 500 μm. Significance indicated as $*P < 0.05$, $**P < 0.01$, or $***P < 0.001$ versus monodispersed.

2.4 Discussion

The vascular potential of ASCs makes them a viable and unique cell source for clinical therapeutics. This study demonstrates that ASCs are capable of spontaneously self-assembling to form three-dimensional vascular networks that contain hollow lumens and are invested with pericytes. This phenomenon requires extensive proliferation of a minority

endothelial sub-population and coordinated heterotypic interactions amongst cells. The monolayer experiments illustrate these complex cellular behaviors and informed the cellular aggregation approach for the 3D fibrin gel experiment, which will be essential for subsequent tissue engineering studies.

In the monolayer experiments, vascular growth only occurred when ASCs were seeded at a high density (20000 cells per cm^2), which allowed for direct contact of CD31+ cells with other cells immediately after plating. While cells seeded at 10000 cells per cm^2 eventually proliferated to the same final cell density as those at 20000 cells per cm^2 and presumably contained half the number of CD31+ cells at the start of the culture period, they did not exhibit CD31+ staining or vessel formation. This suggests that these early cellular interactions may be crucial to vascular assembly.

Intriguingly, the various subpopulations of ASCs appeared to recapitulate some aspects of classic vasculogenesis. During development, endothelial progenitors are induced by FGF-2 and VEGF to elongate and proliferate into nascent vessels. The growing vessels secrete PDGF-B to recruit pericytes (PDGFR-β+) who migrate towards and wrap around the vessels for stability and support [72-74]. In our system, CD31+ cells elongated and proliferated to form vessel-like structures, while the proliferating αSMA+ cells were initially spatially independent. As the vascular structures continued to elongate, both αSMA+ and CD31-/αSMA- cells appeared to migrate towards the vessel, forming dense clusters of cells around the vessel stalks. These cells fully enveloped the vessel, such that the endothelial cells within experienced a three-dimensional microenvironment. This perivascular cell recruitment was blocked with the inclusion of a selective PDGFR inhibitor in the culture medium, resulting in thinner vessels and a substantial reduction of αSMA+ cell vessel coverage.

Vessel tracks were lined with vascular basement membrane proteins, collagen IV and laminin, and the vessels themselves exhibited classic morphology, with a patent lumen, thin multicellular endothelial wall, and cells at sprouting tips containing numerous filopodia.

The serial passaging experiment revealed a significantly smaller percentage of CD31+ cells in the population, which were completely gone by passage 4. This correlated with a similar reduction in vascular density after culture. These findings indicate that this endothelial subpopulation, which likely originated from the adipose microvasculature, is lost with passaging and may be the most robust at earlier passages. Clinically, reducing the extent of cellular manipulation and *ex vivo* expansion is preferable for numerous reasons (preserving cellular potency, safety, cost, time, etc.); therefore in the case of ASCs, the loss of vascular potential is another motivating factor to use the cells at low passage or fresh SVF.

An interesting observation from the monolayer experiments was that the cells spontaneously self-assembled into dense clusters of cells during vascular growth, suggesting that heterotypic cell-cell interactions were important to the process. Moving into a 3D fibrin gel system, we tested the hypothesis that facilitating cellular interactions through forced aggregation would promote more robust vascular assembly. We demonstrated that indeed, aggregating ASCs into spheroids prior to fibrin encapsulation significantly enhanced their vascular network density and interconnectivity, pericyte coverage, and deposition of vascular basement membrane. This novel finding complements previous work demonstrating that aggregation of pure endothelial cells into spheroids or on the surface of microbeads reduces apoptosis and greatly enhances vascular sprouting [75, 76]. ASCs specifically have been shown to reside in perivascular sites in native adipose tissues [46, 47] and stabilize vascular

networks *in vitro* [47, 53]. Therefore, aggregation may also serve to bring the pericyte-like cells closer to the endothelial sub-population to help support and stabilize them.

This spontaneous organization of endothelial and pericyte-like populations from ASCs has significant implications for their therapeutic applications. Multiple tissue engineering therapies have focused on generating capillary networks to vascularize grafts. However, the key to facilitating long-term, stable vascular regeneration may lie in the ability to recruit perivascular cells to endothelial networks to provide support and vasoresponsive properties [77]. In skeletal muscle vascular remodeling, vessel expansion beyond capillary diameter is accompanied by investment by αSMA+ cells [78]. Interaction between endothelial cells and pericytes elicits the deposition of supportive vascular basement membrane [79, 80], and ultimately leads to stabilization, junctional integrity, and maturation [72, 80, 81]. Pericytes can also promote survival and resistance to vascular regression [82-84]. The unique properties of ASCs allow them to perform both roles concurrently.

While donor-to-donor variability is a valid concern with ASCs, we have also demonstrated the ability of numerous additional donors to give rise to similar vascular structures in monolayer and fibrin gels. Given that cellular heterogeneity was a key component of these findings, it will be important to understand how these findings differ depending on a wider variety of donor demographics and harvest techniques. There may also be implications for methods used to culture and expand ASCs: is the trend towards homogeneity with continued passaging beneficial? Ultimately, it may affect clinical application as the ability to harvest all of the necessary cells from a single procedure could potentially reduce cost and recovery time for the patient. Nevertheless, additional studies are required to address these considerations.

2.5 Conclusions

In summary, we have demonstrated that minority sub-populations of vascular cells persist in early passage ASCs and are capable of extensive proliferation and spontaneous self-assembly to form pericyte-stabilized vascular networks. Close cellular contact and endogenous biological signaling are crucial to encouraging this self-assembly process. Further studies are required to determine whether vascular morphogenesis can occur in the culture without negatively impacting the differentiation potential of the remaining non-vascular cells in the culture. However, these studies set an important foundation upon which to vascularize a tissue graft with ASCs.

Chapter 3

Vascularized Bone Model, Part I: Platelet-Derived Growth Factor

3.1 Introduction and Background

Tissue engineering approaches to generate vascularized bone grafts could potentially revolutionize treatment of massive bone loss due to traumatic injuries, cancer, and congenital defects. Vasculature is essential to the long-term functional outcomes of a large bone graft to ensure sufficient nutrient delivery and post-implantation viability. While vasculature plays a necessary and intimate role in bone development, inducing the formation of vascularized bone tissues *in vitro* remains a challenge because the factors that promote each lineage may be detrimental to the other [18, 19, 85]. This incompatibility has led researchers to develop various methods to encourage vasculature to form concurrently or in a sequential manner with osteogenic differentiation, including: precise dosing regimens of induction factors [17, 21, 26], various cocktail media [86, 87], and pre-treating multiple cell types separately followed by recombination in a unified graft [17, 24-26, 88]. Yet each of these approaches relies on mitigating competing factors, resulting in an imbalance with sub-optimal results for one or both of the tissue components. Therefore, there is still an unmet need for a clinically translatable approach to induce robust formation of both vasculature and bone within a unified graft and using a single autologous cell source.

Adipose-derived stromal/stem cells (ASCs) are a promising, clinically relevant cell source to supply both the osteogenic and vascular components of a vascularized bone graft. Our prior studies showed that vascular assembly of ASCs is dependent on heterotypic cell-cell interactions, specifically through dense clustering of cells and endogenous platelet-derived growth factor (PDGF) signaling. This endogenous behavior is reminiscent of what occurs in native tissues, as proliferating endothelial cells in nascent vessels secrete PDGF-BB to recruit pericytes for vascular maturation and stabilization [72, 81]. PDGF-BB is also a major factor secreted by activated platelets to initiate repair mechanisms in wounded tissues such as bone [89-91] (**Fig. 1.1A**). A number of studies have demonstrated that *in vivo* administration of exogenous PDGF-BB significantly enhances bone formation [92-94]. Yet, *in vitro* studies with MSCs have reported that while exogenous PDGF-BB induces greater proliferation, it has no effect on [95-97], or may even be inhibitory to [98, 99], osteogenic differentiation. With regards to ASCs, it has been shown that during osteogenic differentiation their expression of PDGF receptor β (PDGFR-β) is upregulated [100]. However, the ability of PDGF-BB signaling to directly enhance the osteogenic capabilities of ASCs is not known.

The goal of this study is to develop an induction protocol to maximize the co-development of vasculature and bone by ASCs. We do so by first optimizing the concentrations and timing of angiogenic and osteogenic factors. We then assess the hypothesis that exogenous PDGF-BB can synergize complex tissue formation by enhancing vascular stability and osteogenic differentiation.

3.2 Materials and Methods

ASC Isolation

Cellular isolation was performed at the Stem Cell Biology Laboratory, Pennington Biomedical Research Center, under an Institutional Review Board approved protocol (#PBRC 23040) according to published methods [67]. Briefly, fresh human subcutaneous adipose lipoaspirate was obtained under informed consent from female donors (n = 2) undergoing elective liposuction surgery, with an average age of 46 years and average body mass index of 29.1. The lipoaspirate tissue was processed to isolate the adherent population from the SVF, as previously described [101]. The adherent population ("passage 0") was trypsinized and cryopreserved [68] for shipment to Johns Hopkins University.

ASC Expansion & Characterization

ASCs were expanded in growth medium: high glucose DMEM (GIBCO Invitrogen) with 10% FBS (Atlanta Biologicals), 1% penicillin/streptomycin (GIBCO Invitrogen), and 1 ng/ml FGF-2 (PeproTech). Cells were used at passage two for all experiments. Cell phenotype was examined via flow cytometry for mesenchymal (CD73, CD105) and vascular markers (CD31, CD34, VEGFR-2, alpha-smooth muscle actin (αSMA)). Briefly, detached cells were incubated with monoclonal antibodies conjugated to FITC or PE (BD Biosciences) for 30 min at 4 ºC. Cells were analyzed with a flow cytometer (BD Accuri C6).

Spheroid Formation via Hanging Drop

Cells were trypsinized and resuspended at a concentration of 400,000 cells/ml in culture medium containing 0.24% (w/v) methylcellulose (Sigma). The cell suspension was pipetted

as 10 μl drops onto inverted Petri dish caps, which were then reverted and placed on dish bottoms containing sterile water to reduce evaporation. Dishes were incubated at 37 ºC overnight to allow cellular aggregation at the air-liquid interface. The dish caps were then flooded with PBS to allow bulk collection and transfer of the spheroids to conical tubes.

Fibrin Encapsulation

Settled spheroid pellets were resuspended in fibrinogen (8 mg/ml final; Sigma), followed by the addition of thrombin (2 U/ml final; Sigma) to initiate gelation. Fibrin gels (35 μl) containing 40 spheroids each were pipetted into 6-mm diameter wells and incubated at 37 ºC for 30 minutes to allow complete gelation prior to the addition of culture medium. Samples were then cultured for two to three weeks, depending on the experiment, with media changed every other day.

Media Preparation

Vascular medium (VM) consisted of: Endothelial Basal Medium-2 (Lonza), 6% FBS, 1% penicillin/streptomycin, 10 ng/ml $VEGF_{165}$, 1 ng/ml FGF-2, and 1 μg/ml L-ascorbic acid-2-phosphate (Sigma). For monolayer osteogenesis experiments, control medium consisted of low glucose DMEM (GIBCO Invitrogen), 6% FBS, and 1% penicillin/streptomycin; Osteogenic Medium (OM) consisted of control medium plus 10 mM β-glycerophosphate (Sigma) and 50 μM L-ascorbic acid-2-phosphate. For osteogenesis in fibrin gels, OM also included 10 ng/ml $VEGF_{165}$ and 1 ng/ml FGF-2 to support vascular viability. The composition of FGF-2 and dexamethasone in VM and OM were optimized to support both vascular and osteogenic development (**Fig. 3.1**). Media were supplemented with additional

growth factors (i.e. PDGF-BB or bone morphogenetic protein-2 (BMP-2)) depending on the experiment. All growth factors were purchased from PeproTech.

Osteogenic Differentiation Assays

For monolayer experiments, ASCs were seeded at 5000 cells/cm^2 and cultured in either control medium or OM for 21 days, with the addition of either PDGF-BB or PDGF receptor inhibitor tyrphostin AG1295 (Santa Cruz Biotechnology). Mineralization was assessed via Alizarin Red S staining and quantification of calcium content. For fibrin gel experiments, samples were cultured in VM for up to 8 days followed by up to 12 days of OM supplemented with VEGF and FGF-2. Mineralization was assessed via quantification of calcium content normalized to DNA content.

For Alizarin Red S staining, monolayers were washed twice with PBS, fixed with 3.7% formaldehyde for 20 min, and then washed again three times. Samples were subsequently incubated for 10 min with 40 mM Alizarin Red S (Sigma) and washed extensively prior to imaging. To quantify calcium content in each sample, monolayers or whole fibrin gels were washed twice with PBS and then incubated with 0.5 N HCl overnight at 4 ºC with agitation. Calcium content in the sample supernatants was quantified using a colorimetric Calcium LiquiColor Test (Stanbio). DNA content was quantified using a PicoGreen dsDNA quantitation kit (Molecular Probes) as previously described [101].

Whole-Mount Immunostaining

All incubation and washing steps were carried out at 4 ºC with gentle agitation. Samples were fixed with 3.7% formaldehyde for 3 hrs, and then washed with PBS three times for 30 min each. Fixed gels were carefully removed from their wells and transferred to

microcentrifuge tubes for subsequent staining procedures. Gels were permeabilized and blocked for 4 hrs with 0.2% triton X-100 and 5% normal goat serum (Sigma) in PBS with 0.1% Tween (PTw). Samples were then incubated overnight with primary antibodies diluted in blocking solution, followed by three 1-hr washes in PTw. Primary antibodies included: mouse anti-CD31 (4 μg/ml; Santa Cruz Biotechnology) and either rabbit anti-laminin (7 μg/ml; Sigma) or rabbit anti-osteocalcin (10 μg/ml; Santa Cruz Biotechnology). Samples were incubated overnight with DyLight 488-conjugated goat anti-mouse and DyLight 649-conjugated goat anti-rabbit (both 1:400; Jackson ImmunoResearch) diluted in blocking solution, followed by three 1-hr washes in PTw. Lastly, samples were blocked in 5% normal mouse serum for 4 hrs, incubated overnight with Cy3-conjugated mouse anti-αSMA (7 μg/ml; Sigma), and then washed three times for 1 hr each. Gels were mounted in 70% glycerol and imaged using a Zeiss LSM 510 confocal microscope with a 5x objective.

Image Analysis

Confocal z-stacks of immunostained gels were z-projected and thresholded for subsequent quantification of vessel network parameters (n = 6 images per group). Thresholded images were analyzed with AngioQuant software [71] to quantify total vessel length, area, and interconnectivity. ImageJ software (NIH) was used to quantify pericyte coverage of vessels, which was defined as αSMA+ area within at least 5 μm of the abluminal face of vessel networks. Briefly, vessel networks were selected in the CD31 channel of thresholded image composites, and selections were enlarged by 5 μm at all edges. These enlarged selections were applied to the αSMA channel, and percent αSMA+ area within the selection was quantified (denoted as "% vessel pericyte coverage"). The mean intensity of

the αSMA+ population was quantified by measuring the mean pixel intensity within the non-thresholded αSMA channel viewfield. Lastly, to quantify the amount of basement membrane protein deposited along the vessels, the enlarged vessel selection was applied to the non-thresholded laminin channel, and the mean pixel intensity within the selection area was quantified (denoted as "laminin mean intensity").

Statistical Analysis

Quantitative data are expressed as mean ± standard error. Multi-group comparisons were determined by one-way ANOVA with Tukey's test for post-hoc analysis. Significance levels are denoted as *$P < 0.05$, **$P < 0.01$, and ***$P < 0.001$.

3.3 Results

Cell Characterization

ASCs at passage 2 were primarily positive for mesenchymal markers CD73 (98.4%) and CD105 (80.1%) and predominantly negative for markers of the endothelial lineage (5.2% CD34+; 0.3% VEGFR+; 0.8% CD31+) or the pericyte marker αSMA (1.1%). 100% of CD31+ cells were also positive for PDGFR-β, indicating that these cells are capable of responding to PDGF-BB directly.

Media Component Optimization

The concentrations of dexamethasone and FGF-2 were optimized separately in OM and VM formulations to support both tissue components. Osteogenic cultures yielded significantly greater calcium deposition with the addition of 1 ng/ml FGF-2 and with 0 to 10

nM dexamethasone (**Fig. 3.1A,B**). In vascular cultures, dexamethasone substantially inhibited vessel network growth, while increasing pericyte coverage in a dose-dependent manner (**Fig. 3.1C-E**). Addition of FGF-2 increased vessel width (**Fig. 3.1C**), and induced a slight increase in vessel network length and pericyte coverage.

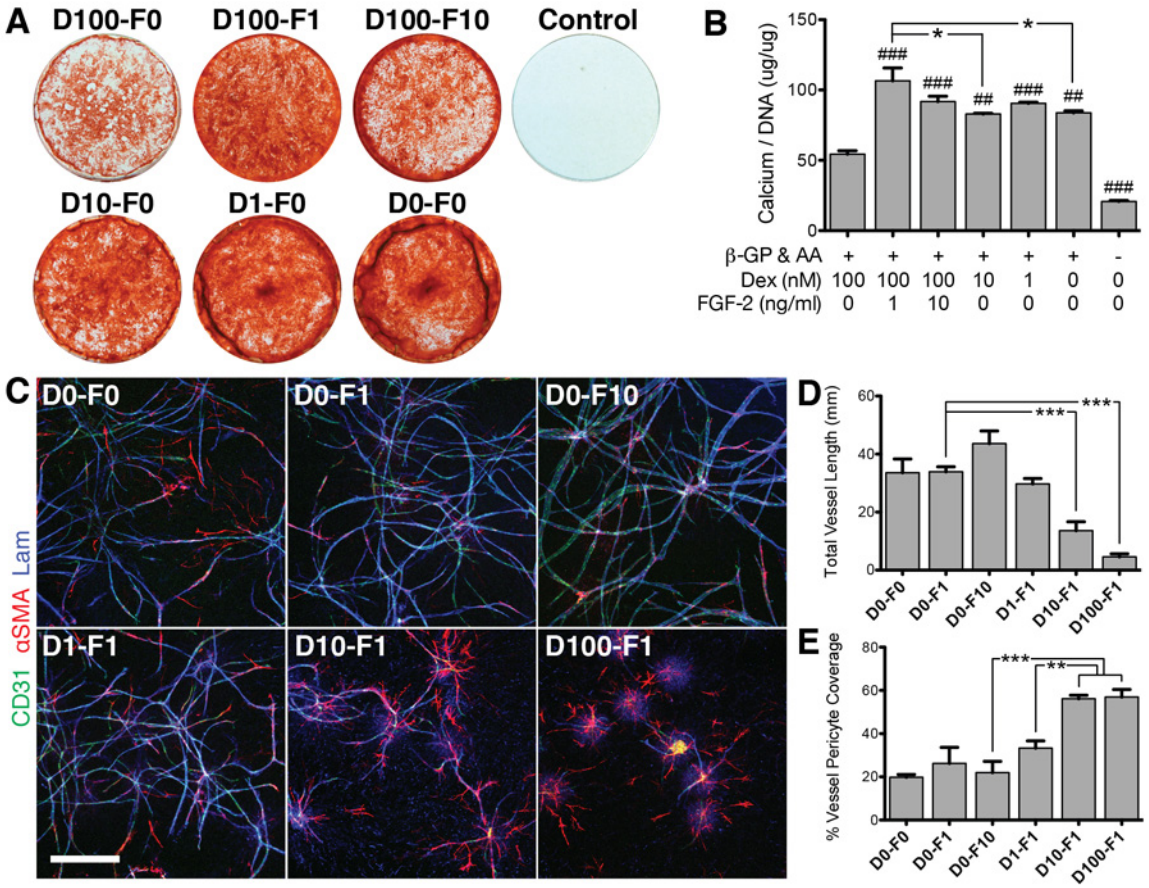

Figure 3.1. Effects of dexamethasone and FGF-2 on each lineage. (**A**) Alizarin Red S staining of mineral in osteogenic monolayers. (**B**) Quantification of calcium content in osteogenic monolayers. (**C**) Vascular networks in 3D fibrin gel. Quantification of vessel network length (**D**) and pericyte coverage of vessels (**E**). Scale bar = 500 μm. Significance indicated by brackets in (**B,D,E**) as $*P < 0.05$, $**P < 0.01$, or $***P < 0.001$. Significance indicated in (**B**) as $\#\#P < 0.01$ or $\#\#\#P < 0.001$ versus D100-F0, and all OM groups were significantly greater ($P < 0.001$) than control. Abbreviations: X nM dexamethasone ("DX"); Y ng/ml FGF-2 ("FY").

Sequential Addition of Factors

To determine the effects of osteogenic factors on vascular morphogenesis, fibrin-encapsulated spheroids were cultured for 0, 4, 8, or 12 days in VM before being transitioned

to OM for the remaining culture period (**Fig. 3.2A**). All groups were cultured for a total of 12 days. ASCs cultured in VM for 8 days prior to the addition of osteogenic factors yielded 3.2-fold longer vascular networks than those cultured in OM for the entire period (**Fig. 3.2B**). Interestingly, the mean αSMA+ intensity increased significantly with increasing length of time in OM (**Fig. 3.2C**), with an apparent increase in the number of αSMA+ and a reduction in their association with the nearby vessels. Extended culture in OM yielded 2.4-fold less laminin deposition around vessels than in VM (**Fig. 3.2D**). Thus, while vascular factors were still present in OM, delaying the addition of osteogenic factors by at least 8 days provided more favorable conditions to induce vascular network growth. This sequential protocol resulted in early mineral deposits located along vessel tracks (**Fig. 3.2E**).

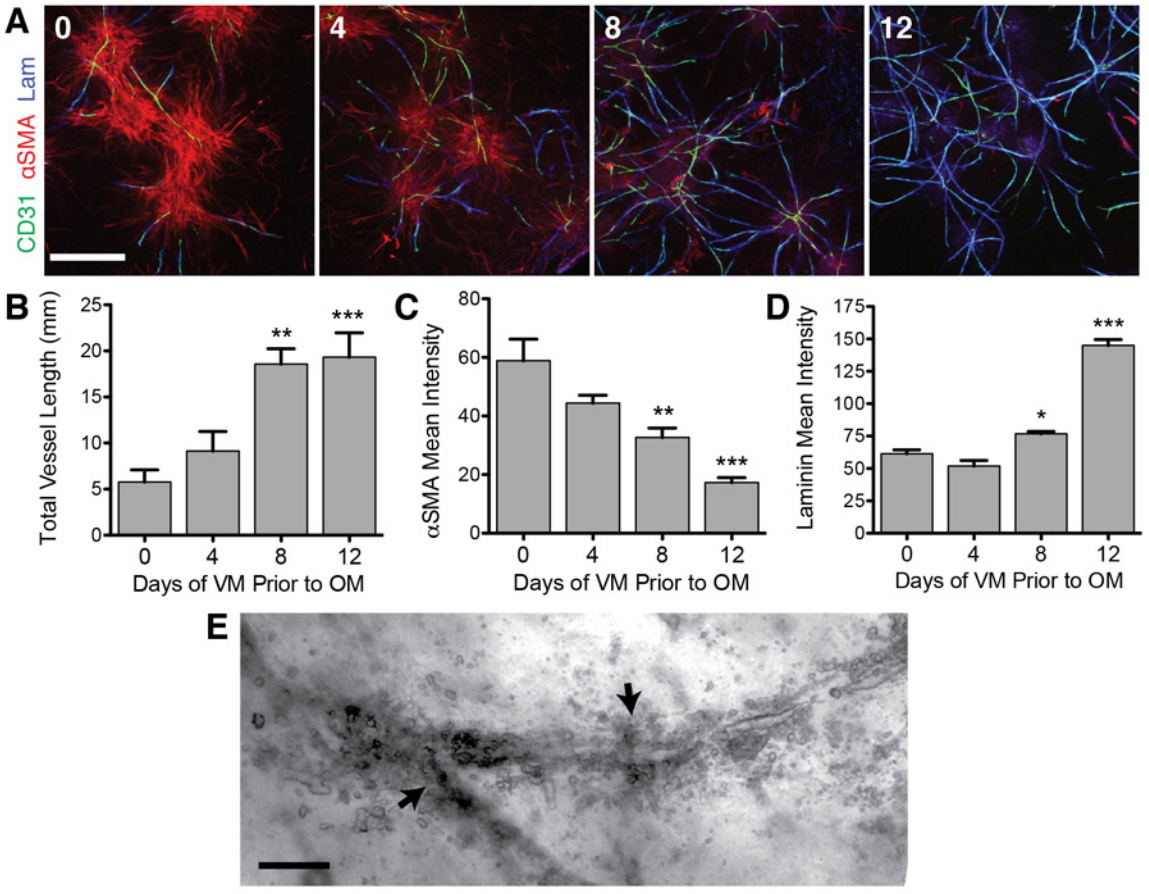

Figure 3.2. Sequential addition of factors. (**A**) Fibrin-encapsulated spheroids were cultured for 0, 4, 8, or 12 days in vascular medium (VM) before switching to osteogenic medium (OM). All samples were cultured for 12 days. (Scale bar = 500 μm). Total vascular network length (**B**) and laminin coverage (**D**) were significantly higher when OM was delayed by several days whereas αSMA staining intensity increased substantially with longer culture periods in OM (**C**). (**B-D**) Significance indicated as $*P < 0.05$, $**P < 0.01$, or $***P < 0.001$ versus 0 days. (**E**) The step-wise protocol resulted in early mineral deposits being deposited in the vicinity of established vessels (arrows). Scale bar = 50 μm.

Independent Effects of Exogenous PDGF-BB on Each Lineage

The effects of exogenous PDGF-BB on osteogenic differentiation and vascular morphogenesis of ASCs were studied independently. ASCs were cultured in OM for 21 days with the addition of either PDGF-BB (0, 2, or 20 ng/ml) or PDGF receptor inhibitor AG1295 (0, 1, or 10 μM). In the presence of exogenous PDGF-BB, ASC calcium deposition was significantly increased in a dose-dependent manner throughout the culture (**Fig. 3.3A**) as well as on a per cell basis (**Fig. 3.3B**). In the presence of AG1295, total calcium deposition was decreased in a dose-dependent manner (**Fig. 3.3A**), whereas calcium deposition per cell was unchanged relative to the OM only group with AG1295 (**Fig. 3.3B**).

In a separate experiment, fibrin-encapsulated spheroids were cultured in VM for 14 days with the addition of PDGF-BB or AG1295. Addition of low concentration (2 ng/ml) PDGF-BB resulted in a slight, 1.4-fold increase in total vessel length (**Fig. 3.3C-D**). Overall however, PDGF stimulation did not have statistically significant effects on total vessel length (**Fig. 3.3D**). Vessels were noticeably wider with the addition of 20 ng/ml PDGF-BB (**Fig. 3.3C**). This was reflected quantitatively with statistically larger total vessel area divided by total vessel length ($P < 0.001$, data not shown). Pericyte coverage was reduced substantially by 2.9 fold in the presence of exogenous PDGF-BB, and only slightly reduced with the addition of AG1295 (**Fig. 3.3E**).

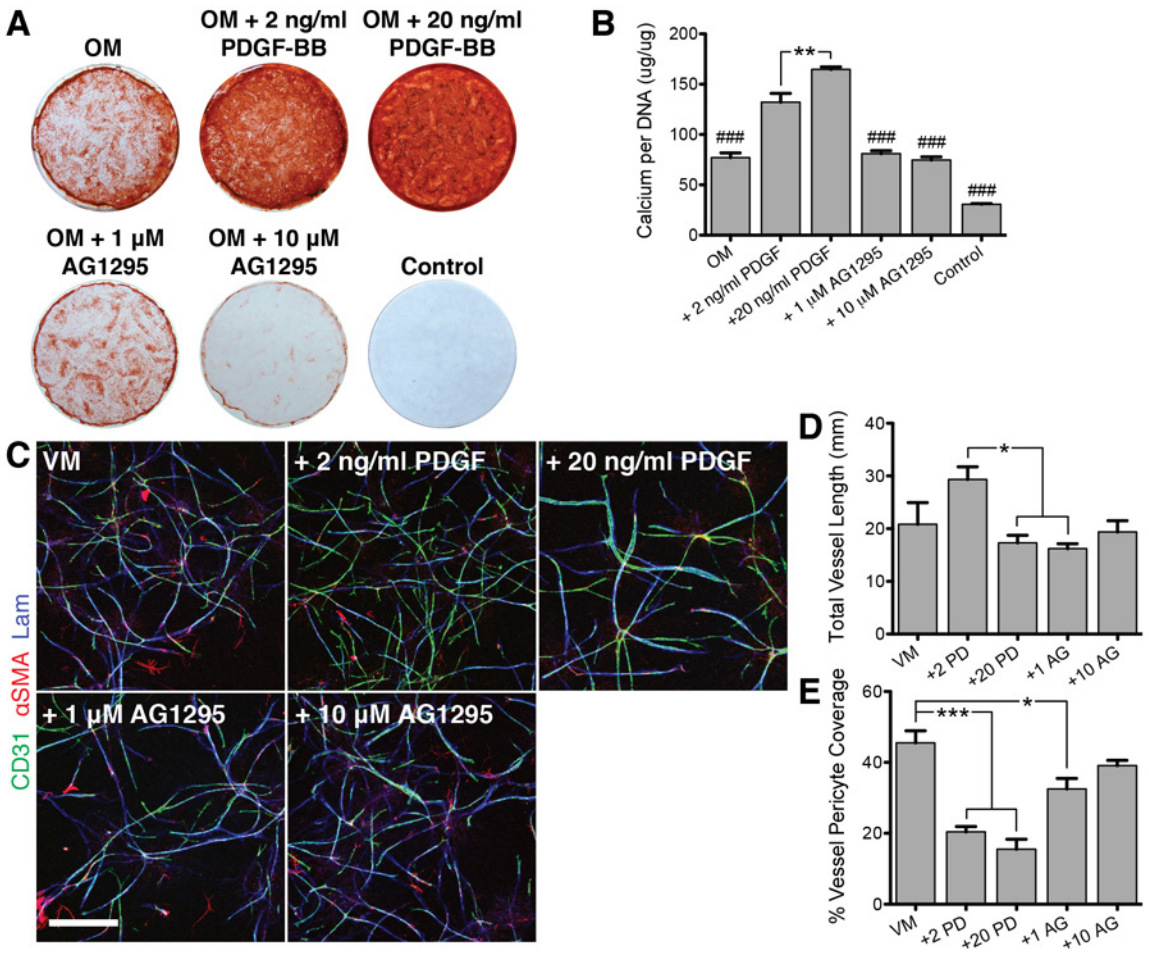

Figure 3.3. Independent effects of exogenous PDGF-BB on each lineage. Mineralization in osteogenic monolayers indicated by (**A**) Alizarin Red S and (**B**) calcium quantification. A separate experiment in 3D fibrin gel demonstrates vessel growth and pericyte coverage (**C-E**). Scale bar = 500 μm. Significance indicated by brackets in (**B,D,E**) as $*P < 0.05$. Significance indicated in (**B**) as $###P < 0.001$ vs. PDGF groups. All OM groups were significantly greater ($P < 0.001$) than control.

Combined Effects of Exogenous PDGF-BB on Vascularized Bone

The effects of PDGF-BB on the co-development of vasculature and bone within the same culture were assessed by inducing fibrin-encapsulated spheroids in a sequential manner (VM for 8 days followed by OM for 12 days) with either 0, 2, or 20 ng/ml PDGF-BB added throughout. Exogenous PDGF-BB resulted in significantly greater vascular density and osteogenic differentiation than cultures without PDGF-BB (**Fig. 3.4D**). Specifically, vascular network length was 2.7 fold greater when 20 ng/ml PDGF-BB was added (**Fig. 3.4A,E**),

and calcium content per cell was 5.2-fold greater (**Fig. 3.4H**). Osteocalcin production was semi-quantitatively measured to be 1.4 fold greater as well (**Fig. 3.4C,G**). Conversely, αSMA intensity was 2.1-fold less in the presence of 20 ng/ml PDGF-BB (**Fig. 3.4B,F**).

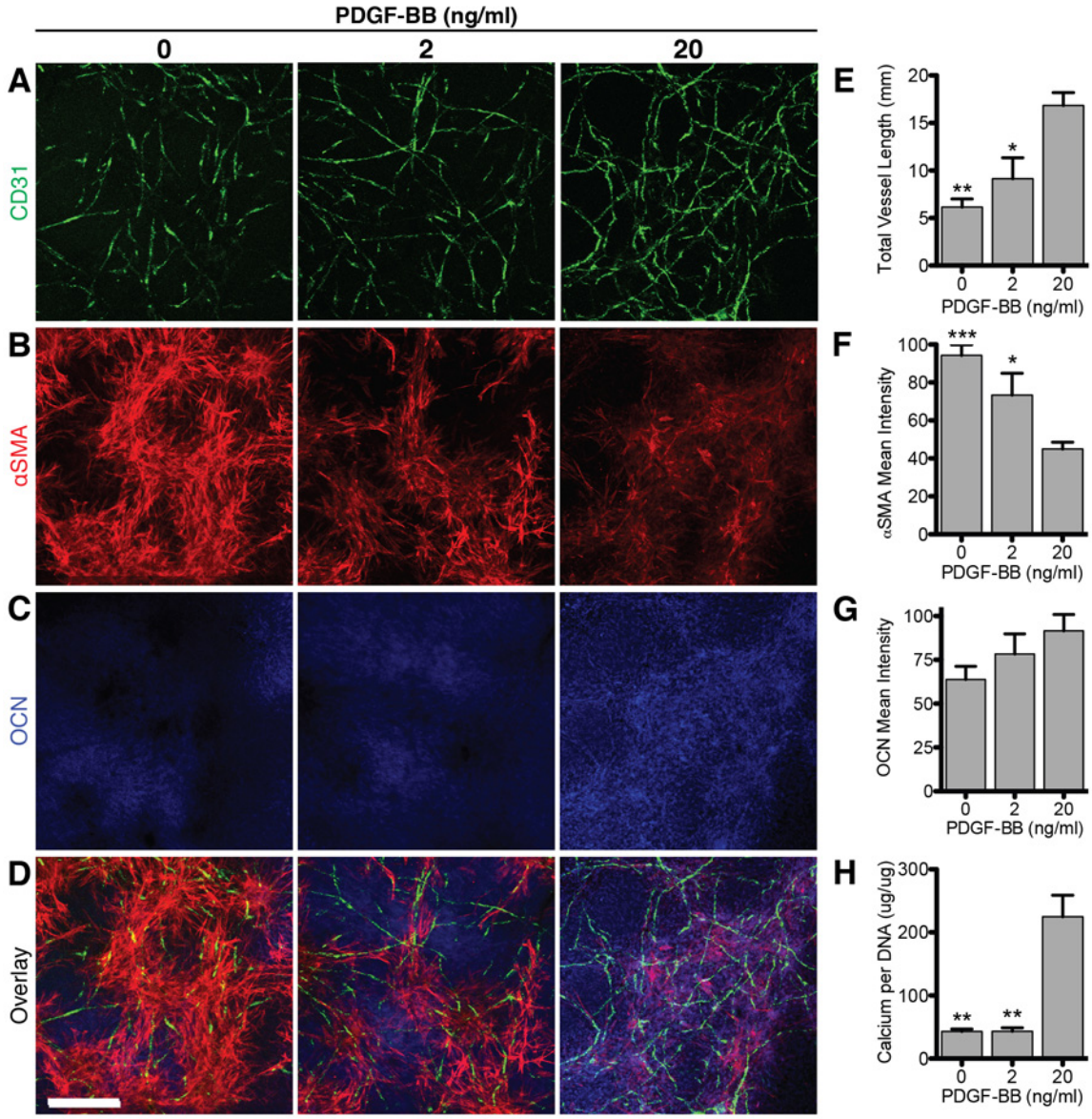

Figure 3.4. Combined effects of exogenous PDGF-BB on vascularized bone. Fibrin-encapsulated spheroids were cultured for 8 days in VM, followed by 12 days of OM with 0, 2, or 20 ng/ml of PDGF-BB added throughout. Total vessel length (A,E), osteocalcin production (C,G), and calcium deposition (H) increased while αSMA staining intensity (B,F) decreased with increasing PDGF-BB concentration. Scale bar = 500 μm. Significance indicated versus 20 ng/ml PDGF-BB.

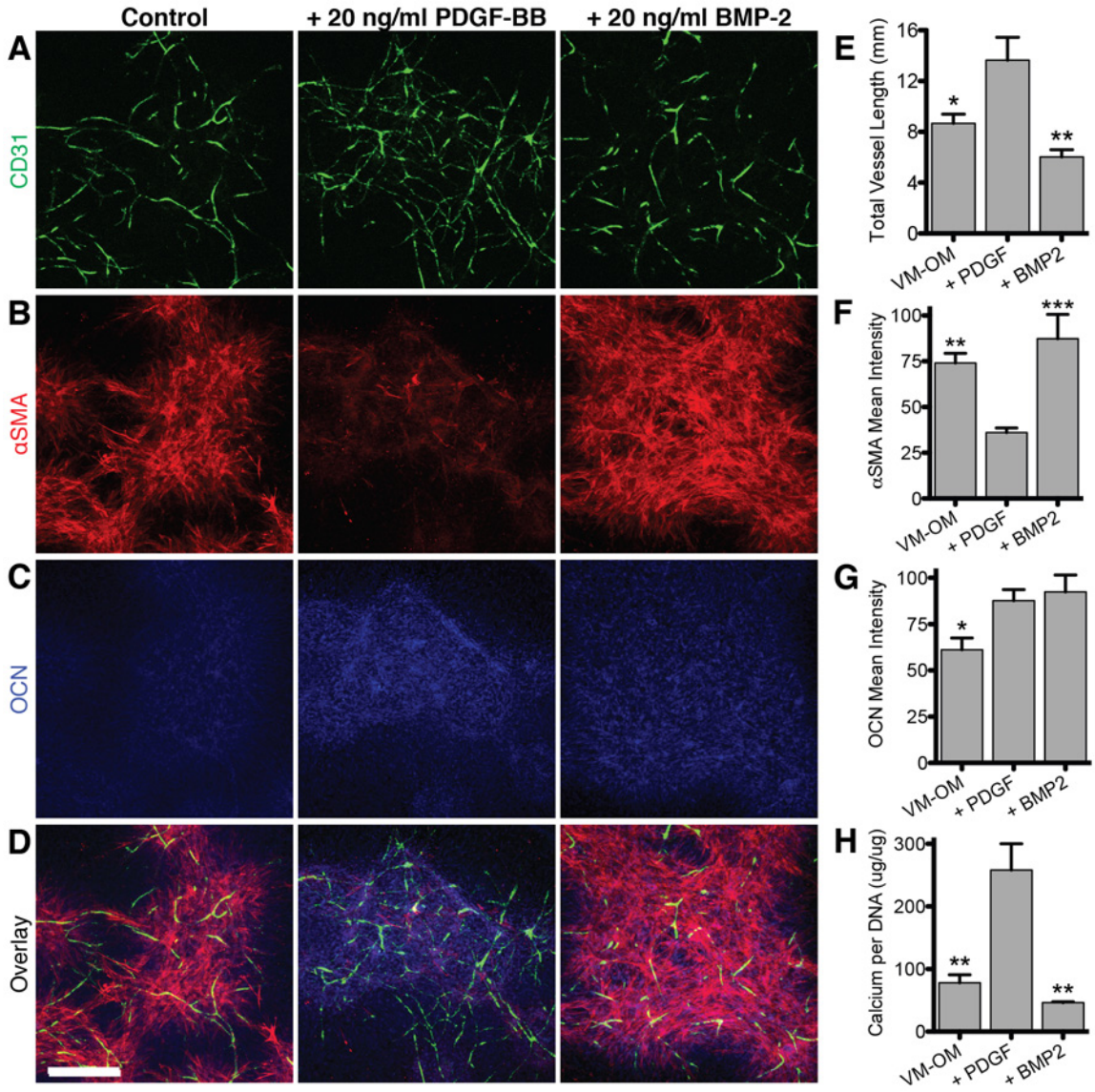

Figure 3.5. Direct comparison of PDGF-BB and BMP-2 on vascularized bone. FVibrin-encapsulated spheroids were induced to form vascularized bone (8 days VM plus 12 days OM) with 20 ng/ml of either PDGF-BB or BMP-2. BMP-2 induced no significant changes in either vascular network length (**A,E**) or calcium content (**H**) versus control, whereas PDGF-BB was substantially greater than both. (**B,F**) αSMA staining intensity was much greater with BMP-2 versus PDGF-BB, but only slightly greater than control. (**C,G**) Osteocalcin staining intensity was similar between PDGF-BB and BMP-2 groups. Scale bar = 500 μm. Significance indicated vs. 20 ng/ml PDGF-BB.

In a similar experiment, we directly compared PDGF-BB with BMP-2 to determine whether these results are unique to PDGF-BB, as BMP-2 has also been shown to be both pro-osteogenic and pro-angiogenic. Encapsulated spheroids were cultured in VM for 8 days followed by OM for 12 days with the addition of either 20 ng/ml PDGF-BB or 20 ng/ml BMP-2. Cultures with PDGF-BB resulted in 4.2 fold greater calcium deposition and 5.6 fold greater calcium per cell than those with BMP-2 (**Fig. 3.5H**). Total vascular network length was also 2.3 fold higher in the presence of PDGF-BB than BMP-2 (**Fig. 3.5A,E**).

3.4 Discussion

Pre-vascularizing tissue-engineered grafts prior to implantation has been shown to accelerate anastomosis with host vasculature and increase the survival of the tissue construct [13, 102, 103]. However, engineering vascularized bone has been a challenge in that the factors that are traditionally used in differentiation medium to induce either osteogenic differentiation or angiogenic behaviors can be mutually inhibitory when combined in mixed cultures [17]. The mutual inhibition is particularly devastating for the vascular component, as vessels have proven to be delicate and unstable in the presence of osteogenic cues *in vitro*. This study has demonstrated that exogenous PDGF-BB helps circumvent these issues by enhancing vascular growth and stability, as well as promoting robust osteogenic differentiation and mineralization. This is the first demonstration of cooperative growth yielding robust vascular networks within dense mineralized matrix.

In the current study, vascular growth by ASCs was severely limited in the presence of osteogenic factors, β-glycerophosphate and higher concentration ascorbic acid, despite the presence of angiogenic factors VEGF and FGF-2. β-glycerophosphate is an essential

initiator of mineralization, as cells cannot synthesize their own phosphate. However, it may be a possible source of vascular inhibition after it is broken down into inorganic phosphate by alkaline phosphatase activity [104]. High inorganic phosphate levels (> 2.5 mM) have been shown to induce endothelial cell apoptosis via increased generation of reactive oxygen species [20]. To compensate for this, delaying the addition of osteogenic factors by one week allowed the vessels to grow and establish stable networks prior to inducing osteogenic differentiation of the non-endothelial sub-population. This sequential process is similar to what occurs in bone development and fracture repair in which invading vasculature is a prerequisite for the entry of osteogenic progenitors and subsequent mineralization [105, 106] (**Fig. 1.1B,C**). This established vascular network serves to bring nutrients and progenitor cells to the highly active site of regeneration [89, 107], as well as serving as a template around which mineral will be deposited [106]. Establishment of vascular networks prior to osteogenesis helped to stabilize the networks with pericytes and increased laminin deposition, possibly shielding them from the inhibitory factors in the second phase.

This study has demonstrated that exogenous PDGF-BB at 20 ng/ml further helps to circumvent issues of mutual inhibition by enhancing both the osteogenic and vascular development of ASCs. In osteogenic cultures, PDGF-BB markedly increased mineral deposition overall and on a per cell basis. Conversely, addition of the inhibitor AG1295 reduced overall mineral deposition, while the relative amount per cell remained unchanged. These results suggest that PDGF signaling might not be required for osteogenic differentiation of ASCs, but it may significantly amplify their responsiveness to osteogenic cues, leading to the production of greater amounts of mineral. This response may be somewhat unique to ASCs, as previous studies have shown that PDGF signaling either has

no effect or even an inhibitory effect on the osteogenic differentiation bone marrow-derived MSCs [95-99].

In vascular cultures, PDGF signaling had minimal effects on vascular network properties, with only low levels of exogenous PDGF-BB contributing to a slight increase in network density. PDGF signaling did, however, significantly affect pericyte coverage of the vessels. Exogenous PDGF-BB caused a significant decrease in pericyte coverage, likely by masking endogenous gradients and stimulating the pericytes to migrate randomly. Interestingly, the inhibitor AG1295 did not significantly reduce pericyte coverage. This is possibly a result of the cellular aggregation prior to encapsulation, in which the growing vessels are already in direct contact with pericyte-like cells, thereby reducing the necessity to recruit pericytes via a PDGF gradient.

PDGF-BB appeared to play a different role in maintaining vascular stability in the presence of osteogenic factors. Using a sequential protocol of a vascular phase followed by an osteogenic phase, the addition of 20 ng/ml PDGF-BB was able to support vascular growth and stability as well as amplify mineral deposition. There are some hypotheses in the literature about how exactly this occurs. A recent review discusses the possible roles of PDGF-BB signaling in terms of bone fracture repair [89]. When bone is injured, high concentrations of PDGF-BB may cause vascular pericytes and other osteoprogenitors to populate the injury site and increase production of mineral. These cells may also respond to PDGF-BB by secreting higher levels of VEGF to recruit angiogenesis towards the regenerating tissue [89, 108]. In the case of our own study, this increased endogenous production of VEGF may be furthering the stability of established vessels in the osteogenic environment. It may also be possible that the vessels in these cultures are responding directly

to PDGF-BB via PDGF receptors. In this study, 100% of CD31+ cells were PDGFR-β+, suggesting that they are indeed capable of sensing PDGF-BB. However, further studies are needed to identify the specific mechanisms underlying these morphogenic events within the ASC cultures.

An interesting observation in our study was that the expression of αSMA changed dramatically throughout the induction period. αSMA aids cellular contractility and is primarily expressed by vascular smooth muscle cells and pericytes [109]. In our study, initial ASC cultures exhibited only 1% αSMA positive population. Prior to the application of osteogenic supplements, αSMA+ cells were primarily located in perivascular locations. However, following exposure to osteogenic supplements, there was a dramatic increase in the intensity and number of cells expressing this marker. This change in expression profile reflects what is observed in native mineralizing bone: Osteoblasts upregulate expression of αSMA during active mineralization, whereas resting osteoblasts and osteocytes do not express αSMA [110]. However, the current study also showed that ASCs treated with 20 ng/ml PDGF-BB in the presence of osteogenic cues exhibited substantially lower αSMA expression at day 20 than those cultured without PDGF-BB even though the mineral content in PDGF-BB cultures was significantly higher suggesting that a αSMA expression alone does not directly correlate with increased osteogenesis.

Lastly, we examined whether this mutually beneficial response exhibited by cells in the presence of PDGF-BB was unique by comparison to BMP-2, the most widely studied and clinically applied pro-osteogenic growth factor. BMP-2 has been shown to significantly enhance osteogenic differentiation and *in vivo* bone growth [111], as well as indirectly enhance vascular growth via promotion of VEGF production [112]. The current study

shows through direct comparison that PDGF-BB is considerably more effective than BMP-2 at both amplifying osteogenic differentiation of ASCs and maintaining vascular stability when applied at 20 ng/ml. Importantly, this concentration of PDGF (20 ng/ml) is only 5 to 10 times the concentration in normal human serum [113] and is within the physiological range measured during bone injury [114]. Clinical safety is imperative, as supra-physiological concentrations may lead to adverse side effects such as bone overgrowth and inflammation [115]. Together, these results indicate that, in combination with ASCs, PDGF-BB may be better suited than BMP-2 for the enhancement of both bone and vasculature at physiological concentrations.

3.5 Conclusions

In summary, we have demonstrated that ASCs can be driven to form robust vascularized bone with the addition of exogenous PDGF-BB. Combined with the delayed addition of osteogenic cues, this protocol recapitulates intrinsic regenerative profiles that instruct the cells to grow into complex tissue grafts with less manipulation compared to existing models. This induction protocol using physiological levels of PDGF-BB can be utilized to engineer vascularized bone grafts with greater efficiency and potential for subsequent integration and functionality.

Chapter 4

Vascularized Bone Model, Part II: Inflammatory Cytokines

4.1 Introduction and Background

Cell-based approaches to bone tissue engineering provide a tremendous opportunity to repair large, non-healing bone defects by enriching the site with regenerative cells. However, the potential benefit is hampered by the need for rapid vascularization to maintain cell viability and also provide complex signaling cues between vasculature, infiltrating inflammatory cells, and osteoprogenitors that guide tissue repair and maturation. Therefore, coupling vascularization strategies with bone tissue engineering may greatly improve functional outcomes.

Our previous studies established a step-wise protocol to engineer robust vascularized bone *in vitro* with the addition of exogenous platelet-derived growth factor (PDGF), which significantly increased both vascularization and mineralization. PDGF is a key regenerative cue that is released by activated platelets following bone injury [89], raising the question of how other elements of normal bone repair may affect bone tissue engineering.

Immediately following bone injury, there is an acute inflammatory phase in which activated platelets and macrophages release a host of factors, including PDGF and pro-inflammatory cytokines [89, 116-118] (**Fig. 1.1A**). These factors play a critical role in the

initiation of healing through the recruitment and activation of regenerative cells, as well as promoting re-vascularization. While normally thought of as intrinsically damaging to tissue repair, pro-inflammatory cytokines such as tumor necrosis factor-α (TNF) have been shown to promote tissue-healing processes in some cases. For example, exogenously applied TNF has been shown to promote angiogenesis *in vivo* [119, 120] and *in vitro* by inducing the endothelial tip cell phenotype [121]. This response appears to be highly sensitive to the timing and dosage, as there are also many reports of the anti-angiogenic effects of TNF [121-124]. In the case of bone, TNF has been shown to improve bone fracture healing *in vivo* [125, 126] and osteogenic differentiation of stem cells *in vitro* [127-130].

The current study aims to understand whether TNF may benefit the development and maintenance of vascular networks within engineered osteogenic tissue. In particular, we study the effects of TNF dose and timing, as well as its combined effects with PDGF. In addition, we generate osteogenic grafts within composite scaffolds to study tissue maturation and integration *in vivo*. We demonstrate that recapitulating the biochemical environment within normal bone healing cascades through the inclusion of the inflammatory mediator TNF improves vascularization of tissue engineered osteogenic grafts.

4.2 Materials and Methods

Ethics Statement

Human subcutaneous adipose tissue was obtained in the form of lipoaspirate from female donors (n = 3) with written informed consent under the approval of the Johns Hopkins Medicine Institutional Review Board. All animal procedures were conducted in strict accordance with the Guide for the Care and Use of Laboratory Animals by the

National Institutes of Health, with every effort taken to minimize animal suffering. The study protocol was approved by the Johns Hopkins University Animal Care and Use Committee. Johns Hopkins University is accredited by the Association for Assessment and Accreditation of Laboratory Animal Care International and holds Public Health Service Animal Welfare Assurance Number A-3272.

ASC Isolation and Culture

ASCs were isolated from lipoaspirate tissue as previously described [101]. Briefly, tissue was digested with collagenase (1 mg/mL; Worthington Biochemical Corp.) to isolate the stromal vascular fraction of cells. These cells were plated onto tissue culture plastic, and were termed "passage 0 ASC" when they reached 80-90% confluence. ASCs were used at passage 2 for all experiments. Growth medium consisted of: high-glucose DMEM (Gibco Invitrogen) with 10% fetal bovine serum (FBS; Atlanta Biologicals), 1% penicillin/streptomycin (Gibco Invitrogen), and 1 ng/mL basic fibroblast growth factor (FGF-2; PeproTech). Experimental results were verified by repeating studies with cells from three separate donors.

Flow Cytometry

Passage 2 ASCs were assessed via flow cytometry for surface expression of mesenchymal (CD73, CD105, PDGFR-β) and endothelial markers (CD31, CD34). Briefly, cells were suspended in phosphate buffered saline (PBS) containing 2% FBS and incubated with monoclonal antibodies for 30 min at 4 ºC. Cells were analyzed with a BD Accuri C6 flow

cytometer. Antibodies were purchased from Santa Cruz Biotech (PDGFR-β) and BD Biosciences (all others).

Cell Aggregation Via Suspension Culture

Cells were trypsinized and resuspended at a concentration of 200,000 cells/mL in growth medium containing 0.24% (w/v) methylcellulose (Sigma). The cell suspension was pipetted into 10-cm petri dishes coated with 2% (w/v) agarose to minimize cellular adherence to the dish. After overnight suspension culture, cellular aggregates (**Fig. 4.1**) were collected with a pipet, and then centrifuged before encapsulation procedures.

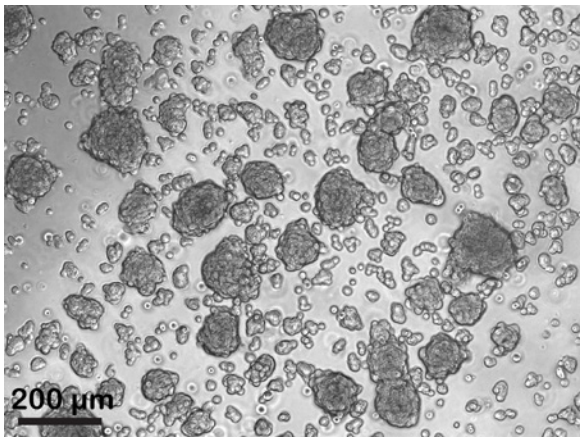

Figure 4.1. Morphology of suspension aggregates.

Cell Encapsulation in Fibrin Gels

Cells were suspended in fibrinogen (8 mg/mL final; Sigma) and thrombin (2 U/mL final; Sigma) at a final cell concentration of 5000 cells/μL. Fibrin gels were formed by pipetting 35 μL of gel solution into 6-mm diameter wells and incubating at 37 ºC for 30 min to allow complete gelation before the addition of culture medium. Samples were cultured for 2 to 3 weeks, depending on the experiment, with medium changed every other day.

PCL Scaffold Fabrication and Seeding

Polycaprolactone (PCL) was utilized as the base scaffold material for these studies to allow handling and implantation of grafts, as well as its biocompatibility, mechanical properties, and in vivo stability [131, 132]. PCL scaffolds were produced as previously described [133]. Briefly, a Syil X4 CNC mill (Syil America) was converted into a custom-built 3D printer with a hot melt pressure extruder attached to the spindle. PCL pellets (Polysciences Inc., Warrington, PA) were melted to 80ºC and extruded at a linear speed of 2.7 mm/sec through a 460-μm nozzle. Scaffold sheets were printed with a 0/90º lay-down pattern and 40% infill density. Cylindrical scaffolds were punched from these sheets with dimensions of 4 mm diameter x 2 mm height (**Fig. 4.2**). Scaffolds were treated with 3M sodium hydroxide for 1 hour to increase hydrophilicity, followed by 1 hour of 70% ethanol to sterilize. Before cell seeding, rinsed scaffolds were incubated with growth medium at 37 ºC for 1 hour, then blotted on sterile Kimwipes immediately prior to seeding. Cells were seeded into the scaffold pore spaces with fibrin gel to facilitate vascular assembly and rapid encapsulation of cells. Briefly, 20 μL of fibrin gel solution containing 6 x 10^5 cells was pipetted into scaffold pore spaces and allowed to solidify at 37 ºC for 30 minutes.

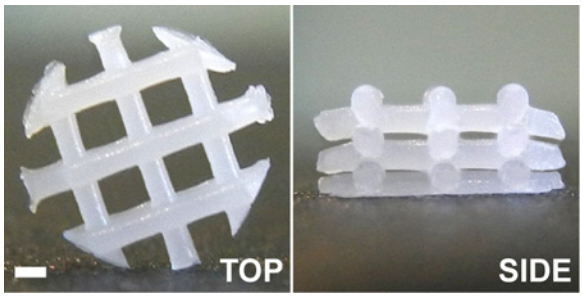

Figure 4.2. Cylindrical polycaprolactone scaffold. Dimensions: 4 mm diameter x 2 mm height, 350 μm average rod diameter, and 750 μm average pore width. Scale bar = 500 μm.

Media Preparation

Vascular Medium (VM) consisted of endothelial basal medium-2 (Lonza), 6% FBS, 1% penicillin/streptomycin, 10 ng/mL vascular endothelial growth factor-165 (VEGF; PeproTech), 1 ng/ml FGF-2, and 1 μg/mL L-ascorbic acid-2-phosphate (Sigma). For monolayer osteogenic differentiation experiments, Control Medium consisted of low glucose DMEM (GIBCO Invitrogen), 6% FBS, and 1% penicillin/streptomycin; Osteogenic Medium (OM) consisted of Control Medium plus 10 mM β-glycerophosphate (Sigma) and 50 μM L-ascorbic acid-2-phosphate. To support both vascular growth and osteogenic differentiation, OM was further supplemented with 10 ng/ml VEGF and 1 ng/ml FGF-2 for studies within fibrin gels and PCL scaffolds.

Osteogenic and Vascular Induction

For monolayer experiments, ASCs were seeded at 5000 cells/cm^2 and cultured in either Control Medium or OM for 21 days. Mineralization was assessed via Alizarin Red S staining, as well as quantification of calcium and DNA content, as previously described [23]. For fibrin gel and scaffold experiments, vascular morphogenesis was induced by culturing cells in VM for up to 14 days. Dual (vascular and osteogenic) induction followed a previously described protocol [23], where samples were cultured in VM for 8 days followed by 13 days of OM supplemented with VEGF and FGF-2. Vascular growth was assessed via immunostaining of fibrin gels (whole-mount) and PCL scaffolds (cryosections). Osteogenic differentiation in 3D samples was also assessed via immunostaining, as well as quantification of calcium content.

Treatment with TNF and PDGF-BB

Different experimental models were employed in this study (**Fig. 4.3**). Initial experiments tested the effects of acute TNF exposure on osteogenesis and vascularization independently (**Fig. 4.3A**). ASCs were cultured in either OM (monolayer) or VM (fibrin gel), with the addition of TNF (0, 0.1, 1, 10, or 100 ng/mL) for the first 48 hours to mimic an acute inflammatory response. In the next experiment, the combined effects of TNF and PDGF-BB on dual (vascular and osteogenic) induction were assessed (**Fig. 4.3B**), as both factors are key mediators in the early bone-healing environment. Fibrin-encapsulated ASCs were treated with 0 or 20 ng/ml PDGF-BB (for the full 21 days of culture) and 0 or 0.1 ng/ml TNF (for 2 or 21 days). To assess tissue development within implantable grafts, ASCs were seeded into PCL scaffolds and underwent vascular and osteogenic induction with the addition of 0 or 0.1 ng/ml TNF (for 2 days) and 20 ng/ml PDGF-BB (for 21 days), and either assessed at the end of in vitro culture (**Fig. 4.3C**) or implanted in vivo to assess the survival and integration of the grafts (**Fig. 4.3D**).

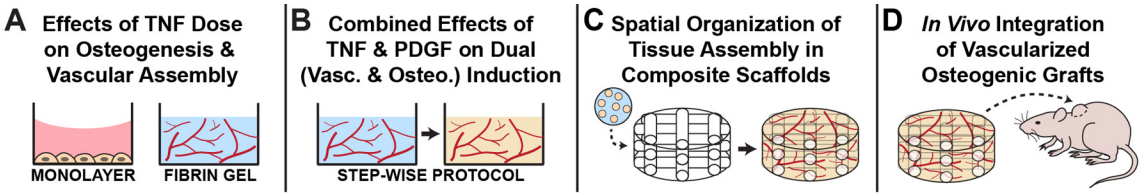

Figure 4.3. Schematic of experimental approaches. (**A**) Osteogenic (monolayer) and vascular (aggregates in fibrin gel) cultures were studied separately in this experiment to study the effects of TNF dose (0 to 100 ng/ml for the first 2 days only) on each lineage. (**B**) Fibrin-encapsulated ASC aggregates underwent dual (vascular and osteogenic) induction using a step-wise approach [23]. The cells were treated with TNF and/or PDGF-BB to study their individual and combined effects. (**C**) ASC aggregates were seeded with fibrin gel into the pores of 3D-printed PCL scaffolds and induced to form vessels and mineral in order to study the spatial organization of tissue assembly within grafts. (**D**) These cultured grafts were implanted subcutaneously in athymic nude rats for 2 weeks to assess *in vivo* integration and maturation of the grafts.

In Vivo Implantation

Male athymic nude rats (7 weeks old, n = 4 per group; Charles River Laboratories) were anesthetized with isofluorane. Two small incisions were made in the dorsal region of the skin to form bilateral subcutaneous pockets. One sample from each treatment group (± TNF) was placed in each rat (one sample per pocket), then the skin was sutured closed. All rats were sacrificed after 14 days for retrieval of scaffold implants, which were fixed in 3.7% formaldehyde at 4 ºC for 24 hours before histological analysis.

Immunostaining and Histology

Fibrin gel samples were fixed in 3.7% formaldehyde at 4 ºC for 3 hours, followed by whole-mount immunostaining, which was performed as previously described [23]. Gels were mounted on glass slides and imaged using a Zeiss LSM 510 confocal microscope with a 5x objective. Fixed PCL scaffold samples were infiltrated with 30% sucrose, frozen in Tissue Tek OCT medium, and cut into 10 μm-thick sections. Cryosections were mounted and dried on Superfrost Plus slides, followed by rehydration in water before staining with either Hematoxylin and Eosin (H&E; Sigma) or immunohistochemistry. Immunohistochemistry was performed by blocking for 30 minutes (10% normal serum / 0.2% Triton X), followed by overnight incubation with primary antibodies at 4 ºC, 1-hour incubation with secondary antibodies at room temperature, and nuclear counterstain for 4'-6-diamidino-2-phenylindole (DAPI; Sigma). Cryosections were imaged using an inverted Zeiss Axio Observer microscope. Primary antibodies included: mouse anti-human CD31 (4 μg/mL, Sigma and Dako), Cy3-conjugated mouse anti-alpha smooth muscle actin (αSMA; 7 μg/ml, Sigma), rabbit anti-laminin (7 μg/ml, Sigma), rabbit anti-osteocalcin (OCN; 10 μg/ml, Santa Cruz

Biotechnology), mouse anti-collagen I (1/1000, Abcam), goat anti-RUNX2 (4 μg/mL, Santa Cruz Biotechnology), and mouse anti-human Lamin A/C (0.5 μg/mL, Abcam). Secondary antibodies (Jackson ImmunoResearch) included: goat anti-mouse (DyLight 488) and goat anti-rabbit (DyLight 649) for in vitro samples; donkey anti-goat (AlexaFluor 488), donkey anti-mouse (Cy3), and donkey anti-rabbit (AlexaFluor 647) for in vivo samples.

Image Analysis

Confocal z-stacks of immunostained gels were z-projected and thresholded for quantification of vessel network parameters (6 images per group). AngioQuant software [71] was used to quantify total vessel length and number of junctions ("interconnectivity"). Cryosectioned scaffold samples were analyzed with Image J software (NIH). A minimum of 3 slices (spaced ≥ 100 μm apart) was analyzed from each independent sample. Nuclear counts (DAPI, RUNX-2, Lamin A/C) were performed with the Analyze Particles command on thresholded images and were normalized to the total graft area. Extracellular matrix deposition ("intensity") was measured by taking the mean grey value of selected regions in non-thresholded images (entire graft region for Col-1 and OCN, and CD31+ overlay region for in vitro laminin). Percent vessel area (either CD31 for human vessels or laminin for rat and human vessels in vivo) was determined in cryosectioned samples by measuring the thresholded vessel area divided by the total graft area (mm^2/mm^2).

Quantitative RT-PCR

Total RNA was isolated using a TRIzol (Invitrogen) extraction method and quantified using a NanoDrop spectrophotometer (Thermo Scientific). Reverse transcription was

performed with 1 μg of total RNA using iScript cDNA Synthesis Kit (BioRAD). Complementary DNA was amplified using SYBR Green PCR Master Mix (Applied Biosystems) and a StepOnePlus Real-Time PCR System (Applied Biosystems). The primer sequences used for PCR analysis are listed in **Table 2.1**. Expression levels were calculated by the comparative C_T method using GAPDH as an endogenous reference gene.

Statistical Analysis

Statistical analyses were performed using GraphPad Prism 5 software. Quantitative data are expressed as mean ± standard error. An unpaired t-test was used for two-group comparisons. Multi-group comparisons were determined by either one-way ANOVA with Tukey's post-test (for single factor studies) or two-way ANOVA with Bonferroni's post-test (for multiple factor studies). Significance is denoted as $*p < 0.05$, $**p < 0.01$, $***p < 0.001$.

4.3 Results

Cell Characterization

Passage 2 ASCs were predominantly positive for mesenchymal markers (97.2% CD73+, 87.1% CD105+, and 99.2% PDGFR-β+), with very few cells positive for endothelial markers (0.64% CD31+ and 2.83% CD34+). All CD31+ cells were positive for PDGFR-β+.

Effects of Acute TNF Exposure on Independent Lineage Induction

The addition of TNF to osteogenic cultures resulted in significantly greater calcium deposition, as shown by Alizarin Red S staining (**Fig. 4.4A**) and quantification of calcium content (**Fig. 4.4C**). This improved response was highest at 10 ng/mL. Calcium normalized

to DNA content (to account for differences in cell number) was not different with any TNF dose (**Fig. 4.4D**). In vascular cultures (**Fig. 4.4B**), 0.1 ng/mL TNF significantly increased vascular network length (**Fig. 4.4E**) and interconnectivity (**Fig. 4.4F**). Higher doses showed no change (1 and 10 ng/mL) or significantly inhibited vascular growth (100 ng/mL).

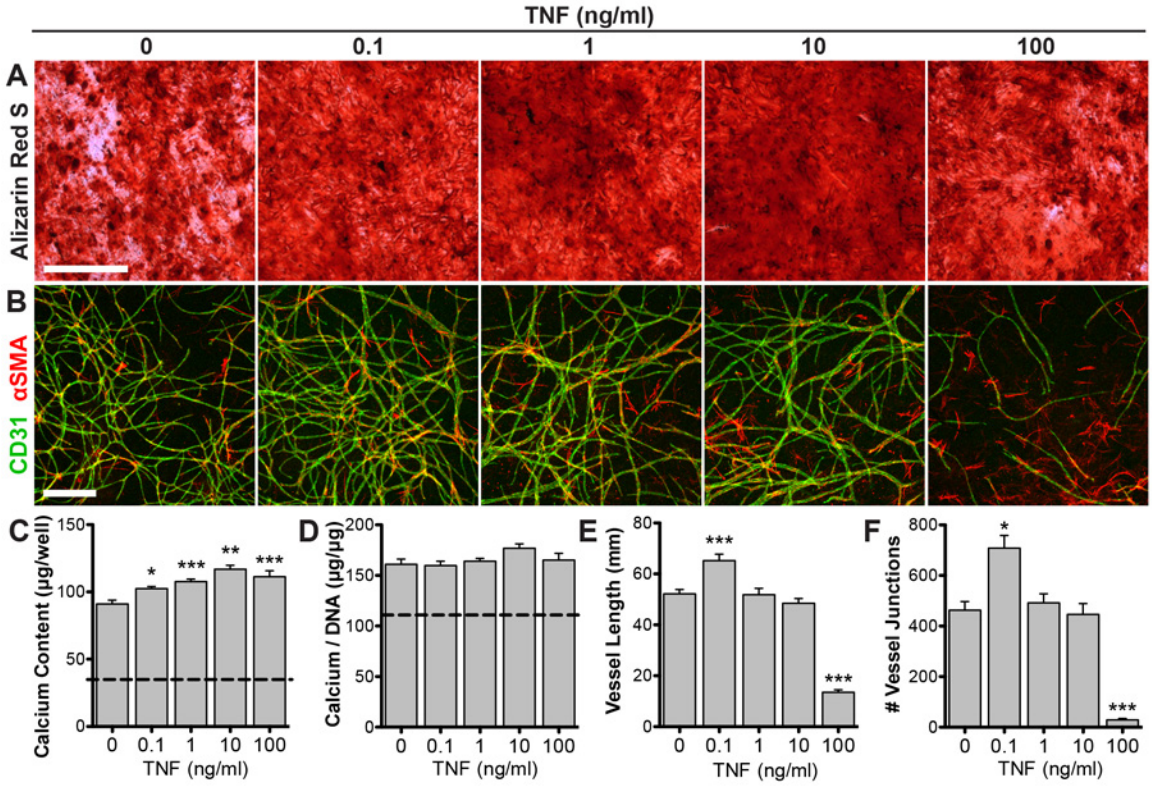

Figure 4.4. Effects of acute TNF exposure on independent lineage induction. ASCs were induced towards either osteogenic differentiation (2D monolayer) or vascular morphogenesis (spheroids in 3D fibrin gel) and treated with varying doses of exogenous TNF for the first 48 hours. Osteogenic cultures were assessed via Alizarin Red S stain for calcium deposits (**A**), as well as quantification of total calcium content (**C**) and calcium normalized to DNA content (**D**) (dotted line: non-osteogenic control). Vascular cultures were assessed via whole-mount immunostaining for CD31 (green) and αSMA (red) (**B**), as well as quantification of vascular network length (**E**) and interconnectivity (**F**). Scale bars = 500 μm. Values shown as mean ± SEM. *$p < 0.05$, **$p < 0.01$, or ***$p < 0.001$ versus 0 ng/ml TNF.

Combined Effects of TNF and PDGF-BB on Dual Induction

Fibrin-encapsulated cell aggregates underwent vascular and osteogenic induction according to a previously established step-wise protocol (**Fig. 4.5A**) [23]. Vascular growth

was enhanced after acute (2 days) TNF exposure (**Fig. 4.5B-D**), similar to the vascular-only cultures (**Fig. 4.4B**). However, chronic (21 days) exposure to the same concentration of TNF significantly reduced vascular growth, and was slightly inhibitory as compared to no TNF treatment. PDGF-BB significantly increased vascular growth in all groups, and demonstrated a synergistic increase in vessel interconnectivity in combination with TNF (interaction p-value = 0.0496). PDGF-BB also induced a significantly increase in osteogenesis (**Fig. 4.5E-G**), whereas TNF exposure did not elicit any significant differences, except for a reduction in osteocalcin staining with chronic (21 day) TNF exposure.

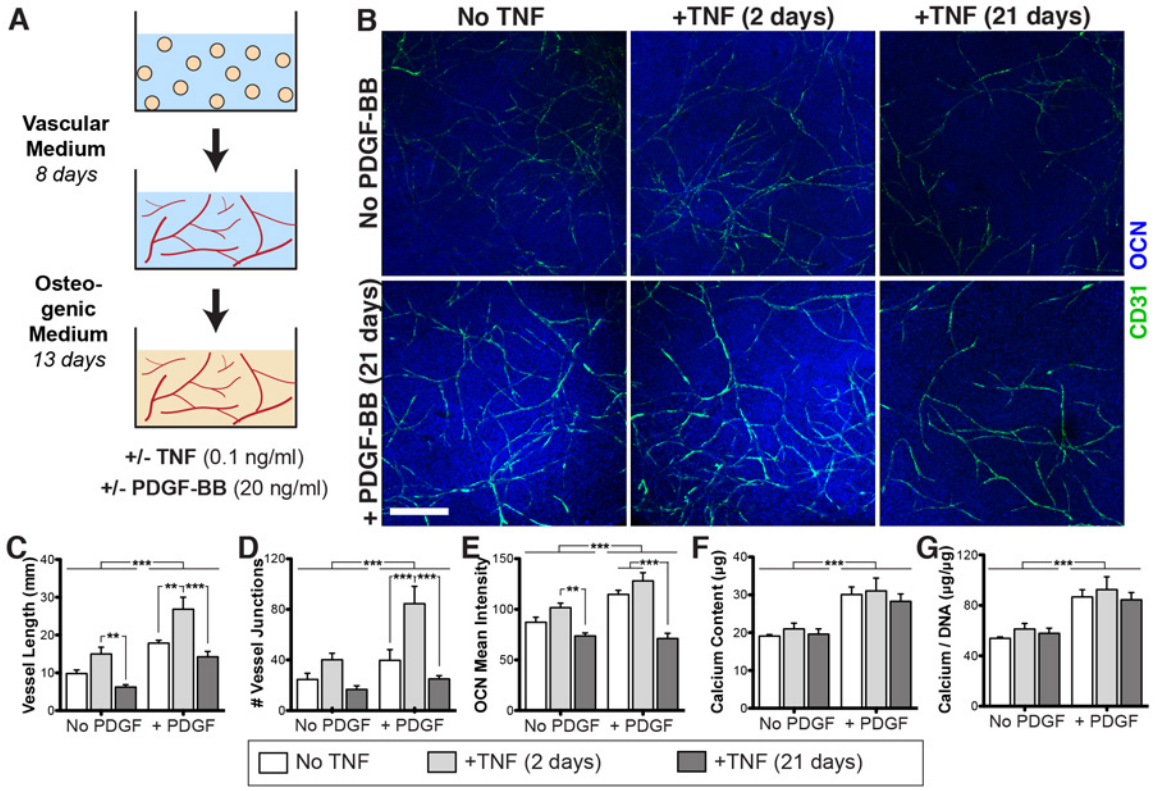

Figure 4.5. Combined effects of TNF and PDGF-BB on vascular and osteogenic induction within fibrin gels. (**A**) Fibrin-encapsulated ASC aggregates underwent dual induction with the addition of TNF and/or PDGF-BB. (**B**) Whole-mount immunostaining for CD31 (green) and OCN (blue). Scale bar = 500 µm. Quantification of immunostains: (**C**) vascular network length, (**D**) vascular network interconnectivity, and (**E**) mean intensity of OCN deposits. (**F**) Total calcium content. (**G**) Calcium content normalized to DNA content. Values shown as mean ± SEM. Significance indicated as $^{**}p < 0.01$ or $^{***}p < 0.001$.

Tissue Assembly in Composite Scaffolds

ASC aggregates seeded with fibrin gel into PCL scaffolds were evenly distributed throughout the pores at day 0 (**Fig. 4.6A,B**). After 21 days of vascular and osteogenic induction, new tissue formed more densely around the periphery of the scaffold, with no noticeable differences amongst treatment groups (**Fig. 4.6C,D**). Immunostaining for bone matrix proteins collagen I and osteocalcin was denser around the periphery of the scaffold, whereas most cells that stained positively for RUNX-2 (early osteogenic transcription factor) were located in the center (**Fig. 4.6E,F**). Quantification of these stains showed no statistical change as a result of TNF treatment (**Fig. 4.6J**). Staining for CD31 and laminin (vascular basement membrane) show vessels throughout the entire scaffold (**Fig. 4.6G,H**), with significantly greater vessel density (1.8-fold increase) and laminin intensity (1.5-fold increase) in scaffolds with acute TNF exposure (**Fig. 4.6J**). At the end of the 21-day induction period, endogenous VEGF-A expression was significantly higher after TNF treatment (**Fig. 4.6I**).

In Vivo Integration of Vascularized Osteogenic Grafts

After 14 days in vivo, graft implants showed greater extracellular matrix production (**Fig. 4.7A,B**) versus pre-implantation. The majority (55-65%) of cells within the grafts were positive for human-specific Lamin A/C (**Fig. 4.7C,D**), with no statistical difference in human cell density as a result of TNF exposure (**Fig. 4.7I**) nor when compared to the pre-implantation density (**Fig. 4.6J**), indicating high cell retention. Staining for bone matrix proteins collagen I and osteocalcin was significantly greater and more uniformly distributed compared to pre-implantation (4-fold and 3-fold change, respectively) and also increased as a result of TNF treatment (**Fig. 4.7E,F,I**). RUNX-2+ cell density was similar amongst groups,

but significantly reduced compared to pre-implantation (0.5-fold change). Some human vessels remained viable within the grafts, although significantly less than what was implanted (0.2-fold change), with no significant difference amongst treatment groups (**Fig. 4.7G,H,I**). However, there was a dense host vessel infiltration in all grafts (indicated by laminin staining), with 1.5-fold greater total vascular area in the TNF-treated group versus control.

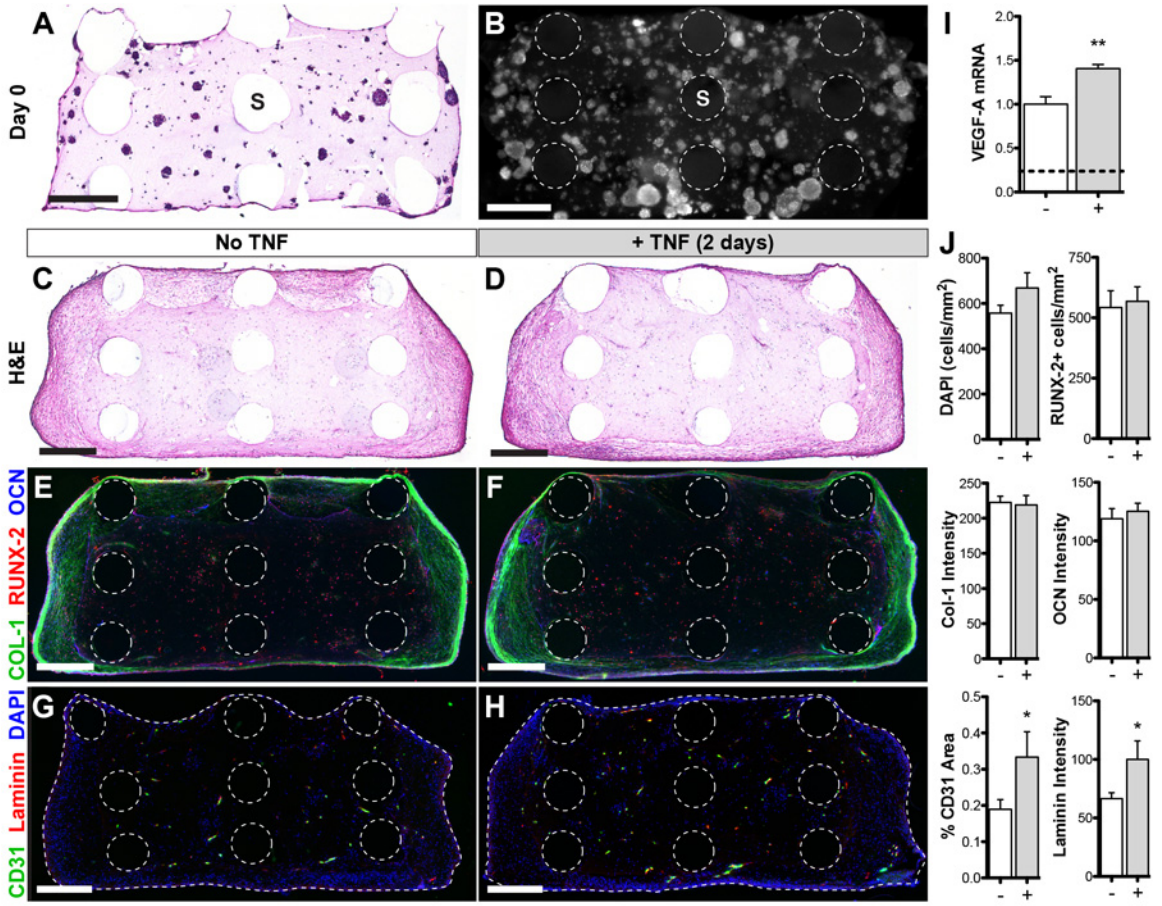

Figure 4.6. Tissue assembly within PCL-fibrin composite scaffolds. ASC aggregates were seeded with fibrin gel into the open pores of PCL scaffolds. Initial cell distribution is shown via H&E staining of a cryosection (**A**) and whole-mount DAPI staining cross-sectional view (**B**) (PCL scaffold rods: 'S'). Samples were induced to form vessels and mineral for 21 days with 20 ng/ml PDGF-BB and either no TNF (**C,E,G**) or 0.1 ng/ml TNF for 48 hours (**D,F,H**). Cryosections (10 µm thick) were stained with H&E (**C,D**) or immunostained for osteogenic (**E**,**F**) and vascular (**G,H**) markers. Dotted lines indicate the scaffold rods and tissue boundary. Scale bars = 500 µm. (**I**) VEGF-A gene expression (dotted line indicates day 0). (**J**) Quantification of immunostaining. Values shown as mean ± SEM. Significance indicated as $*p < 0.05$ or $**p < 0.01$.

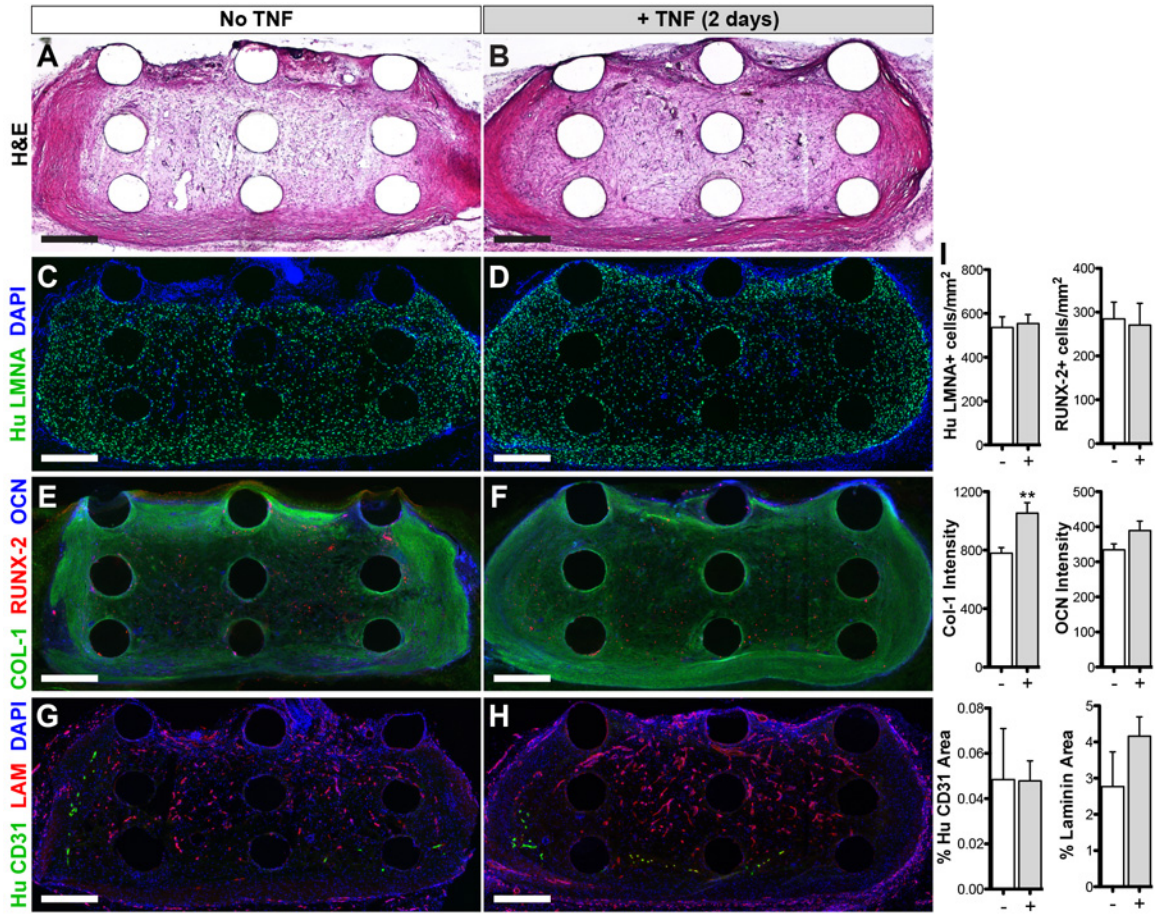

Figure 4.7. In vivo integration of vascularized osteogenic grafts. *In vitro*-induced grafts were implanted subcutaneously in athymic nude rats for 14 days. Staining of cryosections (10 μm thick): (**A,B**) H&E, (**C,D**) human-specific Lamin A/C (LMNA) to label implanted cells, (**E,F**) osteogenic markers, (**G,H**) vascular markers (human-specific CD31 and laminin (LAM) for rat/human vessels). Scale bars = 500 μm. (**I**) Quantification of immunostaining. Values shown as mean ± SEM. Significance indicated as $^{**}p < 0.01$.

4.4 Discussion

Bone is a resilient tissue that has the potential to fully heal itself after moderate injuries. When this happens, normal healing progresses towards full recovery through a tightly regulated cascade of inflammation, cellular and vascular recruitment, and a complex host of signaling molecules. However in the case of large, critical-sized defects, these normal healing cascades are disrupted due to the shear size of the defect, as well as a number of

confounding factors such as infection, mechanical instability, and absent sources of regenerative cues (i.e. periosteum, hematoma) [1, 134]. Historically, tissue engineers have vastly improved upon many of these shortcomings with the application of novel scaffolds, a variety of clinically relevant cells, and growth factors to instruct cells. More recently, inflammatory mediators have gained interest in the field because of their important roles in normal healing processes. The goal of this study was to study the effects of TNF, a key inflammatory cytokine, on vascular assembly and osteogenesis. We demonstrate that TNF acts synergistically with PDGF - another important component of the bone-healing cascade - to enhance vascularization within engineered osteogenic grafts.

Initial studies tested the effects of TNF dose on ASC osteogenesis and vascular morphogenesis in separate cultures, demonstrating that TNF has a beneficial effect on both lineages when supplied at a low dose for 48 hours. While TNF induced a moderate increase in mineralization, this was concomitant with an increase in DNA content, suggesting that the increased mineralization may be due to proliferation. However, previous studies have indicated that TNF induces increased endogenous production of bone morphogenetic protein-2 (BMP-2) in mesenchymal stem cells [128, 129], suggesting that there may be a direct osteogenic effect on the cells. Not all pro-inflammatory cytokines elicit the same response, as we conducted a similar experiment with interleukin-1β (IL-1β) that resulted in a significant increase in mineralization for all concentrations ranging from 0.1 – 100 ng/mL, but a sharp dose-dependent inhibition of vascular assembly.

In the *in vitro* model of vascularized bone development, acute (2-day) treatment with TNF increased vessel length and interconnectivity. However, continuous exposure to the same TNF dose had an adverse effect on vascular network structure. This finding is

supported by studies with endothelial cell cultures that have shown that continuous exposure to TNF can inhibit endothelial cell proliferation and growth factor responsiveness [121, 122]. In contrast to the monolayer osteogenesis experiment, mineralization was not significantly affected by the acute addition of TNF in the dual (vascular and osteogenic) induction model. This is likely due to the fact that TNF was only added during the vascular phase of culture (first two days). With the addition of PDGF, both vascularization and mineralization were improved, as was seen in our previous studies [23]. This PDGF-induced response was slightly synergistic in combination with the effects of TNF on the vascular development but not mineralization in these scaffolds. Ultimately, for in vivo applications, this improved vascular development is critical for graft survival and integration with host tissue.

Tissue development within composite fibrin-PCL scaffolds was studied before *in vivo* implantation because the spatial, mechanical, and biochemical transport properties are more complex than within a homogenous fibrin gel. Despite being uniformly seeded throughout the pores, the tissue formed more densely around the periphery of the scaffold (independent of TNF treatment) following three weeks of *in vitro* induction. This may be due to diffusion-limited gradients of oxygen and nutrients [135], given that cells form a layer of dense tissue on the scaffold periphery that may significantly reduce oxygen transfer to the central regions. Another hypothesis regards the differential constraints on the gel, which may remain fairly soft in the center, while the fibrin fibers near the edges where the PCL rods terminate are free to contract inward and stiffen [136]. Increased mechanical stiffness may play a role in facilitating the osteogenic response of ASCs [137]. Another observation at this time-point was that the majority of the cells in the center of the scaffold expressed RUNX-2, an early marker of osteogenic differentiation, suggesting that these cells may be at an earlier stage of

differentiation. Vascular growth within the scaffolds was significantly improved after TNF treatment, and may be due to an increased endogenous VEGF-A expression. Interestingly, this increase in expression was detected at the end of the 3-week culture period, which was long after the TNF stimulus was removed, indicating a long-term effect on the cells.

After *in vivo* implantation, the pre-vascularized osteogenic grafts continued to mature, as indicated by the increase in H&E staining and greater deposition of collagen I and osteocalcin throughout the center of the graft. The decrease in RUNX-2+ cells (vs. pre-implantation) may indicate progression to a more mature phenotype. Interestingly, almost all of the implanted human cells were retained after 2 weeks *in vivo*. However, the amount of human vessels decreased significantly after implantation, showing no difference in retention as a result of TNF treatment. Previous studies have indicated that pre-engineered vascular networks may lead to faster anastomosis and subsequent remodeling and replacement by host vessels, suggesting that persistence of implanted vessels may not be necessary for a positive outcome [138]. Interestingly, host vascular invasion in this study was greater in the TNF-treated grafts, which may be due to improved remodeling and replacement of human vascular networks and/or elevated endogenous expression levels of VEGF-A and MMP-9 (data not shown), which are known to promote angiogenesis [139-141]. Therefore in the current study, acute TNF treatment had a greater long-term impact on vascularization.

An important consideration regarding these *in vivo* studies is the host inflammatory response. Nude Athymic rats were used for the animal model because they lack T-cells to enable xenograft implantation, but have normal B-cell and macrophage function [142]. In these animals, as well as immuno-competent animals or patients, there will undoubtedly be some level of innate immune response due to surgical implantation. On-going studies will

investigate the role of this response on the development and functional integration of vascularized osteogenic grafts. From a clinical standpoint, the *in vivo* inflammatory environment can change based on the nature of the defect (e.g. an inflamed, compound injury versus congenital defect), infection, and anti-inflammatory drugs that the patient may be taking. While chronic inflammation and recurring infection have been shown to delay or inhibit healing of large bone defects [143, 144], the use of anti-inflammatory drugs have also been shown to slow healing rates [145-147]. These considerations further highlight the need to understand the role of the *in vivo* inflammatory environment in functional bone repair.

4.5 Conclusions

In summary, this study demonstrates how the pro-inflammatory cytokine TNF impacts vascularization of osteogenic grafts with ASCs. We have shown that acute exposure to TNF significantly improves vascular network formation within these grafts while prolonged exposure abrogates this response. The addition of exogenous PDGF synergistically enhances vascular development and simultaneously enhances mineral deposition. While this study demonstrates one application of *in vitro* pre-engineering of these grafts, the findings may have broader significance i.e. the approach may be applied to *in situ* tissue development strategies by controlling the exogenous or endogenous release of TNF *in vivo*. Our study underscores that modulation of the inflammatory response may be a powerful strategy to regulate tissue development during bone regeneration.

Chapter 5

Oxygen Is a Critical Determinant of Vascularization

5.1 Introduction and Background

Rapid vascularization is essential for the effective application of cell-based tissue engineering strategies, as cell survival is critically dependent on adequate supply of oxygen and nutrients. For example, it may take weeks for invading vasculature from the surrounding tissues to fully vascularize clinically sized, centimeter-scaled bone grafts. In the interim, diffusion of oxygen and nutrients into the center of the graft will be slow and countered by high consumption rates by the implanted cells, resulting in diffusion-limited oxygen gradients that can reach near anoxia within hours [148]. This ischemic environment is exacerbated if the surrounding tissue has incurred vascular damage due to trauma.

Previous studies have demonstrated that vascularization and blood perfusion can be accelerated by stimulating endothelial cells (EC) within the graft to form a nascent vascular network that would be capable of anastomosing with host vessels *in vivo* [11-14]. Possible sources of autologous ECs include circulating endothelial progenitor cells and ECs derived from induced pluripotent stem cells [149-151]; however, their low yields necessitate extensive *in vitro* expansion. Adipose-derived stromal/stem cells (ASC) are an abundant, single cell source of stem cells, ECs, and pericytes, making them ideal for tissue engineering

strategies that require stem cell differentiation or trophic signaling combined with vascular support. Our group has previously demonstrated that ASCs can self-assemble into interconnected, pericyte-stabilized vascular networks in fibrin gels *in vitro* [23]. These vessels assemble through EC proliferation and complex heterotypic signaling that is facilitated by aggregating the cells prior to encapsulation [23, 101].

Minimizing *ex vivo* manipulation and pre-cultivation of cells may be advantageous for clinical translation of cell-based tissue engineering approaches, which puts more emphasis on *in situ* tissue assembly and vascularization. However, there still remain several unknowns regarding the ability of ASCs to assemble into functional vascular networks within a metabolically challenging environment. Hypoxia is typically a potent stimulus for angiogenesis *in vivo* through increased expression of vascular endothelial growth factor (VEGF) by hypoxic cells [152]. ASCs similarly upregulate angiogenic factors in response to hypoxia [43, 52, 57, 153], which can promote EC survival and growth. However, when ECs themselves experience hypoxia, this can inhibit vascular assembly and stability [154] and induce apoptosis through increased production of reactive oxygen species [155, 156].

The current study aims to determine whether ASC-derived vessels can grow in hypoxia, and assesses the effects of vessel maturity (i.e. individual cells versus pre-formed vessels) on this hypoxic response. We demonstrate that there is a differential response to hypoxia depending on vessel maturity, which has important implications for vascularization strategies that utilize ASCs.

5.2 Materials and Methods

ASC isolation and culture

Human subcutaneous adipose tissue was obtained in the form of lipoaspirate from female donors (n = 3) with written informed consent under the approval of the Johns Hopkins Medicine Institutional Review Board. ASCs were isolated as previously described [101]. Briefly, tissue was digested with collagenase (1 mg/mL; Worthington Biochemical Corp.) to isolate the stromal vascular fraction of cells. These cells were plated onto tissue culture plastic and were termed "passage 0 ASC" when they reached 80-90% confluence. ASCs were used at passage 2 for all experiments. Growth medium consisted of: high glucose DMEM (Gibco) with 10% fetal bovine serum (FBS; Atlanta Biologicals), 1% penicillin/streptomycin (Gibco), and 1 ng/mL basic fibroblast growth factor (FGF-2; PeproTech). All experiments were conducted with cells from three independent donors.

Flow cytometry

Passage 2 ASCs were assessed via flow cytometry for surface expression of mesenchymal (CD73, CD105) and endothelial markers (CD31, CD34). Briefly, cells were suspended in phosphate buffered saline (PBS) containing 2% FBS and incubated with monoclonal antibodies for 30 min at 4 ºC. Cells were analyzed with a BD Accuri C6 flow cytometer. All antibodies were purchased from BD Biosciences.

Cell aggregation via suspension culture

Cells were trypsinized and resuspended at a concentration of 250,000 cells/mL in growth medium containing 0.24% (w/v) methylcellulose (Sigma). The cell suspension was pipetted into 10-cm petri dishes coated with 2% (w/v) agarose to minimize cellular adherence to the

dish. After overnight suspension culture, cellular aggregates were collected with a pipet, and then centrifuged before encapsulation procedures.

Aggregate encapsulation and culture

Cell aggregates were suspended in fibrinogen (8 mg/mL final; Sigma) and thrombin (2 U/mL final; Sigma) at a final cell concentration of 2 x 10^4 cells/μL. Fibrin gels were formed by pipetting 12 μL of gel solution into 4-mm diameter wells and incubating at 37 ºC for 30 min to allow complete gelation before adding medium. Each gel sample was fed with 1 mL of culture medium containing no added growth factors: Endothelial Basal Medium-2 (EBM-2, Lonza), 10% FBS, and 1% penicillin/streptomycin. To assess *de novo* vascular assembly, freshly encapsulated cells were immediately cultured in either normoxia (20% O_2) or hypoxia (2% or 0.2% O_2) for 6 days with no media changes to allow for cell-driven nutrient depletion. To assess growth / stability of pre-formed vessels, encapsulated cells were first cultured in normoxia for 6 days with media changed every other day to establish vascular networks. At day 6, these samples were fed once more and then cultured in either normoxia or hypoxia for an additional 6 days with no media changes. Normoxic samples were maintained in a 37 ºC incubator with 5% CO_2, 95% ambient air. Hypoxic samples were placed in a modular incubator chamber (Billups-Rothenberg) that was flushed every other day with pre-mixed gas (0.2% or 2% O_2 / 5% CO_2 / N_2 balance) and placed in a 37 ºC incubator.

Viability and metabolism assessments

To assess cell viability, samples were incubated with LIVE/DEAD Viability/Cytotoxicity solution (Molecular Probes) for 30 min at 37 ºC, washed with PBS,

and imaged with a confocal microscope. Total DNA content was measured to gauge total cell number using the Quant-iT PicoGreen dsDNA Assay (Invitrogen) as previously described [101]. Glucose and lactate content in culture media were quantified using Glucose Assay Kit and L-Lactate Assay Kit I (Eton Bioscience) and subtracted from day 0 values to calculate consumption or production, respectively. These values were normalized to DNA content (pmol / cell).

Enzyme-linked immunosorbent assay

To assess endogenous growth factor production, cells were cultured in 0.5 mL of serum-free medium (EBM-2 + 1% penicillin/streptomycin) for 48 hours in either normoxia (20% O_2) or hypoxia (0.2% or 2% O_2). Supernatant was collected and assayed for VEGF and FGF-2 using human ELISA kits (PeproTech) according to the manufacturers protocol. Cells were also harvested and assayed for total DNA content to normalize growth factor production to cell number (ng / 10^6 cells).

BrdU labeling

Cells were incubated with bromodeoxyuridine (BrdU, Sigma) to detect proliferating cells. Briefly, 10 μM BrdU was pipetted into existing culture medium (i.e. medium was not changed), and samples were quickly returned to their appropriate oxygen environment (less than 5 minutes of normoxic exposure) for a 20-hour incubation. Samples were then washed with PBS and fixed with 3.7% formaldehyde. Incorporated BrdU was detected via whole-mount immunostaining.

Whole-mount immunostaining

Whole-mount immunostaining of fibrin gels was performed as previously described [23]. Briefly, samples were fixed with 3.7% formaldehyde for 3 hours at 4 ºC, washed with PBS, and blocked with 5% normal goat serum / 0.2% Triton X-100 / PBS for 3 hours at 4 ºC. Antibodies were incubated overnight at 4 ºC, followed by three 1-hour washes in PBS with 0.1% Tween. Primary antibodies included: mouse anti-human CD31 (4 μg/mL, Sigma) and Cy3-conjugated mouse anti-alpha smooth muscle actin (□SMA; 7 μg/ml, Sigma). One secondary antibody was used: DyLight 488-conjugated goat anti-mouse (1:400, Jackson ImmunoResearch).

Prior to staining for BrdU, samples were stained for all other antigens and post-fixed with 3.7% formaldehyde for 30 min to preserve the stain. Samples were then denatured with 2N HCl / 0.5% Triton X-100 for 45 minutes at room temperature, washed, re-blocked, and then incubated with AlexaFluor 647-conjugated mouse anti-BrdU (4 μg/mL, Invitrogen) overnight at 4 ºC. Cell nuclei were counterstained with 4'-6-diamidino-2-phenylindole (DAPI; Sigma).

Imaging and analysis

Immunostained gels were mounted on glass slides and imaged using a Zeiss LSM 510 confocal microscope (5x and 20x objectives). Confocal z-stacks were z-projected and thresholded for quantification. AngioQuant software [71] was used to quantify total vessel length (sum of the lengths of all vessel branches within a gel). Image J software (NIH) was used for all other image analysis. Pericyte coverage was defined as αSMA+ area within at least 5 μm of the abluminal face of vessel networks. Briefly, vessel networks were selected in

the CD31 channel of thresholded image composites. Selections were enlarged by 5 μm at all edges and applied to the αSMA channel. αSMA+ area fraction within the selected area was measured and displayed as "% Pericyte Coverage". BrdU+ nuclei were counted with the Analyze Particles command. BrdU counts from the whole gel indicate overall proliferation within the culture (displayed as "Total # BrdU+"). To assess proliferation within the vessels only, CD31+ vessel area was selected and applied to the BrdU channel prior to counting within the selected area. This count was normalized to the CD31+ vessel area to account for differences in vessel density and is displayed as "# BrdU+ / CD31 (mm^2)". To approximate the survival / persistence of ECs within the culture, the total number of independent CD31+ units (ranging from solitary cells to small vessels) was counted and divided by the day 0 count. Briefly, whole-gel images were thresholded and assessed with the Analyze Particles command.

Quantitative RT-PCR

Total RNA was isolated using a TRIzol (Invitrogen) extraction method and quantified using a NanoDrop spectrophotometer (Thermo Scientific). Reverse transcription was performed with 1 μg of total RNA using iScript cDNA Synthesis Kit (BioRAD). Complementary DNA was amplified using SYBR Green PCR Master Mix (Applied Biosystems) and a StepOnePlus Real-Time PCR System (Applied Biosystems). Expression levels were calculated by the comparative C_T method using β-Actin as an endogenous reference gene. Primers included:

(i) β-Actin [RefSeq: NM_001101] – sense: 5'-AGTTGCGTTACACCCTTTCTTG-3', antisense: 5'-TCACCTTCACCGTTCCAGTTT-3'

(ii) VEGF-A [RefSeq: NM_001025368] – sense: 5'-GCCTTGCCTTGCTGCTCTA-3', antisense: 5'-GATTCTGCCCTCCTCCTTCTG-3'

(iii) VEGFR-2 [RefSeq: NM_002253] – sense: 5'-AGTCTGTGGCATCTGAAGGC-3', antisense: 5'-ACGGTGGTGTCTGTGTCATC-3'.

Statistical analysis

All experiments were conducted with cells from three independent donors (n = 3 samples per donor). Quantitative data are expressed as mean ± standard error. Statistical analyses were performed using GraphPad Prism 5 software. Statistical significance was determined by one-way ANOVA with Tukey's post-test and is denoted as $*p < 0.05$, $**p < 0.01$, $***p < 0.001$.

5.3 Results

Cell characterization

Passage 2 ASCs from multiple donors were predominantly positive for mesenchymal markers, CD73 (99.3 ± 0.2%), and CD105 (98.7 ± 0.5%), with very few cells positive for the mature endothelial marker CD31 (1.1 ± 0.1%) (**Fig. 5.1A**). Approximately half of the population expressed CD34 (46.9 ± 11%), which is expressed by native ASCs as well as endothelial progenitors.

Spontaneous self-assembly of vessels

Aggregated ASCs (**Fig. 5.1B**) spontaneously self-assembled into vascular networks in 6 days without any exogenously added growth factors (**Fig. 5.1C-D**). This was reproduced

with cells from multiple donors (**Fig. 5.1D**). Vascular assembly still occurred even when medium was not replenished for the entire culture period, which sets the basis for the vascular assay in subsequent experiments. By only feeding at the start of culture, there will be cell-driven nutrient depletion and waste buildup to simulate the ischemic conditions that arise after *in vivo* implantation of avascular grafts.

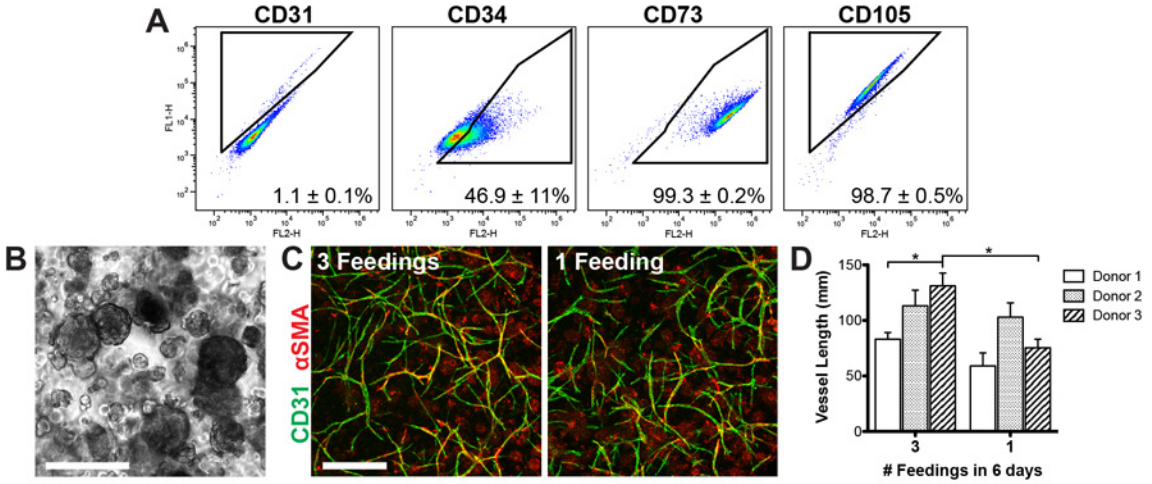

Figure 5.1. Cell characterization and spontaneous vascular assembly. (**A**) Flow cytometric analysis (average of three donors). (**B**) Morphology of cell aggregates immediately after fibrin encapsulation. (**C**) Vessels assembled within 6 days of culture in medium containing no added growth factors with routine (three) feedings or a single feeding at the onset of the culture. (**D**) Quantification of total vascular network length. Scale bars = 200 μm (B), 500 μm (C).

Viability and growth factor production in hypoxia

ASCs cultured for 6 days in 0.2%, 2%, and 20% O_2 all demonstrated high viability (**Fig. 5.2A**) and similar DNA content (**Fig. 5.2B**). Endogenous secretion of the potent angiogenic growth factor VEGF was upregulated in hypoxia (**Fig. 5.2C**) relative to normoxic conditions, while another angiogenic growth factor, FGF-2, was down-regulated at 0.2% and 2% O_2 relative to 20% O_2 cultures (**Fig. 5.2D**).

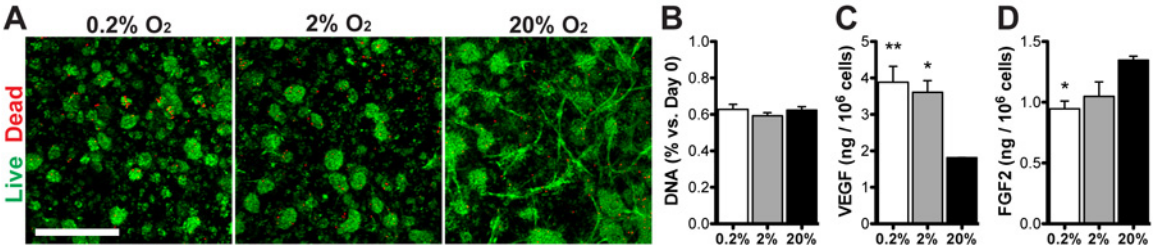

Figure 5.2. ASC viability and growth factor production. ASCs were fed at day 0 and maintained in 0.2%, 2%, or 20% O_2 for 6 days. (**A**) Live/Dead staining was used to assess viability at day 6. The number of viable (green) cells appeared similar in all groups. (**B**) The total DNA content normalized to day 0 was also similar in all groups. (**C,D**) VEGF and FGF2 production was assessed in all groups via ELISA after 48 hours in serum-free medium and normalized to DNA content. Scale bar = 500 μm. Significance indicated versus normoxia (20% O_2).

De novo vascular assembly is inhibited by hypoxia

To assess the effects of hypoxia/ischemia on *de novo* vascular assembly, freshly encapsulated cells were immediately transitioned into the 6-day hypoxia assay (**Fig. 5.3A**). Vascular assembly was substantially inhibited in both moderate (2% O_2) and severe (0.2% O_2) hypoxia (47% and 11% total vessel length versus normoxia, respectively) (**Fig. 5.3B,F**). Pericyte coverage of vessels was 3-fold less in hypoxia (**Fig. 5.3C,G**). Vessel proliferation was also significantly lower in hypoxia (**Fig. 5.3H**), even when normalized to vessel area (**Fig. 5.3D**). Interestingly, the majority of proliferating cells throughout the culture are vascular cells (**Fig. 5.3I**) (62%, 86%, and 90% of BrdU+ nuclei co-localize with CD31 in 0.2%, 2%, and 20% O_2, respectively), which corresponds to a similar reduction in proliferation within the total population (**Fig. 5.3E**). To approximate EC persistence within the cultures, we assessed the total number of spatially distinct CD31+ entities. These numbers were not significantly different in 0.2% or 2% O_2 as compared to the number of CD31+ cells at day 0 (82.0% and 98.4% respectively) indicating that the majority of ECs survived in all oxygen conditions.

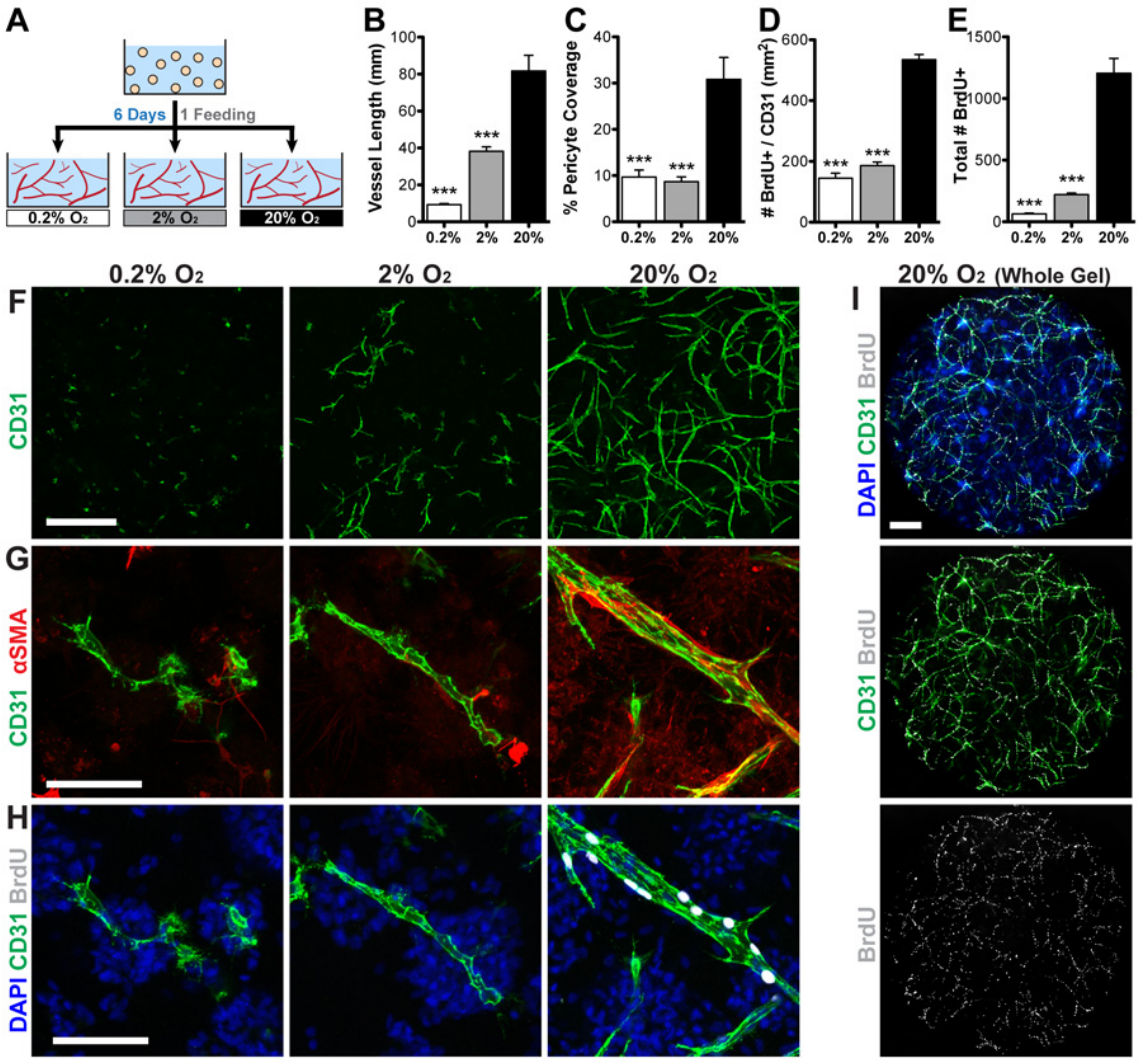

Figure 5.3. Hypoxia inhibits *de novo* vascular assembly. (**A**) Experimental approach. Vascular length (**B,F**) and pericyte coverage (**C,G**) were significantly inhibited in hypoxic conditions versus 20% O_2. Proliferation (BrdU incorporation) was significantly reduced in hypoxia in vascular cells (**D,H**) and the entire population (**E**). Vascular cells constituted the majority of proliferating cells within the culture (**I**). Scale bars = 500 μm (F,I), 100 μm (G,H). Significance indicated vs. 20% O_2.

Pre-formed vessels grow more in hypoxia

To assess the effects of hypoxia on pre-formed vascular networks, ASCs were first allowed to self-assemble into a nascent vascular network for 6 days in normoxia with routine feedings before transitioning into the 6-day hypoxia assay (**Fig. 5.4A**). Contrary to the previous experiment, pre-formed vascular networks survived and continued to grow more in

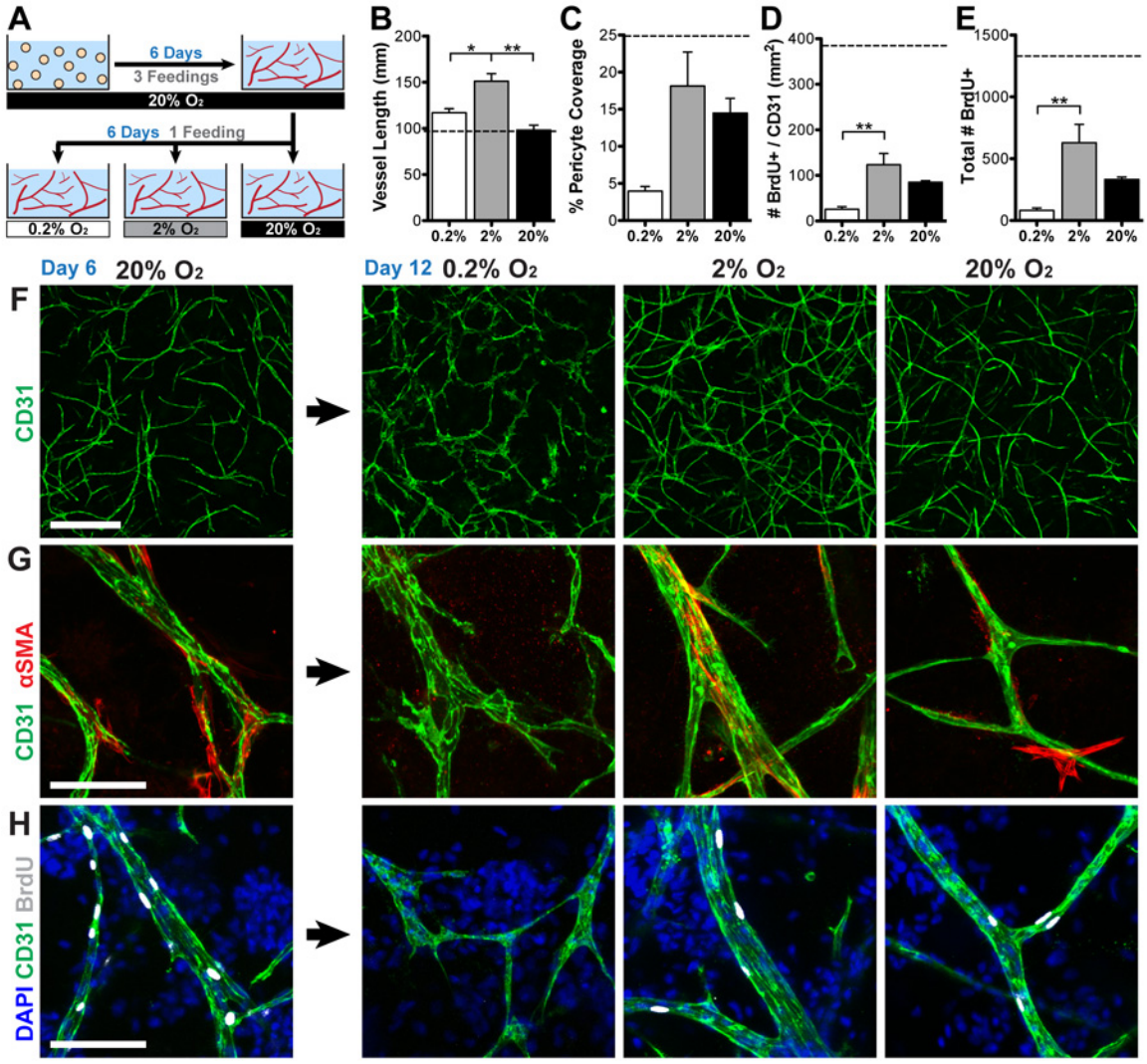

Figure 5.4. Moderate hypoxia enhances the growth and stability of pre-formed vessels. (**A**) Schematic of the experimental approach. (**B,F**) Vessels grew significantly longer in hypoxia by day 12 versus day 6 (dotted line), with the greatest length in 2% O_2. (**C,G**) Pericyte coverage decreased in all groups relative to day 6 (dotted line) but was highest in 2% O_2. (**D,E,H**) Proliferation (BrdU incorporation) decreased in all groups relative to day 6 (dotted lines) but remained highest in the 2% O_2 group. Scale bars = 500 μm (F), 100 μm (G,H). Significance indicated vs. 20% O_2.

hypoxia than normoxia (1.21, 1.56, and 1.01-fold increase in vascular length versus day 6 for 0.2%, 2%, and 20% O_2, respectively) (**Fig. 5.4B,F**). Vessels also became wider in 2% O_2, whereas those in 0.2% O_2 developed a highly destabilized morphology. Pericyte coverage

(**Fig. 5.4C,G**) and cell proliferation (**Fig. 5.4D,E,H**) decreased in all groups after continued culture (versus day 6); however, they remained highest in 2% O_2 and lowest in 0.2% O_2.

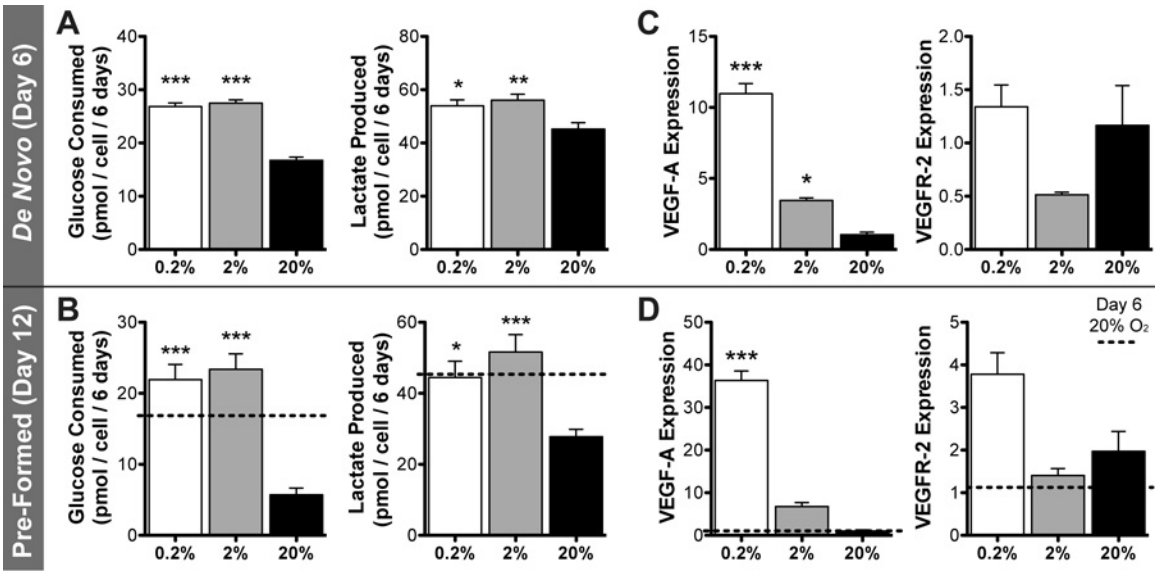

Figure 5.5. Comparison of ASC metabolic activity and gene expression immediate versus delayed hypoxia. Glucose consumption and lactate production increased in 0.2% and 2% O_2 relative to 20% O_2 after 6 days of immediate hypoxia (*de novo* vascular assembly) (**A**) and delayed hypoxia (6 days of pre-culture in normoxia) (**B**). By day 12, continued normoxic culture resulted in reduced glucose and lactate metabolism versus day 6 (dotted lines), whereas hypoxic conditions increased glucose consumption. (**C**) mRNA expression of VEGF-A was substantially upregulated in hypoxia, with highest expression in 0.2% O_2. VEGFR-2 expression was reduced in 2% O_2, but unchanged in 0.2% O_2 relative to normoxia. (**D**) Changes in VEGF-A and VEGFR-2 expression were even greater following delayed-onset hypoxia. Significance indicated versus normoxia (20% O_2).

Metabolism & gene expression

ASCs in hypoxia significantly increased glucose consumption and lactate production (**Fig. 5.5A**). When cells were pre-cultured in normoxia for 6 days before the onset of hypoxia, there was an even greater glycolytic increase in hypoxia relative to normoxia by day 12 (**Fig. 5.5B**); however, basal levels of glucose consumption and lactate production were significantly lower after extended culture (2.9- and 1.6-fold decrease, respectively; day 12 vs. day 6). Expression of VEGF-A mRNA increased substantially after 6 days in hypoxia (**Fig. 5.5C**) and was an additional two- to three-fold higher in cells that were pre-cultured for 6

days before hypoxia (**Fig. 5.5D**). VEGF receptor-2 (VEGFR-2) mRNA expression was lower in 2% O_2, but similar in 0.2% O_2 versus normoxia (**Fig. 5.5C**). Samples that were pre-cultured before hypoxia demonstrated elevated VEGFR-2 expression at day 12 versus day 6 (end of pre-culture) and the highest expression in 0.2% O_2 (**Fig. 5.5D**).

5.4 Discussion

Rapid vascularization is critical for the survival of cell-seeded tissue grafts after implantation, as inadequate diffusion of oxygen and nutrients may lead to cell death and tissue necrosis. ASCs, which exhibit spontaneous vascular self-assembly, may be a suitable cell population for providing tissue engineered grafts with an intrinsic vascular network [23]. In this study, we tested whether this capacity for vascular assembly would be impacted by hypoxia, which might be expected following *in vivo* implantation into a defect site. We demonstrated that hypoxia severely inhibits *de novo* vascular assembly of ASCs, but promotes further growth of pre-formed vascular networks.

In this study, we removed all exogenously added growth factors (except for what may be in FBS) and demonstrated that ASCs are still able to rapidly and spontaneously assemble into vascular networks. This finding suggests that endogenous biochemical and physical signals may be instructing this cellular self-assembly. For example, ASCs express detectable levels of angiogenic growth factors VEGF and FGF-2 (1.81 and 1.35 ng / 10^6 cells / 2 days in normoxia, respectively). For this study, growing the cells without exogenous growth factors allows for a more direct assessment of cellular behavior in response to hypoxia.

In addition to low oxygen tension, transplanted cells will also experience cell-driven nutrient depletion and waste build-up, making the environment gradually ischemic. To

replicate this environment, cells were only fed at the start of the 6-day "simulated implantation" period during which oxygen tension was varied. A direct comparison of multiple media changes versus none shows that vessel network growth is slightly reduced but only significantly in one of the three tested donors.

Viability of ASCs remained high in all oxygen tensions, with no significant difference in cell number even in 0.2% oxygen. The cells may have compensated for reduced oxygen availability by shifting their metabolism more towards anaerobic glycolysis, as glucose consumption and lactate production were both significantly higher in hypoxia. Similar hypoxic resiliency and metabolic shifts have been demonstrated in ASCs [157] and other cell types [158, 159]. This finding is promising regarding the ability of ASCs to endure harsh ischemic environments after transplantation.

Hypoxic ASCs increased endogenous expression of the potent angiogenic factor VEGF. This is in agreement with previous reports that ASCs increase angiogenic factor production in hypoxia [43, 52, 57, 153]. Interestingly, expression of another important angiogenic factor, FGF-2, was reduced in hypoxia. Despite the high overall viability and increased VEGF expression, *de novo* vascular assembly of ASCs was substantially inhibited in hypoxia. This finding is likely due to reduced proliferation of ECs, as BrdU incorporation was significantly reduced within vessels. Substantial apoptosis is unlikely, as the total number of independent vessel structures (often individual cells in 0.2% O_2 and small vessels in 2% O_2; **Fig. 3F**) was not significantly reduced when compared to the number of ECs encapsulated at day 0. This metric of counting vessels and cells alike as just one cell is based on our earlier studies that demonstrated that each vessel arises from an individual EC [101]. Pericyte coverage was significantly reduced on hypoxic vessels, which is similar to our previous findings in

monolayer ASC cultures [101]. Those monolayer experiments, however, demonstrated no significant change in vessel length when grown in hypoxia, which is an interesting observation that warrants further investigation.

Hypoxia is a potent stimulus for angiogenesis *in vivo*, inducing increased VEGF expression that recruits the sprouting and growth of pre-formed vessels. Angiogenic vessels may not experience severe hypoxia themselves, as they are constantly near a source of blood, only responding to indirect indicators of hypoxic stress. The *de novo* vascular assembly model presented in this study is fundamentally different from angiogenic sprouting in a number of ways, including the fact that the ECs are immature and are not a part of a vessel when the metabolic insult begins. Therefore, we assessed the effects of hypoxia on vessels that were first grown in a normoxic environment with routine media changes to establish healthy vascular network structures. Surprisingly, hypoxia induced increased vascular growth versus normoxia when vessels were pre-formed. By day 12, vessels demonstrated maximal growth, proliferation, and pericyte coverage in 2% O_2. While the vascular networks in 0.2% O_2 also increased in length, endothelial morphology indicated destabilization of the vascular structure. This observation may be due to the 36-fold increase in endogenous VEGF-A expression, which can cause pericyte detachment and loosening of EC junctions to prime vessels for sprouting [160].

The results of these experiments indicate a differential response of ECs within ASC cultures towards hypoxia depending on whether they are individual cells or incorporated into a pericyte-stabilized tissue structure. Despite similar global changes in metabolism and growth factor expression in each experimental approach, there were marked differences in EC proliferation and overall vessel growth. Vessel maturity and stabilization likely plays a

role in this complex system. Pericyte investment promotes EC survival through the expression of VEGF-A and anti-apoptotic factors [161]. Interestingly, the extended culture period experienced by the pre-formed vessels resulted in decreased glycolytic activity and proliferation, but increased expression of VEGF-A and VEGFR-2 versus earlier timepoints. It is possible that the early phase of *de novo* vascular assembly requires higher proliferation and metabolic activity in order to initiate the nascent vascular plexus, and is therefore dramatically inhibited when the oxygen tension is reduced.

The findings of this study have important implications on vascularization strategies for tissue engineering. Immediate encapsulation and implantation of ASCs into hypoxic tissues may impair their ability to assemble into functional vascular networks. However, delaying this exposure to hypoxia may result in improved vascularization. This may be achieved by pre-assembly of vascular networks prior to implantation or through oxygen delivery strategies *in situ* [162-164]. The *in vivo* tissue environment is certainly much more complex, with inflammation, cellular invasion, and other biological signaling occurring after implantation of a cell-seeded graft. On-going *in vivo* studies are necessary to completely understand the impact of this complex post-implantation environment on the ability of ASCs to functionally vascularize a graft *in situ*.

5.5 Conclusions

This study reveals striking phenomena and provides important insights into the differential responses of ASC-derived vessels to hypoxia. ASCs are a heterogeneous population of stem cells. Sub-populations of ECs and pericytes present within the ASCs can spontaneously self-assemble through tightly orchestrated heterotypic interactions, but this

system is remarkably sensitive to changes in oxygen levels. Depending on the stage of tissue assembly and maturity, hypoxia may have disparate effects. We demonstrated that moderate hypoxia has a negative impact on *de novo* vascular assembly but positively impacts the stability and growth of pre-formed vessels. These novel findings are of importance to the tissue engineering field and may instruct future vascularization strategies.

Chapter 6

Conclusions and Future Perspectives

The data presented here demonstrate the ability of a heterogeneous cell source to build a complex tissue through endogenous self-assembly mechanisms and exogenously controlled biochemical environments. This final chapter summarizes the most important conclusions, contributions, and future research directions that have resulted from this work.

6.1 Conclusions and Contributions

Aim 1 Conclusions

Chapter 2 describes the ability of ASCs to spontaneously self-assemble into three-dimensional (3D) vascular networks. These surprisingly mature vessels displayed classic morphology: patent lumens, sprouting endothelial tip cells, invested pericytes, and vascular basement membrane. Observations from a detailed time course study and a serial passaging experiment revealed that these complex vessels originated from existing sub-populations (<1%) of endothelial cells and pericytes that were likely derived from the adipose tissue microvasculature and diminish *in vitro* through continuous passaging. Vascular growth required extensive endothelial proliferation and was facilitated by increasing direct cell-cell contacts (e.g. high cell density in monolayer and spheroid aggregation in 3D gel culture). Pericyte recruitment was mediated by PDGF receptor signaling.

This chapter established a 3D vascularization model: ASCs were aggregated into multicellular spheroids overnight, encapsulated in fibrin gels, and cultured for up to 14 days

in medium containing angiogenic growth factors. This experimental model yields highly interconnected vascular networks, setting the foundation upon which the remainder of this thesis was built. The body of work described in this aim resulted in one journal publication (featured on the cover), six conference abstracts, and a pre-doctoral fellowship application (successfully funded).

Aim 2 Conclusions

The body of work that spans Chapters 3 and 4 established an *in vitro* model to induce vascularized bone development by recapitulating key factors that initiate native bone repair. It was first demonstrated that the classic inductive factors in osteogenic medium are inhibitory to ASC vascular assembly. This necessitated the development of a step-wise approach in which vessels are allowed to grow and stabilize for one week in purely vascular medium before osteogenic factors are added. While this approach mitigated the initial inhibition of growth, vessel stability in the presence of osteogenic factors was poor, leading to gradual regression. After extensive literature review, key factors were identified that initiate angiogenesis and osteoprogenitor recruitment / activation in native bone injury: PDGF (released by activated platelets) and pro-inflammatory cytokines (released by activated macrophages; eventually narrowed down to TNF). Each of these factors was studied in great detail, looking at their effects on osteogenesis and vascular assembly separately and in the vascularized bone model.

Chapter 3 describes the unique ability of a single growth factor, PDGF-BB, to substantially increase both osteogenesis and vascular stability, resulting in greatly improved vascularized bone constructs compared to existing *in vitro* literature. Chapter 4 further

improved upon this model by demonstrating that acute (48-hour) exposure to TNF significantly improves vascular assembly in vascularized bone grafts, and provides synergistic improvement when combined with PDGF-BB. These pre-engineered vascularized bone grafts were tested *in vivo* in a subcutaneous model. Bone matrix continued to mature *in vivo,* and was combined with extensive host angiogenic ingrowth. However, engineered vessels became less dense, either because of regression or remodeling by the host.

This aim illustrated several important points: (i) ASCs are capable of forming vessels and mineralized matrix in the same tissue construct, (ii) a biomimetic approach towards vascularized bone engineering yields improved development of complex tissue structures, (iii) additional unknowns remain regarding how the *in vivo* environment will impact ASC vascularization. This body of work resulted in five journal publications (one featured on the cover), seven conference abstracts, and one provisional patent.

Aim 3 Conclusions

Chapter 5 demonstrated that oxygen tension is a critical determinant of ASC vascular morphogenesis. This topic was of great interest given the ischemic environment that cells would face in a large bone defect environment. Initial experiments demonstrated high cell viability and increased endogenous production of VEGF in hypoxia. However, the major finding was that hypoxia severely inhibits *de novo* vascular assembly, but promotes growth and stability when the onset of hypoxia is delayed until after vessels have assembled. This finding correlated with changes in endothelial proliferation, suggesting that hypoxia differentially impacts endothelial growth depending on the maturity of the tissue. The findings in this study have will instruct future *in vivo* research directions in our lab and may

have important implications for the vascular tissue engineering field as a whole. This work resulted in one journal publication and one conference abstract.

6.2 Future Perspectives

This dissertation established feasibility for the use of ASCs to engineer vascularized bone and identified numerous factors that guide the cells towards more robust tissue formation. The majority of the work was conducted *in vitro*, which allowed for a controlled microenvironment in which to study cellular behavior. However, *in vivo* studies are the necessary next step to understand the real therapeutic potential of this approach, as the complexity and dynamics of *in vivo* environments will undoubtedly affect cellular behavior. Additionally, the development of a clinically translatable approach will likely require reduced *ex vivo* manipulation and pre-cultivation of cells, working towards the ideal of achieving complete tissue assembly from freshly implanted cells within the defect site (i.e. *in situ*).

An important question that arises when moving from *in vitro* to *in vivo* is – "How much of what we have learned holds true *in vivo*?" An essential study will be to assess the dynamics of ASC vascular morphogenesis *in vivo* within a bone defect. As was demonstrated in Chapters 4 and 5, ASC vascular assembly is drastically impacted by inflammatory cytokines and changes in oxygen tension. Therefore, the complexity and dynamics of the innate immune response and local ischemia within a bone defect will have an impact that is not yet known. Depending on the nature of the study, it may be advantageous to utilize autologous or syngeneic ASC sources within an immunocompetent animal model (e.g. mouse ASC into mouse model) so that the cells may be studied in the context of a completely intact immune response.

Modulating the bone defect microenvironment through controlled release of factors or biomaterial modifications may allow for tighter control of cellular responses. For example, a study could expand upon the findings in Chapter 3 to understand how exogenous PDGF-BB impacts ASC vascularization and osteogenesis *in vivo*. This study would be fundamentally different from my existing work because bone provides a more complex osteoinductive environment than the factors provided *in vitro*.

The insights gained in Chapter 5 illustrate the need to tune the oxygen environment in order to maximize ASC vascular assembly and growth. ASCs placed in an ischemic environment and/or a very large, densely seeded scaffold will rapidly experience hypoxia. This scenario resulted in poor vascular assembly in my *in vitro* studies. As discussed in Chapter 5, methods to delay the onset of hypoxia may greatly improve the ability of vessels to pre-form and become stabilized. Therefore, future studies could address this challenge by locally producing / delivering oxygen from the scaffold through chemical [162-164] or physical means [unpublished method from our lab].

Clinical adoption of cell therapies for tissue regeneration has been limited by challenges such as safety, efficacy, reproducibility, and cost. Currently, intraoperative procedures appear be the most viable option to lower these hurdles by minimizing *ex vivo* manipulation and culture of cells. This means that the cells would be isolated, processed, and transplanted back *in vivo* without leaving the operating room. Therefore, freshly isolated SVF may be more translatable than cultured ASCs. Uncultured SVF contains at least 10-fold greater endothelial population than what was used in my studies, which may result in improved vascularization potential. Additional studies are required to assess the vascular and osteogenic properties of SVF, both *in vitro* and *in vivo*.

Appendix: Supplementary Protocols

A1. Isolation of Adipose-Derived Stem Cells

1. Transfer lipoaspirate into multiple 50 ml tubes (up to 20 ml / tube). Add an equal volume of warm collagenase solution (1 mg/mL Collagenase Type I + 10 mg/mL bovine serum albumin + PBS with Ca^{2+}). Shake tube to mix well.
2. Place all tubes on an orbital shaker (laying sideways for ample agitation) inside a 37ºC incubator for 1 hour or until the tissue appears smooth.
3. Centrifuge the tubes at 300 g for 5 min. Shake the tubes to disrupt the cell pellet. Centrifuge again at 300 g for 5 min (dislodges residual adipocytes from pellet).
4. Using a serological pipet, carefully remove the top (oil / fatty tissue) and middle (mostly collagenase) layers, and discard into a waste bottle. Leave the bottom ~5mL to avoid disrupting the SVF pellet.
5. Resuspend the pellet with ~20 mL of PBS. Pass the cell suspension through a 100-μm cell strainer. Collect in fresh 50 ml tubes. Bring volume up to 50 mL with PBS. Centrifuge at 300 g for 5 min. Remove all oil and PBS with a pipet.
6. Resuspend pellet in 10 - 20 ml of 1X RBC lysis buffer. Incubate 7 min. Pour PBS into the tubes to dilute the buffer, then centrifuge at 300 g for 5 min.
7. Resuspend the cell pellet in 10 ml of medium. Count cells.
8. Split cells into the appropriate number of flasks (T-175 flask: ~ 33 ml of lipoaspirate tissue or 10 - 15 x 10^6 cells). Culture in high glucose DMEM + 10% FBS + 1% pen/strep + 1 ng/mL FGF-2 until ~80% confluent (~4-6 days).

A2. Cell Aggregation in Suspension Culture

1. Prepare a 1.2% (w/v) methylcellulose stock solution in basal medium. Advanced preparation requires autoclaving the powder and overnight mixing steps [165].
2. Dilute methylcellulose 1:5 in culture medium. Warm to 37ºC.
3. Coat 10-cm petri dishes (non-TC-treated is fine) with 6 mL of sterile 2% agarose. While still liquid, swirl the dishes to evenly distribute the agarose. Set at room temperature for 10 min, followed by 10 min at 4ºC. Add 6 mL of basal medium to each dish. Equilibrate at 37ºC for at least 30 min. Carefully aspirate the DMEM from each dish prior to adding cells.
4. Suspend trypsinized cells to 250,000 cells/mL in methylcellulose working solution. Pipet 5 – 6 mL of cell suspension into each dish ($1.25 – 1.5 \times 10^6$ cells/dish).
5. Transfer dishes to 37ºC incubator overnight (~15-20 hours). Do not stack more than 2 dishes together. Taller stacks result in larger, more heterogeneously sized clusters.

A3. Preparation of PDMS Molds for Casting Gels

1. Obtain Polydimethylsiloxane (PDMS) – Dow Corning Sylgard 184 kit
2. Mix the PDMS base and curing agent at a 10:1 ratio (w/w). Weigh in a medium-sized disposable weigh boat. Stir well with a disposable spatula.
3. Remove air bubbles by placing the mixed solution in a vacuum desiccator for 10 min.
4. Pour the PDMS solution into a mold to cast a flat sheet (e.g. large-sized disposable weigh boat). Note that the quantity of PDMS solution and the geometry of the mold will determine the thickness of the resulting sheet. Optimize according to the desired final thickness (e.g. 1.2 – 1.5 mm). Equilibrate for 5 min at room temperature.

5. Incubate at 80ºC for 20-60 min or until fully solidified.
6. Remove the solid PDMS sheet from the mold. Punch custom cylindrical molds using biopsy punches (e.g. a ring shape with 6 mm I.D. and 12 mm O.D.). The inner diameter represents the size of the hydrogel.
7. Autoclave molds to sterilize. Place molds in tissue culture multi-well plates using sterile forceps. Clean PDMS (i.e. no dust) should stick / bond completely to the plate such that liquid cannot pass underneath.

A4. Cell Encapsulation in Fibrin Gels

1. Prepare 10 mg/mL fibrinogen in PBS without Ca^{2+}. Sterile filter prior to use. Store at 4ºC and use within 1 day. Prepare 10 U/mL thrombin in PBS with Ca^{2+} from sterile stocks. Make fresh each day.
2. Suspend cells in fibrinogen at 25% greater concentration than desired to account for the addition of thrombin. Aliquot the suspension into multiple 0.5 mL tubes with each containing enough volume for only 3 gels (e.g. 92 μL of fibrinogen for 3 x 35 μL fibrin gels) because gelation will be fairly rapid (< 1 min) after thrombin is added.
3. To each aliquot of fibrinogen + cells, add thrombin at a 1:4 ratio. Final concentrations should be 8 mg/mL fibrinogen and 2 U/mL thrombin.
4. Mix well and pipet 3 gel volumes into PDMS molds (e.g. 15 μL into 4 mm I.D. or 35 μL into 6 mm I.D. results in a gel with 1 mm thickness). Change pipet tips and repeat for each aliquot.
5. Incubate for 30 min at 37ºC for complete gelation before adding medium to the well. Gels will stay inside the PDMS for the entire culture period.

A5. Whole-Mount Immunostaining

1. Technical Notes: All steps occur at 4ºC on a rocker. Transfer samples into 2 mL round-bottom tubes for improved agitation. Biological replicates can be combined into the same tube. Keep tubes upright at ~125 rpm during small-volume incubation steps and side-ways at ~75 rpm during large-volume wash steps. All wash steps are in 1.5 mL of 0.1% Tween-20 in PBS (PTw). Antibodies are diluted in 5% normal serum in PTw and utilize a minimal volume to cover the samples (e.g. 100 μL).
2. Gently release the gels from their PDMS molds by cutting the edges of the gel with an equal-sized biopsy punch. Transfer gels to 2 mL tubes.
3. Block and permeabilize in 5% normal serum + 0.2% Triton X + PBS for 2+ hours
4. Incubate with primary antibodies overnight. Wash 3 x 1 hour.
5. Incubate with secondary antibodies for overnight (can be shortened to several hours at room temperature, but may increase background). Wash 3 x 1 hour.
6. Note: Co-staining with two mouse primaries (e.g. CD31 and αSMA) must be done sequentially. Follow the complete staining protocol (through Step 5) for the unconjugated primary, then re-block with mouse serum for 1 hour before incubating with the conjugated primary overnight. This lengthens the entire process by 1 day.
7. Mount onto glass slides for imaging

Bibliography

1. J.P. Schmitz and J.O. Hollinger, *The critical size defect as an experimental model for craniomandibulofacial nonunions*. Clin Orthop Relat Res, 1986. 205): 299-308.
2. *2010 Bone Grafts and Bone Substitutes*. Orthopedic Network News, 2010. 21(4): 16-19.
3. H.C. Pape, A. Evans and P. Kobbe, *Autologous bone graft: properties and techniques*. J Orthop Trauma, 2010. 24 Suppl 1(S36-40.
4. K.M. Dupont, K. Sharma, H.Y. Stevens, J.D. Boerckel, A.J. Garcia and R.E. Guldberg, *Human stem cell delivery for treatment of large segmental bone defects*. Proc Natl Acad Sci U S A, 2010. 107(8): 3305-3310.
5. V. Viateau, G. Guillemin, V. Bousson, K. Oudina, D. Hannouche, L. Sedel, D. Logeart-Avramoglou and H. Petite, *Long-bone critical-size defects treated with tissue-engineered grafts: a study on sheep*. J Orthop Res, 2007. 25(6): 741-749.
6. Y. He, Z.Y. Zhang, H.G. Zhu, W. Qiu, X. Jiang and W. Guo, *Experimental study on reconstruction of segmental mandible defects using tissue engineered bone combined bone marrow stromal cells with three-dimensional tricalcium phosphate*. J Craniofac Surg, 2007. 18(4): 800-805.
7. K. Mesimaki, B. Lindroos, J. Tornwall, J. Mauno, C. Lindqvist, R. Kontio, S. Miettinen and R. Suuronen, *Novel maxillary reconstruction with ectopic bone formation by GMP adipose stem cells*. Int J Oral Maxillofac Surg, 2009. 38(3): 201-209.
8. R. Quarto, M. Mastrogiacomo, R. Cancedda, S.M. Kutepov, V. Mukhachev, A. Lavroukov, E. Kon and M. Marcacci, *Repair of large bone defects with the use of autologous bone marrow stromal cells*. N Engl J Med, 2001. 344(5): 385-386.

9. P.H. Warnke, I.N. Springer, J. Wiltfang, Y. Acil, H. Eufinger, M. Wehmoller, P.A. Russo, H. Bolte, E. Sherry, E. Behrens and H. Terheyden, *Growth and transplantation of a custom vascularised bone graft in a man*. Lancet, 2004. 364(9436): 766-770.

10. M. Jakob, F. Saxer, C. Scotti, S. Schreiner, P. Studer, A. Scherberich, M. Heberer and I. Martin, *Perspective on the evolution of cell-based bone tissue engineering strategies*. Eur Surg Res, 2012. 49(1): 1-7.

11. A. Lesman, J. Koffler, R. Atlas, Y.J. Blinder, Z. Kam and S. Levenberg, *Engineering vessel-like networks within multicellular fibrin-based constructs*. Biomaterials, 2011. 32(31): 7856-7869.

12. S. Singh, B.M. Wu and J.C. Dunn, *Accelerating vascularization in polycaprolactone scaffolds by endothelial progenitor cells*. Tissue Eng Part A, 2011. 17(13-14): 1819-1830.

13. R.E. Unger, S. Ghanaati, C. Orth, A. Sartoris, M. Barbeck, S. Halstenberg, A. Motta, C. Migliaresi and C.J. Kirkpatrick, *The rapid anastomosis between prevascularized networks on silk fibroin scaffolds generated in vitro with cocultures of human microvascular endothelial and osteoblast cells and the host vasculature*. Biomaterials, 2010. 31(27): 6959-6967.

14. G. Cheng, S. Liao, H. Kit Wong, D.A. Lacorre, E. di Tomaso, P. Au, D. Fukumura, R.K. Jain and L.L. Munn, *Engineered blood vessel networks connect to host vasculature via wrapping-and-tapping anastomosis*. Blood, 2011. 118(17): 4740-4749.

15. Y. Liu, J.K. Chan and S.H. Teoh, *Review of vascularised bone tissue-engineering strategies with a focus on co-culture systems*. J Tissue Eng Regen Med, 2012.

16. R.A.D. Carano and E.H. Filvaroff, *Angiogenesis and bone repair*. Drug Discovery Today, 2003. 8(21): 980-989.

17. C. Correia, W.L. Grayson, M. Park, D. Hutton, B. Zhou, X.E. Guo, L. Niklason, R.A. Sousa, R.L. Reis and G. Vunjak-Novakovic, *In vitro model of vascularized bone: synergizing vascular development and osteogenesis*. PLoS One, 2011. 6(12): e28352.

18. T. Meury, S. Verrier and M. Alini, *Human endothelial cells inhibit BMSC differentiation into mature osteoblasts in vitro by interfering with osterix expression*. J Cell Biochem, 2006. 98(4): 992-1006.

19. N. Quarto and M.T. Longaker, *FGF-2 inhibits osteogenesis in mouse adipose tissue-derived stromal cells and sustains their proliferative and osteogenic potential state*. Tissue Eng, 2006. 12(6): 1405-1418.

20. G.S. Di Marco, M. Hausberg, U. Hillebrand, P. Rustemeyer, W. Wittkowski, D. Lang and H. Pavenstadt, *Increased inorganic phosphate induces human endothelial cell apoptosis in vitro*. Am J Physiol Renal Physiol, 2008. 294(6): F1381-1387.

21. C. Correia, W. Grayson, R. Eton, J.M. Gimble, R.A. Sousa, R.L. Reis and G. Vunjak-Novakovic, *Human adipose-derived cells can serve as a single-cell source for the in vitro cultivation of vascularized bone grafts*. J Tissue Eng Regen Med, 2012.

22. N.C. Rivron, C.C. Raiss, J. Liu, A. Nandakumar, C. Sticht, N. Gretz, R. Truckenmuller, J. Rouwkema and C.A. van Blitterswijk, *Sonic Hedgehog-activated engineered blood vessels enhance bone tissue formation*. Proc Natl Acad Sci U S A, 2012. 109(12): 4413-4418.

23. D.L. Hutton, E.M. Moore, J.M. Gimble and W.L. Grayson, *Platelet-Derived Growth Factor and Spatiotemporal Cues Induce Development of Vascularized Bone Tissue by Adipose-Derived Stem Cells*. Tissue Eng Part A, 2013. 19(17-18): 2076-2086.

24. S. Koob, N. Torio-Padron, G.B. Stark, C. Hannig, Z. Stankovic and G. Finkenzeller, *Bone formation and neovascularization mediated by mesenchymal stem cells and endothelial cells in critical-sized calvarial defects*. Tissue Eng Part A, 2011. 17(3-4): 311-321.

25. M. Nishi, R. Matsumoto, J. Dong and T. Uemura, *Engineered bone tissue associated with vascularization utilizing a rotating wall vessel bioreactor*. J Biomed Mater Res A, 2012.

26. O. Tsigkou, I. Pomerantseva, J.A. Spencer, P.A. Redondo, A.R. Hart, E. O'Doherty, Y. Lin, C.C. Friedrich, L. Daheron, C.P. Lin, C.A. Sundback, J.P. Vacanti and C. Neville, *Engineered vascularized bone grafts*. Proc Natl Acad Sci U S A, 2010. 107(8): 3311-3316.

27. R. Zhang, Z. Gao, W. Geng, X. Yan, F. Chen and Y. Liu, *Engineering vascularized bone graft with osteogenic and angiogenic lineage differentiated bone marrow mesenchymal stem cells*. Artif Organs, 2012. 36(12): 1036-1046.

28. W.L. Grayson, M. Frohlich, K. Yeager, S. Bhumiratana, M.E. Chan, C. Cannizzaro, L.Q. Wan, X.S. Liu, X.E. Guo and G. Vunjak-Novakovic, *Engineering anatomically shaped human bone grafts*. Proc Natl Acad Sci U S A, 2010. 107(8): 3299-3304.

29. Y. Liu, S.H. Teoh, M.S. Chong, C.H. Yeow, R.D. Kamm, M. Choolani and J.K. Chan, *Contrasting effects of vasculogenic induction upon biaxial bioreactor stimulation of mesenchymal stem cells and endothelial progenitor cells cocultures in three-dimensional scaffolds under in vitro and in vivo paradigms for vascularized bone tissue engineering*. Tissue Eng Part A, 2013. 19(7-8): 893-904.

30. Z.Y. Zhang, S.H. Teoh, M.S. Chong, E.S. Lee, L.G. Tan, C.N. Mattar, N.M. Fisk, M. Choolani and J. Chan, *Neo-vascularization and bone formation mediated by fetal mesenchymal*

stem cell tissue-engineered bone grafts in critical-size femoral defects. Biomaterials, 2010. 31(4): 608-620.

31. A.M. Boos, J.S. Loew, A. Weigand, G. Deschler, D. Klumpp, A. Arkudas, O. Bleiziffer, H. Gulle, U. Kneser, R.E. Horch and J.P. Beier, *Engineering axially vascularized bone in the sheep arteriovenous-loop model*. J Tissue Eng Regen Med, 2013. 7(8): 654-664.

32. A. Arkudas, J.P. Beier, K. Heidner, J. Tjiawi, E. Polykandriotis, S. Srour, M. Sturzl, R.E. Horch and U. Kneser, *Axial prevascularization of porous matrices using an arteriovenous loop promotes survival and differentiation of transplanted autologous osteoblasts*. Tissue Eng, 2007. 13(7): 1549-1560.

33. P.H. Warnke, J. Wiltfang, I. Springer, Y. Acil, H. Bolte, M. Kosmahl, P.A. Russo, E. Sherry, U. Lutzen, S. Wolfart and H. Terheyden, *Man as living bioreactor: fate of an exogenously prepared customized tissue-engineered mandible*. Biomaterials, 2006. 27(17): 3163-3167.

34. Y.J. Koh, B.I. Koh, H. Kim, H.J. Joo, H.K. Jin, J. Jeon, C. Choi, D.H. Lee, J.H. Chung, C.H. Cho, W.S. Park, J.K. Ryu, J.K. Suh and G.Y. Koh, *Stromal vascular fraction from adipose tissue forms profound vascular network through the dynamic reassembly of blood endothelial cells*. Arterioscler Thromb Vasc Biol, 2011. 31(5): 1141-1150.

35. J.B. Mitchell, K. McIntosh, S. Zvonic, S. Garrett, Z.E. Floyd, A. Kloster, Y. Di Halvorsen, R.W. Storms, B. Goh, G. Kilroy, X. Wu and J.M. Gimble, *Immunophenotype of human adipose-derived cells: temporal changes in stromal-associated and stem cell-associated markers*. Stem Cells, 2006. 24(2): 376-385.

36. L. Zimmerlin, V.S. Donnenberg, M.E. Pfeifer, E.M. Meyer, B. Péault, J.P. Rubin and A.D. Donnenberg, *Stromal vascular progenitors in adult human adipose tissue*. Cytometry Part A, 2010. 77A(1): 22-30.

37. C. Seebach, D. Henrich, K. Wilhelm, J.H. Barker and I. Marzi, *Endothelial progenitor cells improve directly and indirectly early vascularization of mesenchymal stem cell-driven bone regeneration in a critical bone defect in rats*. Cell Transplant, 2012. 21(8): 1667-1677.

38. H. Zigdon-Giladi, T. Bick, D. Lewinson and E.E. Machtei, *Mesenchymal Stem Cells and Endothelial Progenitor Cells Stimulate Bone Regeneration and Mineral Density*. J Periodontol, 2013.

39. H. Zigdon-Giladi, T. Bick, D. Lewinson and E.E. Machtei, *Co-Transplantation of Endothelial Progenitor Cells and Mesenchymal Stem Cells Promote Neovascularization and Bone Regeneration*. Clin Implant Dent Relat Res, 2013.

40. Y. Cao, Z. Sun, L. Liao, Y. Meng, Q. Han and R.C. Zhao, *Human adipose tissue-derived stem cells differentiate into endothelial cells in vitro and improve postnatal neovascularization in vivo*. Biochem Biophys Res Commun, 2005. 332(2): 370-379.

41. A. Miranville, C. Heeschen, C. Sengenes, C.A. Curat, R. Busse and A. Bouloumie, *Improvement of postnatal neovascularization by human adipose tissue-derived stem cells*. Circulation, 2004. 110(3): 349-355.

42. V. Planat-Benard, J.S. Silvestre, B. Cousin, M. Andre, M. Nibbelink, R. Tamarat, M. Clergue, C. Manneville, C. Saillan-Barreau, M. Duriez, A. Tedgui, B. Levy, L. Penicaud and L. Casteilla, *Plasticity of human adipose lineage cells toward endothelial cells: physiological and therapeutic perspectives*. Circulation, 2004. 109(5): 656-663.

43. J. Rehman, D. Traktuev, J. Li, S. Merfeld-Clauss, C.J. Temm-Grove, J.E. Bovenkerk, C.L. Pell, B.H. Johnstone, R.V. Considine and K.L. March, *Secretion of angiogenic and antiapoptotic factors by human adipose stromal cells*. Circulation, 2004. 109(10): 1292-1298.

44. A.C. Zannettino, S. Paton, A. Arthur, F. Khor, S. Itescu, J.M. Gimble and S. Gronthos, *Multipotential human adipose-derived stromal stem cells exhibit a perivascular phenotype in vitro and in vivo*. J Cell Physiol, 2008. 214(2): 413-421.

45. P.J. Amos, H. Shang, A.M. Bailey, A. Taylor, A.J. Katz and S.M. Peirce, *IFATS collection: The role of human adipose-derived stromal cells in inflammatory microvascular remodeling and evidence of a perivascular phenotype*. Stem Cells, 2008. 26(10): 2682-2690.

46. M. Crisan, S. Yap, L. Casteilla, C.W. Chen, M. Corselli, T.S. Park, G. Andriolo, B. Sun, B. Zheng, L. Zhang, C. Norotte, P.N. Teng, J. Traas, R. Schugar, B.M. Deasy, S. Badylak, H.J. Buhring, J.P. Giacobino, L. Lazzari, J. Huard and B. Peault, *A perivascular origin for mesenchymal stem cells in multiple human organs*. Cell Stem Cell, 2008. 3(3): 301-313.

47. D.O. Traktuev, S. Merfeld-Clauss, J. Li, M. Kolonin, W. Arap, R. Pasqualini, B.H. Johnstone and K.L. March, *A population of multipotent CD34-positive adipose stromal cells share pericyte and mesenchymal surface markers, reside in a periendothelial location, and stabilize endothelial networks*. Circ Res, 2008. 102(1): 77-85.

48. R.R. Chen, E.A. Silva, W.W. Yuen and D.J. Mooney, *Spatio-temporal VEGF and PDGF delivery patterns blood vessel formation and maturation*. Pharm Res, 2007. 24(2): 258-264.

49. R. Cao, E. Brakenhielm, R. Pawliuk, D. Wariaro, M.J. Post, E. Wahlberg, P. Leboulch and Y. Cao, *Angiogenic synergism, vascular stability and improvement of hind-limb ischemia by a combination of PDGF-BB and FGF-2*. Nat Med, 2003. 9(5): 604-613.

50. J.M. Gimble, A.J. Katz and B.A. Bunnell, *Adipose-derived stem cells for regenerative medicine*. Circ Res, 2007. 100(9): 1249-1260.

51. P.A. Zuk, M. Zhu, H. Mizuno, J. Huang, J.W. Futrell, A.J. Katz, P. Benhaim, H.P. Lorenz and M.H. Hedrick, *Multilineage cells from human adipose tissue: implications for cell-based therapies*. Tissue Eng, 2001. 7(2): 211-228.

52. J.G. Rasmussen, O. Frobert, L. Pilgaard, J. Kastrup, U. Simonsen, V. Zachar and T. Fink, *Prolonged hypoxic culture and trypsinization increase the pro-angiogenic potential of human adipose tissue-derived stem cells*. Cytotherapy, 2011. 13(3): 318-328.

53. F. Verseijden, S.J. Posthumus-van Sluijs, P. Pavljasevic, S.O. Hofer, G.J. van Osch and E. Farrell, *Adult human bone marrow- and adipose tissue-derived stromal cells support the formation of prevascular-like structures from endothelial cells in vitro*. Tissue Eng Part A, 2010. 16(1): 101-114.

54. J. Basu, C.W. Genheimer, K.I. Guthrie, N. Sangha, S.F. Quinlan, A.T. Bruce, B. Reavis, C. Halberstadt, R.M. Ilagan and J.W. Ludlow, *Expansion of the human adipose-derived stromal vascular cell fraction yields a population of smooth muscle-like cells with markedly distinct phenotypic and functional properties relative to mesenchymal stem cells*. Tissue Eng Part C Methods, 2011. 17(8): 843-860.

55. H. Ning, G. Liu, G. Lin, R. Yang, T.F. Lue and C.S. Lin, *Fibroblast growth factor 2 promotes endothelial differentiation of adipose tissue-derived stem cells*. J Sex Med, 2009. 6(4): 967-979.

56. H. Suga, D. Matsumoto, H. Eto, K. Inoue, N. Aoi, H. Kato, J. Araki and K. Yoshimura, *Functional implications of CD34 expression in human adipose-derived stem/progenitor cells*. Stem Cells Dev, 2009. 18(8): 1201-1210.

57. H. Thangarajah, I.N. Vial, E. Chang, S. El-Ftesi, M. Januszyk, E.I. Chang, J. Paterno, E. Neofytou, M.T. Longaker and G.C. Gurtner, *IFATS collection: Adipose stromal cells adopt a proangiogenic phenotype under the influence of hypoxia*. Stem Cells, 2009. 27(1): 266-274.

58. L.J. Fischer, S. McIlhenny, T. Tulenko, N. Golesorkhi, P. Zhang, R. Larson, J. Lombardi, I. Shapiro and P.J. DiMuzio, *Endothelial differentiation of adipose-derived stem cells: effects of endothelial cell growth supplement and shear force*. J Surg Res, 2009. 152(1): 157-166.

59. P. Zhang, N. Moudgill, E. Hager, N. Tarola, C. Dimatteo, S. McIlhenny, T. Tulenko and P.J. Dimuzio, *Endothelial differentiation of adipose-derived stem cells from elderly patients with cardiovascular disease*. Stem Cells Dev, 2011. 20(6): 977-988.

60. S. Natesan, G. Zhang, D.G. Baer, T.J. Walters, R.J. Christy and L.J. Suggs, *A bilayer construct controls adipose-derived stem cell differentiation into endothelial cells and pericytes without growth factor stimulation*. Tissue Eng Part A, 2011. 17(7-8): 941-953.

61. A.C. Boquest, A. Noer, A.L. Sorensen, K. Vekterud and P. Collas, *CpG methylation profiles of endothelial cell-specific gene promoter regions in adipose tissue stem cells suggest limited differentiation potential toward the endothelial cell lineage*. Stem Cells, 2007. 25(4): 852-861.

62. B.A. Bunnell, M. Flaat, C. Gagliardi, B. Patel and C. Ripoll, *Adipose-derived stem cells: Isolation, expansion and differentiation*. Methods, 2008. 45(2): 115-120.

63. J.M. Gimble, B.A. Bunnell and F. Guilak, *Human adipose-derived cells: an update on the transition to clinical translation*. Regen Med, 2012. 7(2): 225-235.

64. H. Suga, T. Shigeura, D. Matsumoto, K. Inoue, H. Kato, N. Aoi, S. Murase, K. Sato, K. Gonda, I. Koshima and K. Yoshimura, *Rapid expansion of human adipose-derived stromal cells preserving multipotency*. Cytotherapy, 2007. 9(8): 738-745.

65. M. Wosnitza, K. Hemmrich, A. Groger, S. Graber and N. Pallua, *Plasticity of human adipose stem cells to perform adipogenic and endothelial differentiation*. Differentiation, 2007. 75(1): 12-23.

66. F. Guilak, K.E. Lott, H.A. Awad, Q. Cao, K.C. Hicok, B. Fermor and J.M. Gimble, *Clonal analysis of the differentiation potential of human adipose-derived adult stem cells*. J Cell Physiol, 2006. 206(1): 229-237.

67. S.G. Dubois, E.Z. Floyd, S. Zvonic, G. Kilroy, X. Wu, S. Carling, Y.D. Halvorsen, E. Ravussin and J.M. Gimble, *Isolation of human adipose-derived stem cells from biopsies and liposuction specimens*. Methods Mol Biol, 2008. 449(69-79.

68. B.C. Goh, S. Thirumala, G. Kilroy, R.V. Devireddy and J.M. Gimble, *Cryopreservation characteristics of adipose-derived stem cells: maintenance of differentiation potential and viability*. J Tissue Eng Regen Med, 2007. 1(4): 322-324.

69. K. Gonda, T. Shigeura, T. Sato, D. Matsumoto, H. Suga, K. Inoue, N. Aoi, H. Kato, K. Sato, S. Murase, I. Koshima and K. Yoshimura, *Preserved proliferative capacity and multipotency of human adipose-derived stem cells after long-term cryopreservation*. Plast Reconstr Surg, 2008. 121(2): 401-410.

70. G. Liu, H. Zhou, Y. Li, G. Li, L. Cui, W. Liu and Y. Cao, *Evaluation of the viability and osteogenic differentiation of cryopreserved human adipose-derived stem cells*. Cryobiology, 2008. 57(1): 18-24.

71. A. Niemisto, V. Dunmire, O. Yli-Harja, W. Zhang and I. Shmulevich, *Robust quantification of in vitro angiogenesis through image analysis*. IEEE Trans Med Imaging, 2005. 24(4): 549-553.

72. A. Armulik, A. Abramsson and C. Betsholtz, *Endothelial/pericyte interactions*. Circ Res, 2005. 97(6): 512-523.

73. M. Hellstrom, M. Kalen, P. Lindahl, A. Abramsson and C. Betsholtz, *Role of PDGF-B and PDGFR-beta in recruitment of vascular smooth muscle cells and pericytes during embryonic blood vessel formation in the mouse*. Development, 1999. 126(14): 3047-3055.

74. K.K. Hirschi, T.C. Skalak, S.M. Peirce and C.D. Little, *Vascular assembly in natural and engineered tissues*. Ann N Y Acad Sci, 2002. 961(223-242.

75. L. Martineau and C.J. Doillon, *Angiogenic response of endothelial cells seeded dispersed versus on beads in fibrin gels*. Angiogenesis, 2007. 10(4): 269-277.

76. T. Korff and H.G. Augustin, *Integration of endothelial cells in multicellular spheroids prevents apoptosis and induces differentiation*. J Cell Biol, 1998. 143(5): 1341-1352.

77. M.J. Frontini, Z. Nong, R. Gros, M. Drangova, C. O'Neil, M.N. Rahman, O. Akawi, H. Yin, C.G. Ellis and J.G. Pickering, *Fibroblast growth factor 9 delivery during angiogenesis produces durable, vasoresponsive microvessels wrapped by smooth muscle cells*. Nat Biotechnol, 2011. 29(5): 421-427.

78. F. Mac Gabhann and S.M. Peirce, *Collateral capillary arterialization following arteriolar ligation in murine skeletal muscle*. Microcirculation, 2010. 17(5): 333-347.

79. L. Diaz-Flores, R. Gutierrez, J.F. Madrid, H. Varela, F. Valladares, E. Acosta, P. Martin-Vasallo and L. Diaz-Flores, Jr., *Pericytes. Morphofunction, interactions and pathology in a quiescent and activated mesenchymal cell niche*. Histol Histopathol, 2009. 24(7): 909-969.

80. A.N. Stratman, K.M. Malotte, R.D. Mahan, M.J. Davis and G.E. Davis, *Pericyte recruitment during vasculogenic tube assembly stimulates endothelial basement membrane matrix formation*. Blood, 2009. 114(24): 5091-5101.

81. G. Bergers and S. Song, *The role of pericytes in blood-vessel formation and maintenance*. Neuro Oncol, 2005. 7(4): 452-464.

82. L.E. Benjamin, D. Golijanin, A. Itin, D. Pode and E. Keshet, *Selective ablation of immature blood vessels in established human tumors follows vascular endothelial growth factor withdrawal*. J Clin Invest, 1999. 103(2): 159-165.

83. L.E. Benjamin, I. Hemo and E. Keshet, *A plasticity window for blood vessel remodelling is defined by pericyte coverage of the preformed endothelial network and is regulated by PDGF-B and VEGF*. Development, 1998. 125(9): 1591-1598.

84. M. Enge, M. Bjarnegard, H. Gerhardt, E. Gustafsson, M. Kalen, N. Asker, H.P. Hammes, M. Shani, R. Fassler and C. Betsholtz, *Endothelium-specific platelet-derived growth factor-B ablation mimics diabetic retinopathy*. EMBO J, 2002. 21(16): 4307-4316.

85. Y. Hori, D.E. Hu, K. Yasui, R.L. Smither, G.A. Gresham and T.P. Fan, *Differential effects of angiostatic steroids and dexamethasone on angiogenesis and cytokine levels in rat sponge implants*. Br J Pharmacol, 1996. 118(7): 1584-1591.

86. J. Rouwkema, J. de Boer and C.A. Van Blitterswijk, *Endothelial cells assemble into a 3-dimensional prevascular network in a bone tissue engineering construct*. Tissue Eng, 2006. 12(9): 2685-2693.

87. Y. Liu, S.H. Teoh, M.S. Chong, E.S. Lee, C.N. Mattar, N.K. Randhawa, Z.Y. Zhang, R.J. Medina, R.D. Kamm, N.M. Fisk, M. Choolani and J.K. Chan, *Vasculogenic and osteogenesis-enhancing potential of human umbilical cord blood endothelial colony-forming cells*. Stem Cells, 2012. 30(9): 1911-1924.

88. K. Usami, H. Mizuno, K. Okada, Y. Narita, M. Aoki, T. Kondo, D. Mizuno, J. Mase, H. Nishiguchi, H. Kagami and M. Ueda, *Composite implantation of mesenchymal stem cells with endothelial progenitor cells enhances tissue-engineered bone formation*. J Biomed Mater Res A, 2009. 90(3): 730-741.

89. A.I. Caplan and D. Correa, *PDGF in bone formation and regeneration: new insights into a novel mechanism involving MSCs*. J Orthop Res, 2011. 29(12): 1795-1803.

90. E. Solheim, *Growth factors in bone*. Int Orthop, 1998. 22(6): 410-416.

91. J.G. Andrew, J.A. Hoyland, A.J. Freemont and D.R. Marsh, *Platelet-derived growth factor expression in normally healing human fractures*. Bone, 1995. 16(4): 455-460.

92. S. Graham, A. Leonidou, M. Lester, M. Heliotis, A. Mantalaris and E. Tsiridis, *Investigating the role of PDGF as a potential drug therapy in bone formation and fracture healing*. Expert Opin Investig Drugs, 2009. 18(11): 1633-1654.

93. Y.J. Park, Y.M. Lee, S.N. Park, S.Y. Sheen, C.P. Chung and S.J. Lee, *Platelet derived growth factor releasing chitosan sponge for periodontal bone regeneration*. Biomaterials, 2000. 21(2): 153-159.

94. T.J. Nash, C.R. Howlett, C. Martin, J. Steele, K.A. Johnson and D.J. Hicklin, *Effect of platelet-derived growth factor on tibial osteotomies in rabbits*. Bone, 1994. 15(2): 203-208.

95. L.R. Chaudhary, A.M. Hofmeister and K.A. Hruska, *Differential growth factor control of bone formation through osteoprogenitor differentiation*. Bone, 2004. 34(3): 402-411.

96. A. Kumar, B.P. Salimath, G.B. Stark and G. Finkenzeller, *Platelet-derived growth factor receptor signaling is not involved in osteogenic differentiation of human mesenchymal stem cells*. Tissue Eng Part A, 2010. 16(3): 983-993.

97. H. Tanaka and C.T. Liang, *Effect of platelet-derived growth factor on DNA synthesis and gene expression in bone marrow stromal cells derived from adult and old rats*. J Cell Physiol, 1995. 164(2): 367-375.

98. R. Gruber, F. Karreth, B. Kandler, G. Fuerst, A. Rot, M.B. Fischer and G. Watzek, *Platelet-released supernatants increase migration and proliferation, and decrease osteogenic differentiation of bone marrow-derived mesenchymal progenitor cells under in vitro conditions*. Platelets, 2004. 15(1): 29-35.

99. A. Tokunaga, T. Oya, Y. Ishii, H. Motomura, C. Nakamura, S. Ishizawa, T. Fujimori, Y. Nabeshima, A. Umezawa, M. Kanamori, T. Kimura and M. Sasahara, *PDGF receptor beta is a potent regulator of mesenchymal stromal cell function*. J Bone Miner Res, 2008. 23(9): 1519-1528.

100. J. Lee, D. Gupta, N.J. Panetta, B. Levi, A.W. James, D. Wan, G.W. Commons and M.T. Longaker, *Elucidating mechanisms of osteogenesis in human adipose-derived stromal cells via microarray analysis*. J Craniofac Surg, 2010. 21(4): 1136-1141.

101. D.L. Hutton, E.A. Logsdon, E.M. Moore, F. Mac Gabhann, J.M. Gimble and W.L. Grayson, *Vascular morphogenesis of adipose-derived stem cells is mediated by heterotypic cell-cell interactions*. Tissue Eng Part A, 2012. 18(15-16): 1729-1740.

102. X. Chen, A.S. Aledia, C.M. Ghajar, C.K. Griffith, A.J. Putnam, C.C. Hughes and S.C. George, *Prevascularization of a fibrin-based tissue construct accelerates the formation of functional anastomosis with host vasculature*. Tissue Eng Part A, 2009. 15(6): 1363-1371.

103. S. Levenberg, J. Rouwkema, M. Macdonald, E.S. Garfein, D.S. Kohane, D.C. Darland, R. Marini, C.A. van Blitterswijk, R.C. Mulligan, P.A. D'Amore and R. Langer, *Engineering vascularized skeletal muscle tissue*. Nat Biotechnol, 2005. 23(7): 879-884.

104. C.G. Bellows, J.N. Heersche and J.E. Aubin, *Inorganic phosphate added exogenously or released from beta-glycerophosphate initiates mineralization of osteoid nodules in vitro*. Bone Miner, 1992. 17(1): 15-29.

105. C. Maes, T. Kobayashi, M.K. Selig, S. Torrekens, S.I. Roth, S. Mackem, G. Carmeliet and H.M. Kronenberg, *Osteoblast precursors, but not mature osteoblasts, move into developing and fractured bones along with invading blood vessels*. Dev Cell, 2010. 19(2): 329-344.

106. A.G. Mikos, S.W. Herring, P. Ochareon, J. Elisseeff, H.H. Lu, R. Kandel, F.J. Schoen, M. Toner, D. Mooney, A. Atala, M.E. Van Dyke, D. Kaplan and G. Vunjak-Novakovic, *Engineering complex tissues*. Tissue Eng, 2006. 12(12): 3307-3339.

107. R.A. Carano and E.H. Filvaroff, *Angiogenesis and bone repair*. Drug Discov Today, 2003. 8(21): 980-989.

108. N. Sato, J.G. Beitz, J. Kato, M. Yamamoto, J.W. Clark, P. Calabresi, A. Raymond and A.R. Frackelton, Jr., *Platelet-derived growth factor indirectly stimulates angiogenesis in vitro*. Am J Pathol, 1993. 142(4): 1119-1130.

109. G. Allt and J.G. Lawrenson, *Pericytes: cell biology and pathology*. Cells Tissues Organs, 2001. 169(1): 1-11.

110. B. Kinner and M. Spector, *Expression of smooth muscle actin in osteoblasts in human bone*. J Orthop Res, 2002. 20(3): 622-632.

111. J.M. Schmitt, K. Hwang, S.R. Winn and J.O. Hollinger, *Bone morphogenetic proteins: an update on basic biology and clinical relevance*. J Orthop Res, 1999. 17(2): 269-278.

112. M.M. Deckers, R.L. van Bezooijen, G. van der Horst, J. Hoogendam, C. van Der Bent, S.E. Papapoulos and C.W. Lowik, *Bone morphogenetic proteins stimulate angiogenesis through osteoblast-derived vascular endothelial growth factor A*. Endocrinology, 2002. 143(4): 1545-1553.

113. B. Czarkowska-Paczek, I. Bartlomiejczyk and J. Przybylski, *The serum levels of growth factors: PDGF, TGF-beta and VEGF are increased after strenuous physical exercise*. J Physiol Pharmacol, 2006. 57(2): 189-197.

114. P.V. Giannoudis, I. Pountos, J. Morley, S. Perry, H.I. Tarkin and H.C. Pape, *Growth factor release following femoral nailing*. Bone, 2008. 42(4): 751-757.

115. E.J. Carragee, E.L. Hurwitz and B.K. Weiner, *A critical review of recombinant human bone morphogenetic protein-2 trials in spinal surgery: emerging safety concerns and lessons learned*. Spine J, 2011. 11(6): 471-491.

116. Z.S. Ai-Aql, A.S. Alagl, D.T. Graves, L.C. Gerstenfeld and T.A. Einhorn, *Molecular mechanisms controlling bone formation during fracture healing and distraction osteogenesis*. J Dent Res, 2008. 87(2): 107-118.

117. P. Kolar, K. Schmidt-Bleek, H. Schell, T. Gaber, D. Toben, G. Schmidmaier, C. Perka, F. Buttgereit and G.N. Duda, *The early fracture hematoma and its potential role in fracture healing*. Tissue Eng Part B Rev, 2010. 16(4): 427-434.

118. P.M. Mountziaris and A.G. Mikos, *Modulation of the inflammatory response for enhanced bone tissue regeneration*. Tissue Eng Part B Rev, 2008. 14(2): 179-186.

119. M. Frater-Schroder, W. Risau, R. Hallmann, P. Gautschi and P. Bohlen, *Tumor necrosis factor type alpha, a potent inhibitor of endothelial cell growth in vitro, is angiogenic in vivo*. Proc Natl Acad Sci U S A, 1987. 84(15): 5277-5281.

120. S.J. Leibovich, P.J. Polverini, H.M. Shepard, D.M. Wiseman, V. Shively and N. Nuseir, *Macrophage-induced angiogenesis is mediated by tumour necrosis factor-alpha*. Nature, 1987. 329(6140): 630-632.

121. R.C. Sainson, D.A. Johnston, H.C. Chu, M.T. Holderfield, M.N. Nakatsu, S.P. Crampton, J. Davis, E. Conn and C.C. Hughes, *TNF primes endothelial cells for angiogenic sprouting by inducing a tip cell phenotype*. Blood, 2008. 111(10): 4997-5007.

122. H. Nakagami, T.X. Cui, M. Iwai, T. Shiuchi, Y. Takeda-Matsubara, L. Wu and M. Horiuchi, *Tumor necrosis factor-alpha inhibits growth factor-mediated cell proliferation through SHP-1 activation in endothelial cells*. Arterioscler Thromb Vasc Biol, 2002. 22(2): 238-242.

123. N. Sato, T. Goto, K. Haranaka, N. Satomi, H. Nariuchi, Y. Mano-Hirano and Y. Sawasaki, *Actions of tumor necrosis factor on cultured vascular endothelial cells: morphologic modulation, growth inhibition, and cytotoxicity*. J Natl Cancer Inst, 1986. 76(6): 1113-1121.

124. A. Yilmaz, G. Bieler, O. Spertini, F.J. Lejeune and C. Ruegg, *Pulse treatment of human vascular endothelial cells with high doses of tumor necrosis factor and interferon-gamma results in simultaneous synergistic and reversible effects on proliferation and morphology*. Int J Cancer, 1998. 77(4): 592-599.

125. L.C. Gerstenfeld, T.J. Cho, T. Kon, T. Aizawa, A. Tsay, J. Fitch, G.L. Barnes, D.T. Graves and T.A. Einhorn, *Impaired fracture healing in the absence of TNF-alpha signaling:*

the role of TNF-alpha in endochondral cartilage resorption. J Bone Miner Res, 2003. 18(9): 1584-1592.

126. G.E. Glass, J.K. Chan, A. Freidin, M. Feldmann, N.J. Horwood and J. Nanchahal, *TNF-alpha promotes fracture repair by augmenting the recruitment and differentiation of muscle-derived stromal cells*. Proc Natl Acad Sci U S A, 2011. 108(4): 1585-1590.

127. J. Ding, O. Ghali, P. Lencel, O. Broux, C. Chauveau, J.C. Devedjian, P. Hardouin and D. Magne, *TNF-alpha and IL-1beta inhibit RUNX2 and collagen expression but increase alkaline phosphatase activity and mineralization in human mesenchymal stem cells*. Life Sci, 2009. 84(15-16): 499-504.

128. K. Hess, A. Ushmorov, J. Fiedler, R.E. Brenner and T. Wirth, *TNFalpha promotes osteogenic differentiation of human mesenchymal stem cells by triggering the NF-kappaB signaling pathway*. Bone, 2009. 45(2): 367-376.

129. Z. Lu, G. Wang, C.R. Dunstan and H. Zreiqat, *Short-term exposure to tumor necrosis factor-alpha enables human osteoblasts to direct adipose tissue-derived mesenchymal stem cells into osteogenic differentiation*. Stem Cells Dev, 2012. 21(13): 2420-2429.

130. P.M. Mountziaris, E. Dennis Lehman, I. Mountziaris, D.C. Sing, F.K. Kasper and A.G. Mikos, *Effect of temporally patterned TNF-alpha delivery on in vitro osteogenic differentiation of mesenchymal stem cells cultured on biodegradable polymer scaffolds*. J Biomater Sci Polym Ed, 2013. 24(15): 1794-1813.

131. C.X. Lam, D.W. Hutmacher, J.T. Schantz, M.A. Woodruff and S.H. Teoh, *Evaluation of polycaprolactone scaffold degradation for 6 months in vitro and in vivo*. J Biomed Mater Res A, 2009. 90(3): 906-919.

132. M.A. Woodruff and D.W. Hutmacher, *The return of a forgotten polymer—Polycaprolactone in the 21st century*. Progress in Polymer Science, 2010. 35(10): 1217-1256.

133. J.P. Temple, D.L. Hutton, B.P. Hung, P.Y. Huri, C.A. Cook, R. Kondragunta, X. Jia and W.L. Grayson, *Engineering anatomically shaped vascularized bone grafts with hASCs and 3D-printed PCL scaffolds*. J Biomed Mater Res A, 2014.

134. D.L. Hutton and W.L. Grayson, *Stem cell-based approaches to engineering vascularized bone*. Current Opinion in Chemical Engineering, 2014. 3(1): 75-82.

135. M. Frohlich, W.L. Grayson, D. Marolt, J.M. Gimble, N. Kregar-Velikonja and G. Vunjak-Novakovic, *Bone grafts engineered from human adipose-derived stem cells in perfusion bioreactor culture*. Tissue Eng Part A, 2010. 16(1): 179-189.

136. E.A. Sander, V.H. Barocas and R.T. Tranquillo, *Initial fiber alignment pattern alters extracellular matrix synthesis in fibroblast-populated fibrin gel cruciforms and correlates with predicted tension*. Ann Biomed Eng, 2011. 39(2): 714-729.

137. B.P. Hung, D.L. Hutton and W.L. Grayson, *Mechanical control of tissue-engineered bone*. Stem Cell Res Ther, 2013. 4(1): 10.

138. J. Koffler, K. Kaufman-Francis, Y. Shandalov, D. Egozi, D.A. Pavlov, A. Landesberg and S. Levenberg, *Improved vascular organization enhances functional integration of engineered skeletal muscle grafts*. Proc Natl Acad Sci U S A, 2011. 108(36): 14789-14794.

139. M.P. Bendeck, *Macrophage matrix metalloproteinase-9 regulates angiogenesis in ischemic muscle*. Circ Res, 2004. 94(2): 138-139.

140. L.J. Hawinkels, K. Zuidwijk, H.W. Verspaget, E.S. de Jonge-Muller, W. van Duijn, V. Ferreira, R.D. Fontijn, G. David, D.W. Hommes, C.B. Lamers and C.F. Sier, *VEGF*

release by MMP-9 mediated heparan sulphate cleavage induces colorectal cancer angiogenesis. Eur J Cancer, 2008. 44(13): 1904-1913.

141. H. Zheng, H. Takahashi, Y. Murai, Z. Cui, K. Nomoto, H. Niwa, K. Tsuneyama and Y. Takano, *Expressions of MMP-2, MMP-9 and VEGF are closely linked to growth, invasion, metastasis and angiogenesis of gastric carcinoma*. Anticancer Res, 2006. 26(5A): 3579-3583.

142. J.G. Vos, J.G. Kreeftenberg, B.C. Kruijt, W. Kruizinga and P. Steerenberg, *The athymic nude rat. II. Immunological characteristics*. Clin Immunol Immunopathol, 1980. 15(2): 229-237.

143. M.V. Thomas and D.A. Puleo, *Infection, inflammation, and bone regeneration: a paradoxical relationship*. J Dent Res, 2011. 90(9): 1052-1061.

144. P.M. Mountziaris, P.P. Spicer, F.K. Kasper and A.G. Mikos, *Harnessing and modulating inflammation in strategies for bone regeneration*. Tissue Eng Part B Rev, 2011. 17(6): 393-402.

145. M.S. Gaston and A.H. Simpson, *Inhibition of fracture healing*. J Bone Joint Surg Br, 2007. 89(12): 1553-1560.

146. M. Murnaghan, G. Li and D.R. Marsh, *Nonsteroidal anti-inflammatory drug-induced fracture nonunion: an inhibition of angiogenesis?* J Bone Joint Surg Am, 2006. 88 Suppl 3(140-147.

147. I. Pountos, T. Georgouli, T.J. Blokhuis, H.C. Pape and P.V. Giannoudis, *Pharmacological agents and impairment of fracture healing: what is the evidence?* Injury, 2008. 39(4): 384-394.

148. S.M. Ehsan and S.C. George, *Nonsteady state oxygen transport in engineered tissue: implications for design*. Tissue Eng Part A, 2013. 19(11-12): 1433-1442.

149. L.B. Bertelsen, A.B. Bohn, M. Smith, B. Mølgaard, B. Møller, H. Stødkilde-Jørgensen and P. Kristensen, *Are endothelial outgrowth cells a potential source for future re-vascularization therapy?* Experimental Gerontology, 2014. 58(0): 132-138.

150. Y.J. Blinder, D.J. Mooney and S. Levenberg, *Engineering approaches for inducing blood vessel formation*. Current Opinion in Chemical Engineering, 2014. 3(0): 56-61.

151. R. Samuel, L. Daheron, S. Liao, T. Vardam, W.S. Kamoun, A. Batista, C. Buecker, R. Schäfer, X. Han, P. Au, D.T. Scadden, D.G. Duda, D. Fukumura and R.K. Jain, *Generation of functionally competent and durable engineered blood vessels from human induced pluripotent stem cells*. Proceedings of the National Academy of Sciences, 2013. 110(31): 12774-12779.

152. K. Hirota and G.L. Semenza, *Regulation of angiogenesis by hypoxia-inducible factor 1*. Crit Rev Oncol Hematol, 2006. 59(1): 15-26.

153. S.T. Hsiao, R.J. Dilley, G.J. Dusting and S.Y. Lim, *Ischemic preconditioning for cell-based therapy and tissue engineering*. Pharmacol Ther, 2014. 142(2): 141-153.

154. C.K. Griffith and S.C. George, *The effect of hypoxia on in vitro prevascularization of a thick soft tissue*. Tissue Eng Part A, 2009. 15(9): 2423-2434.

155. R. Eguchi, A. Suzuki, S. Miyakaze, K. Kaji and T. Ohta, *Hypoxia induces apoptosis of HUVECs in an in vitro capillary model by activating proapoptotic signal p38 through suppression of ERK1/2*. Cell Signal, 2007. 19(6): 1121-1131.

156. T. Ohta, R. Eguchi, A. Suzuki, S. Miyakaze, R. Ayuzawa and K. Kaji, *Hypoxia-induced apoptosis and tube breakdown are regulated by p38 MAPK but not by caspase cascade in an in vitro capillary model composed of human endothelial cells*. J Cell Physiol, 2007. 211(3): 673-681.

157. H. Moriyama, M. Moriyama, H. Isshi, S. Ishihara, H. Okura, A. Ichinose, T. Ozawa, A. Matsuyama and T. Hayakawa, *Role of notch signaling in the maintenance of human mesenchymal stem cells under hypoxic conditions*. Stem Cells Dev, 2014. 23(18): 2211-2224.

158. N.C. Denko, *Hypoxia, HIF1 and glucose metabolism in the solid tumour*. Nat Rev Cancer, 2008. 8(9): 705-713.

159. M. Deschepper, K. Oudina, B. David, V. Myrtil, C. Collet, M. Bensidhoum, D. Logeart-Avramoglou and H. Petite, *Survival and function of mesenchymal stem cells (MSCs) depend on glucose to overcome exposure to long-term, severe and continuous hypoxia*. J Cell Mol Med, 2011. 15(7): 1505-1514.

160. P. Carmeliet and R.K. Jain, *Molecular mechanisms and clinical applications of angiogenesis*. Nature, 2011. 473(7347): 298-307.

161. M. Franco, P. Roswall, E. Cortez, D. Hanahan and K. Pietras, *Pericytes promote endothelial cell survival through induction of autocrine VEGF-A signaling and Bcl-w expression*. Blood, 2011. 118(10): 2906-2917.

162. S. Benjamin, D. Sheyn, S. Ben-David, A. Oh, I. Kallai, N. Li, D. Gazit and Z. Gazit, *Oxygenated environment enhances both stem cell survival and osteogenic differentiation*. Tissue Eng Part A, 2013. 19(5-6): 748-758.

163. S.H. Oh, C.L. Ward, A. Atala, J.J. Yoo and B.S. Harrison, *Oxygen generating scaffolds for enhancing engineered tissue survival*. Biomaterials, 2009. 30(5): 757-762.

164. E. Pedraza, M.M. Coronel, C.A. Fraker, C. Ricordi and C.L. Stabler, *Preventing hypoxia-induced cell death in beta cells and islets via hydrolytically activated, oxygen-generating biomaterials*. Proc Natl Acad Sci U S A, 2012. 109(11): 4245-4250.

165. A.M. Laib, A. Bartol, A. Alajati, T. Korff, H. Weber and H.G. Augustin, *Spheroid-based human endothelial cell microvessel formation in vivo*. Nat Protoc, 2009. 4(8): 1202-1215.

Vita

Daphne earned her B.S. in Biomedical Engineering from the Georgia Institute of Technology in 2009. She conducted research as an undergraduate in the laboratory of Barbara D. Boyan, where she studied the biological responses of osteoblasts and stem cells to titanium orthopedic implant materials. This work resulted in 5 journal publications, 7 conference abstracts (1 oral presentation), and undergraduate research awards.

Daphne entered the Biomedical Engineering Ph.D. program at Johns Hopkins University in 2009 and was the first graduate student to join the brand new lab of Warren L. Grayson. Her project, presented in this dissertation, was to develop methods to engineer vascularized bone using a single cell source. During her tenure as a Ph.D. student, Daphne authored 13 journal publications (6 first author, 2 featured on the cover), 21 conference abstracts (2 oral presentations), and one provisional patent. She was also awarded the American Heart Association Pre-Doctoral Fellowship.